

**Queensland Climate Change
Centre of Excellence**

Research Report

Rainfall in Queensland

**Part 5: Projected changes in
Queensland rainfall under double-
CO₂ conditions in the HiGEM model**

Prepared by Nicholas Klingaman

August 2012



Prepared by: Queensland Climate Change Centre of Excellence
Department of Science, Information Technology, Innovation and the Arts

© The State of Queensland (Department of Science, Information Technology, Innovation and the Arts) 2012

Copyright inquiries should be addressed to <enquiries@derm.qld.gov.au> or the Department of Science, Information Technology, Innovation and the Arts, Level 19, Forestry House, Brisbane QLD 4000.

ISBN 978-09805641-5-0

Disclaimer

This document has been prepared with all due diligence and care, based on the best available information at the time of publication. The department holds no responsibility for any errors or omissions within this document. Any decisions made by other parties based on this document are solely the responsibility of those parties. Information contained in this document is from a number of sources and, as such, does not necessarily represent government or departmental policy.

If you need to access this document in a language other than English, please call the Translating and Interpreting Service (TIS National) on 131 450 and ask them to telephone Library Services on +61 7 3224 8412. This publication can be made available in an alternative format (e.g. large print or audiotape) on request for people with vision impairment; phone +61 7 3224 8412 or email <library@derm.qld.gov.au>.

Citation

Klingaman N. 2012. Projected changes in Queensland rainfall under double CO₂ conditions in the HiGEM model. QCCCE research report: Rainfall in Queensland. Part. 5. Queensland Department of Science, Information Technology, Innovation and the Arts, Brisbane, Australia. Available online at <www.longpaddock.qld.gov.au/about/publications/index.html>

Acknowledgements

Dr Nicholas Klingaman was funded by a grant from the Queensland Government, under a collaboration between the Queensland Climate Change Centre of Excellence (QCCCE) and the Walker Institute for Climate System Research at the University of Reading. Dr Klingaman was supervised by Steve Woolnough of the Walker Institute and Jozef Syktus of QCCCE. Dr Klingaman acknowledges productive discussions with Ken Day of QCCCE.

SILO rainfall data were provided by the Queensland Government. 20th Century Reanalysis V2 data were provided by the NOAA/OAR/ESRL PSD, Boulder, Colorado, USA, from their website <www.esrl.noaa.gov/psd/>. Support for the Twentieth Century Reanalysis Project dataset is provided by the U.S. Department of Energy, Office of Science Innovative and Novel Computational Impact on Theory and Experiment (DOE INCITE) program, and Office of Biological and Environmental Research (BER), and by the National Oceanic and Atmospheric Administration Climate Program Office. HadISST SSTs were provided by the British Atmospheric Data Centre, under agreement with the U.K. Met Office. IBTrACS data were provided by the U.S. National Climatic Data Centre. HiGEM model output data were provided by the National Centre for Atmospheric Science in the United Kingdom. Tropical cyclone tracking was kindly performed by Dr Jane Strachan of the University of Reading.

To contact the author:

Email: <n.p.klingaman@reading.ac.uk>

Post: Department of Meteorology
University of Reading
Earley Gate, PO Box 243
Reading, Berkshire RG6 6BB
United Kingdom

Published August 2012

Contents

Contents	ii
List of Figures	iii
List of Tables	iv
1 Executive Summary	1
2 Introduction & Objectives	2
3 Model, data and methods	3
3.1 HiGEM simulations	3
3.2 SILO rainfall	4
3.3 EOT Analysis	4
3.4 Seasonal and Annual Means.....	5
4 Projected changes in mean climate	6
4.1 Surface temperature	6
4.2 850 hPa circulation	9
4.3 Rainfall	11
4.3.1 Mean rainfall	11
4.3.2 Significance of mean rainfall changes	12
4.3.3 Frequency and intensity of daily rainfall.....	17
4.4 Tropical cyclones	19
5 Projected changes in rainfall extremes	21
5.1 Daily extremes	21
5.2 Rainfall duration and event size	23
5.2.1 Rainfall Duration	23
5.2.2 Rainfall size event.....	24
Compression of the Queensland wet season.....	28
6.1 Onset and termination dates	28
6.2 Contributions of individual months to wet season totals	30
7 Projected changes in inter-annual variability	31
7.1 Inter-annual variability in seasonal means	31
7.2 Empirical Orthogonal Teleconnection patterns	34
7.2.1 December - February EOTs	35
7.2.2 March - May EOTs.....	37
7.2.3 June - August EOTs.....	41
7.2.4 September - November EOTs	44
8 Discussion.....	51
9 Summary and conclusions	54
10 References	56

List of Figures

- Figure 1: (a–d) The difference in seasonal-mean climatological surface temperature for 2 x CO₂ minus CTL for (a) DJF, (b) MAM, (c) JJA and (d) SON; (e–p) the difference in seasonal-mean climatological surface temperature for 2 x CO₂ minus 50 year periods of CTL, using (e, h, k, n) years 1–50, (f, i, l, o) years 51–100 and (g, j, m, p) years 101–150 for (e–g) DJF, (h–j) MAM, (k–m) JJA and (n–p) SON. 6
- Figure 2: CTL Seasonal-mean climatological (vectors) 850 hPa wind direction and (colours) 850 hPa wind speed from CTL for (a) DJF, (b) MAM, (c) JJA and (d) SON 8
- Figure 3: As in Fig. 1, but for the change in (vectors) 850 hPa wind direction and (colours) 850 hPa wind speed. 9
- Figure 4: The difference (2 x CO₂ minus CTL) in climatological rainfall for (a) May–April (mm year⁻¹), (b) December–February (mm season⁻¹), (c) March–May (mm season⁻¹), (d) June–August (mm season⁻¹) and (e) September–November (mm season⁻¹). The mean of all 150 years of CTL were used as the baseline against which 2 x CO₂ was compared. The contour interval for (a) is 50 mm year⁻¹, while for (b–e) it is 24 mm season⁻¹. 13
- Figure 5: As in Fig. 3, but for ratios of rainfall (2 x CO₂ divided by CTL) for (a, f–h) May–April, (b, i–k) December–February, (c, l–n) March–May, (d, o–q) June–August and (e, r–t) September–November. 14
- Figure 6: The fraction of 50-year periods in CTL with mean rainfall less than the mean rainfall in 2 x CO₂ for (a) the May–April annual-mean and seasonal means of (b) December–February, (c) March–May, (d) June–August and (e) September–November. The quantity shown is effectively the confidence level for a drying, or unity minus the confidence level for an increase in rainfall. White regions represent values between 0.20 and 0.80, which correspond to 2 x CO₂ mean rainfall that is statistically indistinguishable from CTL mean rainfall. 16
- Figure 7: Using a 1 mm day⁻¹ threshold and for 2 x CO₂ minus or divided by CTL, (leftmost column) the difference in the mean number of wet days; (centre-left) the ratio of the mean number of wet days; (centre-right) the difference in the mean rainfall amount per wet day; (rightmost) the ratio of the mean rainfall amount per wet day. Differences and ratios are taken for (a–d) the May–April year, (e–h) December–February, (i–l) March–May, (m–p) June–August and (q–t) September–November. Regions where fewer than 5% of days in CTL and 2 x CO₂ are above the rainfall threshold are shown in white. 18
- Figure 8: As in Fig. 7 but for a 5 mm day⁻¹ wet-day threshold. 20
- Figure 9: For (left column) 2 x CO₂, (centre) CTL and (right) 2 x CO₂ minus CTL, climatological densities [storms year⁻¹ (106 km²)⁻¹] of (a–c) cyclone tracks, (d–f) genesis locations and (g–i) lysis locations. Cyclones are tracked in all months between October and May. Note that the contour intervals change between each row of panels. 21
- Figure 10: Cumulative distributions of daily rainfall for all land points in Queensland for (a) May–April, (b) December–February, (c) March–May, (d) June–August, (e) September–November using data from (solid black) all years of CTL, (solid red) all years of 2 x CO₂ and (dashed black) years 1–50, 51–100 and 101–150 of CTL. The blue lines show ratios of (solid) 2 x CO₂ to all years of CTL and (dashed) 2 x CO₂ to years 1–50, 51–100 and 101–150 of CTL. 22
- Figure 11: The frequency (events year⁻¹ gridpoint⁻¹) of consecutive days of precipitation exceeding a percentile threshold, using CTL rainfall to compute the percentiles, for (a) CTL for May–April rainfall, (b) 2 x CO₂ divided by CTL for May–April rainfall, (c) CTL for December–February rainfall, (d) 2 x CO₂ divided by CTL for December–February rainfall, (e) CTL for March–May rainfall and (f) 2 x CO₂ divided by CTL. Rainfall percentiles are computed from CTL for the season or year in question using all days with greater than 1 mm accumulation. 25

- Figure 12: For all land gridpoints in Queensland, (a–c) the size distribution of CTL rain events exceeding each percentile of daily rainfall, expressed for each area bin (vertical axis, in 104 km²) as a fraction of all events that exceed the given percentile (horizontal axis) for (a) May–April, (b) December–February and (c) March–May; (d–f) as in (a–c), but for the ratio of the 2 x CO₂ fractions to the CTL fractions. In (d–f), blue colours indicate rainfall event sizes that occur relatively more frequently in 2 x CO₂ than in CTL, while orange colours indicate event sizes that occur relatively less frequently; ratios are not shown for event sizes that occur less than 2% in CTL [equal to the 0.02 fractional frequency in (a–c)]. In all panels, the percentiles of daily rainfall are computed from CTL for the seasonal or annual period shown in the panel. 26
- Figure 13: The mean over all Queensland land gridpoints of (a, b) duration of events (in days) exceeding each daily percentile threshold from CTL and (c, d) size of daily events (in 104 km²) exceeding each percentile threshold from CTL for (black lines) CTL and (red lines) 2 x CO₂ using data from (a, c) DJF and (b, d) MAM. These are the means of the distributions from Fig. 11 for rainfall duration and Fig. 12 for event size. 27
- Figure 14: For the (a, b) wet-season onset date and (c, d) wet-season termination date, (a, c) the mean dates from CTL and (b, d) the differences in the mean dates between 2 x CO₂ and CTL. 29
- Figure 15: Linear regressions (mm mm⁻¹) of monthly rainfall on September–April total rainfall for (left column) SILO, (centre) CTL and (right) 2 x CO₂ for (a–c) November, (d–f) December, (g–i) January, (j–l) February, (m–o) March and (p–r) April. Regression coefficients are shown only where statistically significant at the 5 per cent level. 32
- Figure 16: Probability distribution functions (PDFs) of the coefficient of variation (CoV, unitless) in Queensland area-averaged rainfall for (a) May–April, (b) December–February, (c) March–May, (d) June–August and (e) September–November. Lines show the PDFs for CoVs computed over (solid black) 50 year periods of 2 x CO₂ (100 samples), (dashed purple) 10 year periods within each 50 year block of CTL (40 samples), (dashed red) 10 year periods within the 50 year 2 x CO₂. The vertical lines show the CoV using all years of (black) CTL and (red) 2 x CO₂. 34
- Figure 17: December–February Empirical Orthogonal Teleconnection patterns for (a–d) CTL and (e–h) 2 x CO₂, where the 2 x CO₂ patterns have been constrained to have the same central points as the CTL patterns. The values shown are the correlation coefficients of every point with the central point; stippling indicates correlations that are statistically significant at the 5% level. 36
- Figure 18: Coefficients of linear regression for gridpoint timeseries of DJF-mean (left column) SST (K); (centre, colours) mean-sea-level pressure (hPa) and (vectors) 850 hPa winds (m, s⁻¹); (right, colours) 500 hPa specific humidity (g, kg⁻¹ and (vectors) 500 hPa winds (m, s⁻¹) regressed on the timeseries of (a–c) CTL DJF EOT1; (d–f) 2 x CO₂ DJF EOT2; (g–i) CTL DJF EOT2; (j–l) 2 x CO₂ DJF EOT2; (m–o) CTL DJF EOT3; (p–r) CTL DJF EOT4; and (s–u) 2 x CO₂ DJF EOT4. 38
- Figure 19: For (a, b) CTL DJF EOT4 and (c, d) 2 x CO₂ EOT4, the regression of tropical-cyclone (a, c) track density and (b, d) genesis density on the EOT timeseries. Units are storms season⁻¹ (106 km²)⁻¹ around each gridpoint for a one standard-deviation change in the rainfall EOT timeseries. 40
- Figure 20: As in Fig. 17 but for March–May EOTs. 41
- Figure 21: As in Fig.18 but for MAM seasonal-mean quantities regressed on the timeseries of MAM EOTs. 42
- Figure 22: As in Fig. 17 but for June–August EOTs. 44
- Figure 23: As in Fig.18 but for JJA seasonal-mean quantities regressed on the timeseries of JJA EOTs. 45
- Figure 24: As in Fig. 17 but for September–November EOTs. 47

- Figure 25: As in Fig. 18 but for SON seasonal-mean quantities regressed on the timeseries of SON EOTs. 48
- Figure 26: (a) As in Fig. 25a but for MSLP only; (b) as in Fig. 25d but for MSLP only. 50
- Figure 27: Linear correlations between seasonal-mean Nino 4 SSTs and gridpoint rainfall for (left column) 2 x CO₂ and (right column) CTL in (a, b) December–February, (c, d) March–May, (e, f) June–August and (g, h) September–November. The 2 x CO₂ rainfall and SSTs were detrended prior to computing the correlation. 52

List of Tables

- Table 1: For each HiGEM CTL EOT identified in (Klingaman, 2012a): the corresponding SILO EOT, if any, based on the analysis in (Klingaman, 2012a); the region of Queensland for which the EOT describes rainfall variations; the climate driver of the EOT, as determined in (Klingaman, 2012a); and a summary of the projected changes to that EOT based on the analysis in this report. 36

1 Executive Summary

This report analyses projected changes in Queensland rainfall from the HiGEM global climate model under atmospheric carbon dioxide (CO₂) concentrations of approximately 690 parts per million (ppm), equivalent to the CO₂ concentration in the late 21st century under a moderate (IPCC SRES (2012) A1B) emissions scenario.

HiGEM is a high-resolution version of the U.K. Met Office model (HadGEM1). Previously reported research found that with present-day CO₂, HiGEM accurately simulated many observed climate drivers of Queensland rainfall, including the El Niño Southern Oscillation; this increases our confidence in the model's projections of rainfall change.

The HiGEM model projects that average surface temperatures in Queensland will warm by approximately 2°C under doubled CO₂, with the strongest warming in autumn and winter. Consistent with many other studies, the land warms by more than the ocean, leading to greater warming inland in Queensland and less along the coast.

While HiGEM projects small changes to annual-total rainfall, the November–April wet season becomes compressed: 10–20 per cent more rain falls during January and February, with 10–40 per cent less in November, March and April. The Queensland wet season begins up to 10 days later—particularly along the coast—and ends up to 20 days earlier—particularly in the southwest. Precipitation falls in fewer but much more intense events.

The HiGEM model projects that Queensland will rely more strongly upon heavy mid-summer rains for its annual precipitation. This has important consequences for agriculture and for water storage. The frequency of extreme rain days (greater than 100 millimetre accumulation) in HiGEM increases by up to 40 per cent, particularly in summer during the intensified monsoon. HiGEM also projects that the average duration of extreme rainfall will rise (by 20 per cent) as will the area covered by each event (15 per cent). The number of light rain days (1–5 millimetre) is projected to decrease by 5–10 per cent. Tropical cyclones become slightly less frequent near Queensland.

The HiGEM model projects that many climate drivers of rainfall will remain robust in a warmer world. The correlation with ENSO declines, but there are an inadequate number of ENSO events in the future-climate simulation on which to base firm conclusions. Rainfall variations in southwest and southeast Queensland become less connected to those in the rest of the state, mostly due to an earlier end of the wet season in those regions.

2 Introduction & Objectives

The impacts of anthropogenic climate change on Queensland's rainfall remain highly uncertain. Among the climate-model simulations performed for the Third Coupled Model Intercomparison Project (CMIP3), Suppiah et al. (2007) reported that the spread in Queensland rainfall changes, per degree of global warming, ranged from 20 per cent wetter to 20 per cent drier. Several CMIP3 models showed no change in rainfall.

Moise and Hudson (2008) constructed a weighted ensemble of the CMIP3 models, with greater weight given to those models with low biases in their present-day climates and with convergent responses to climate change. The authors found a bi-model distribution of rainfall changes over tropical Australia, including Queensland, indicating that rainfall increases and decreases were equally likely.

This lack of consistency among models provides little useful information to policymakers making decisions on how best to adapt to climate change.

Further, these techniques assess only the effect of global warming on the mean rainfall, neglecting potential changes in inter-annual and decadal variability. Queensland experiences considerable variability on these temporal scales (e.g. Lough, 1997; Klingaman, 2012a), which have a substantial impact upon the state's agriculture, hydrology and infrastructure. It is therefore critical to consider the potential impact of climate change on rainfall variability as well as on the mean state.

This project has adopted the opposite approach to the model inter-comparison efforts noted above. It has analysed one model in considerable detail, to understand and assess its ability to simulate not only the mean rainfall in Queensland and its variability, but also the climate drivers of that rainfall variability.

The model under consideration is the U.K. High-resolution Global Environment Model (HiGEM), which has considerably finer resolution than most of the models that contributed to CMIP3. This improved resolution may give HiGEM the ability to more reliably simulate regional climate variability and change. Klingaman (2012a) concluded that HiGEM accurately simulated many of the key climate drivers of Queensland's rainfall—identified using observations and the 20th Century Reanalysis (Compo et al., 2011) in Klingaman (2012b)—when the model was run for present-day conditions (i.e. present-day concentrations of greenhouse gases and aerosols).

In this report, the response of Queensland rainfall in HiGEM to a doubling of atmospheric carbon dioxide (CO₂) is assessed. Changes in annual- and seasonal-mean rainfall, inter-annual rainfall variability and the climate drivers thereof, daily rainfall frequency and intensity and daily rainfall extremes are analysed to provide a synthesis of how HiGEM projects Queensland's rainfall to change in a warmer world.

This report seeks to draw together the previously reported research under this project—how the frequency and intensity of Queensland's rainfall vary between wet and dry years (Klingaman, 2012c), the climate drivers of Queensland's rainfall variability in observations and reanalysis data (Klingaman, 2012b), and the assessment of the HiGEM present-day control simulation (Klingaman, 2012a)—to form conclusions on how Queensland's rainfall may change as the world warms.

3 Model, data and methods

3.1 HiGEM simulations

This report analyses the output from three simulations of the HiGEM version 1.1 coupled atmosphere–ocean Global Climate Model (GCM), which are described in the paragraph below. HiGEM is a high-resolution version of the Hadley Centre Global Environmental Model (HadGEM1; Ringer et al. 2006), with an atmospheric horizontal resolution of 1.25° longitude × 0.83° latitude and 38 vertical gridpoints. The oceanic horizontal resolution is 0.33° longitude × 0.33° latitude, with 40 vertical points; the first ocean vertical layer is 10 metres deep. HiGEM was described in Klingaman (2012a). Further details on the model and its ability to simulate global climate can be found in Shaffrey et al. (2009) and Roberts et al. (2009).

The three simulations analysed in this report are:

- (a) the 150 year present-day “control” simulation evaluated by Klingaman (2012a) to determine the ability of HiGEM to simulate the climate drivers of Queensland rainfall;
- (b) a “transient” simulation in which the atmospheric CO₂ concentration is increased by 2 per cent year⁻¹;
- (c) a “fixed” double-CO₂ simulation in which the atmospheric CO₂ concentration is maintained at twice the concentration used in the control simulation.

The fixed simulation is bifurcated from the transient simulation when the atmospheric CO₂ in the transient simulation reaches twice the control value. The control simulation employed a 345 ppm CO₂ concentration, approximately equal to the concentration in 1985 (Shaffrey et al., 2009); the concentration in the fixed simulation is therefore 690 ppm. For reference, the 2090 CO₂ concentration under the Intergovernmental Panel on Climate Change (IPCC) Special Report on Emissions Scenarios (SRES) pathway A1B—a moderate emissions scenario—is approximately 680 ppm. The fixed simulation is not equivalent to the A1B scenario, however, because the concentrations of other anthropogenic and natural forcing agents (e.g. ozone, methane, aerosols) remain equal to the present-day concentrations in the fixed simulation.

It is important to note that the prescribed 2 per cent year⁻¹ CO₂ increase in the transient simulation is twice the commonly used 1 per cent year⁻¹ rate of increase. The higher rate was applied to reduce the computational cost of the transient simulation. The design of these simulations was outside the control of this project. The transient simulation is 70 years long; the atmospheric CO₂ concentration reaches twice the control value after 35 years and four times the control value after 70 years.

The fixed integration (at 690 ppm) is 30 years long. Although the CO₂ concentration is stable throughout this integration, the climate system—particularly the oceans—will still be adjusting to the radiative forcing produced by the increased CO₂. This adjustment may be particularly strong given the accelerated nature of the transient simulation. A longer fixed integration would have provided a greater opportunity for the climate system to come into balance with the additional CO₂, but such an integration was not possible given the computational cost of the high-resolution HiGEM model. Thus, while the CO₂ is stable during this integration, the climate system should not be considered to be in balance.

To provide a longer integration period for a more robust analysis of inter-annual and decadal variability in Queensland climate, 20 years from the 2 per cent transient simulation were concatenated with the 30 year fixed integration. The 20 years of the transient simulation were taken from around the time of CO₂ doubling: years 25–44. For timeseries analysis, years 25–34 of the transient were placed before the fixed simulation, while years 36–44 were placed after the fixed simulation. The mean CO₂ concentration across these years is 1.993 times that in the control—with a range of 1.64 to 2.39 times the control—which is comparable to the fixed simulation. As the fixed simulation is not in

balance, adding years from the transient simulation—which is also not balance, due to the steadily increasing forcing—is unlikely to greatly affect the results. The resulting 50 year integration (hereafter “2 x CO₂”) is highly similar to the 30 year integration in all aspects of Queensland climate that were examined for this report, including all changes in rainfall.

All analysis presented in this report compares the 150 year control simulation (“CTL”) to the 50 year amalgamation of the transient and fixed simulations (“2 x CO₂”). This comparison gives the response of the model to an increase in CO₂ only; as noted above, concentrations of other radiative-forcing agents are identical in CTL and 2 x CO₂. In many cases, in addition to comparing the mean of 2 x CO₂ to the mean of CTL, the mean of 2 x CO₂ is compared to three individual 50 year means of CTL, taken from years 1–50, 51–100 and 101–150. If common signals are found in the differences between 2 x CO₂ and the 50 year means from CTL, this demonstrates the robustness of the difference between 2 x CO₂ and the full CTL integration (i.e., the 50 year 2 x CO₂ period is outside the range of the 50 year periods from CTL).

3.2 SILO rainfall

The SILO gridded rainfall dataset (Jeffrey, 2001) is employed in section 5.2 for analysis of the contributions of each month of the Queensland wet season (November–April) to the wet-season total rainfall. These quantities from SILO are compared against the corresponding quantities from HiGEM CTL and 2 x CO₂. The 5 km SILO monthly mean rainfall data for 1900–2010 were interpolated onto the HiGEM horizontal grid (section 2.1) prior to analysis, using an area-weighted linear interpolation technique.

3.3 EOT Analysis

Empirical Orthogonal Teleconnection (EOT) analysis is applied to the seasonal rainfall from HiGEM 2 x CO₂, to evaluate how doubling the atmospheric CO₂ concentration has affected the seasonal patterns of inter-annual Queensland rainfall variability that Klingaman (2012a) identified in CTL.

EOT analysis produces a set of basis functions that are orthogonal in time through repeated linear correlation analysis, correlating timeseries of seasonal rainfall at gridpoint in Queensland with the Queensland-averaged seasonal rainfall timeseries. Each EOT pattern is described by a “central point”—the point which shows the highest correlation with the average—and the spatial pattern of correlations between each other gridpoint and the central point. Each pattern is removed from the field by linear regression, prior to computing the next EOT pattern using the residual timeseries. Smith (2004), Klingaman (2012a) and Klingaman (2012b) describe the EOT technique in detail.

Straightforward EOT analysis of 2 x CO₂—using the method from Klingaman (2012b)—would not permit a direct comparison of the 2 x CO₂ and CTL patterns. Since EOT patterns are orthogonal in time, each pattern depends upon those computed previously. EOTs from one climate (e.g. the HiGEM CTL climate) are therefore not directly comparable to those from another climate (e.g. HiGEM 2 x CO₂). In other words, straightforward EOT analysis would not permit an understanding of how the CTL EOTs had changed in the 2 x CO₂ climate, as the different mean climate of 2 x CO₂ would result in a set of EOTs that could not be cleanly compared to their CTL counterparts.

While projecting the 2 x CO₂ data onto the CTL EOT patterns would allow an evaluation of how the CTL EOTs had changed—via analysing the timeseries of the projected data—the CTL EOTs no longer form an orthogonal set of basis functions in the 2 x CO₂ climate. Thus, the timeseries of the projections of 2xCO₂ onto two CTL EOTs from the same season would be correlated; untangling the relationships between the projected timeseries would be cumbersome.

Projection is therefore not an effective technique when dealing with two potentially radically different mean climates. February (DJF) rainfall as an example, the central point of CTL DJF EOT1 is

assumed to be the central point of 2 x CO₂ DJF EOT1. The timeseries of 2 x CO₂ DJF EOT1 is then the timeseries of DJF seasonal-mean rainfall in 2 x CO₂ at that central point; the spatial pattern is the correlation of the timeseries of 2 x CO₂ seasonal-mean rainfall at every point against that at the central point. This pattern is then removed at all points by linear regression. The next EOT, 2 x CO₂ DJF EOT2, is then computed by forcing the central point of CTL DJF EOT2; the process is repeated for the first four EOTs. This ensures that (a) the EOTs from 2 x CO₂ are linearly orthogonal in time; (b) the 2 x CO₂ EOTs are more directly comparable to the CTL EOTs, since they use the same central points; and crucially (c) the technique accounts for how climate change may alter the correlations between each CTL central points and the rest of Queensland.

The forced technique cannot, however, account for how climate change may alter the spatial coherence in seasonal Queensland rainfall. The 2 x CO₂ EOTs are also not necessarily the patterns that explain the most variance in 2 x CO₂ rainfall. The object, however, is not to determine such patterns, but to understand how the CTL patterns change as a result of increased CO₂.

3.4 Seasonal and Annual Means

The analysis in this report focuses on changes in seasonal- and annual-mean quantities (e.g. rainfall, temperatures, circulation patterns). To avoid blending two November–April wet seasons in Queensland, the annual mean is defined as May–April. Seasonal means are defined using the normal boundaries: summer (December– February; DJF), autumn (March–May; MAM), winter (June– August; JJA) and spring (September–November; SON). Because Queensland receives nearly 80 per cent of its rainfall in DJF and MAM, this report focuses on the differences between 2 x CO₂ and CTL in those seasons.

4 Projected changes in mean climate

In this section, the 2 x CO₂ annual- and seasonal-mean climates are compared to those from CTL in terms of surface temperature (section 3.1); low-level, 850 hPa circulation (section 3.2) and rainfall (section 3.3). For rainfall, the significance of the mean rainfall changes (section 3.3.2) and the seasonal differences in the daily frequency and intensity of rainfall (section 3.3.3) are also examined. The objective is not to provide a complete description of the mean climate of 2 x CO₂, but to give a brief indication of the impact of doubled CO₂ on several basic thermodynamic fields (temperature and low-level circulation) that are strongly linked to rainfall.

4.1 Surface temperature

In common with many other GCM's, HiGEM shows greater surface warming over the land than the oceans in all seasons in response to increased atmospheric CO₂ (Fig. 1a–d). The Northern Hemisphere warms more than the Southern Hemisphere (not shown). The high latitudes of the Southern Hemisphere show particularly little warming, except along the immediate Antarctic coastline where the temperature changes are driven by the disappearance of sea ice (not shown). The smaller warming in the Southern Hemisphere has frequently been associated with the high heat uptake by the Southern Ocean—driven by the strong, circumpolar westerly jet and the greater fraction of land in the Northern Hemisphere (e.g. Flato and Boer, 2001). Northern Australia warms more than southern Australia and New Zealand, in agreement with the meridional gradient in the zonal mean temperature change in the Southern Hemisphere.

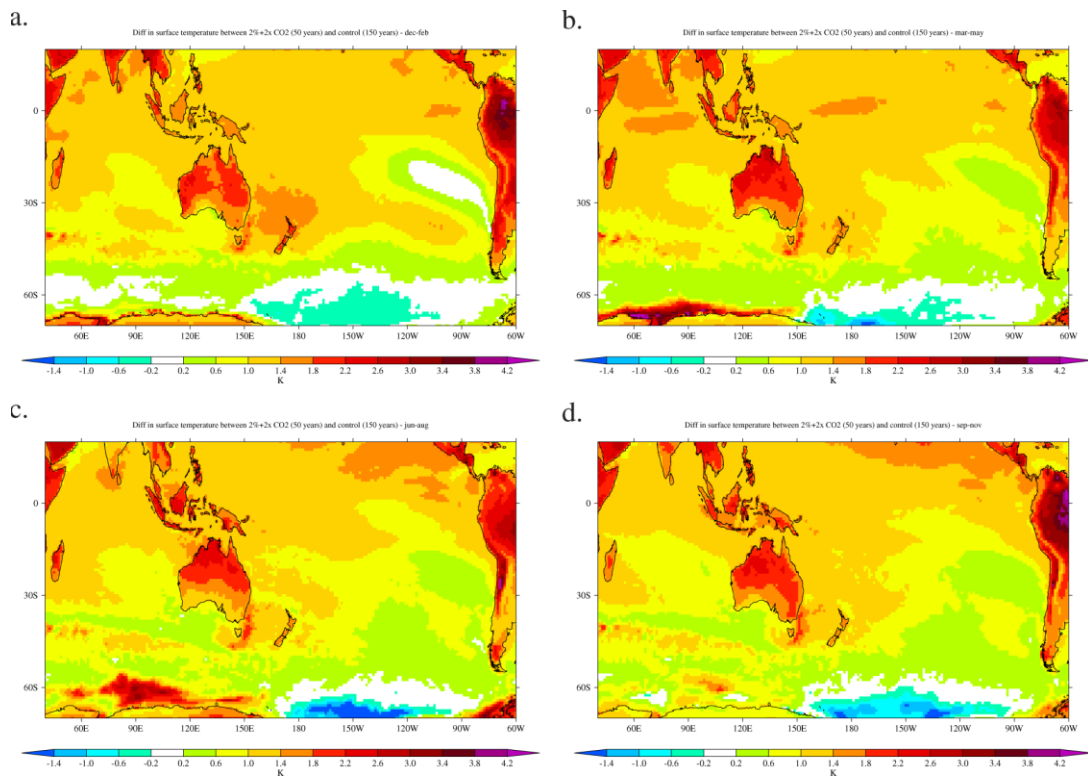


Figure 1: (a–d) The difference in seasonal-mean climatological surface temperature for 2 x CO₂ minus CTL for (a) DJF, (b) MAM, (c) JJA and (d) SON; (e–p) the difference in seasonal-mean climatological surface temperature for 2 x CO₂ minus 50 year periods of CTL, using (e, h, k, n) years 1–50, (f, i, l, o) years 51–100 and (g, j, m, p) years 101–150 for (e–g) DJF, (h–j) MAM, (k–m) JJA and (n–p) SON.

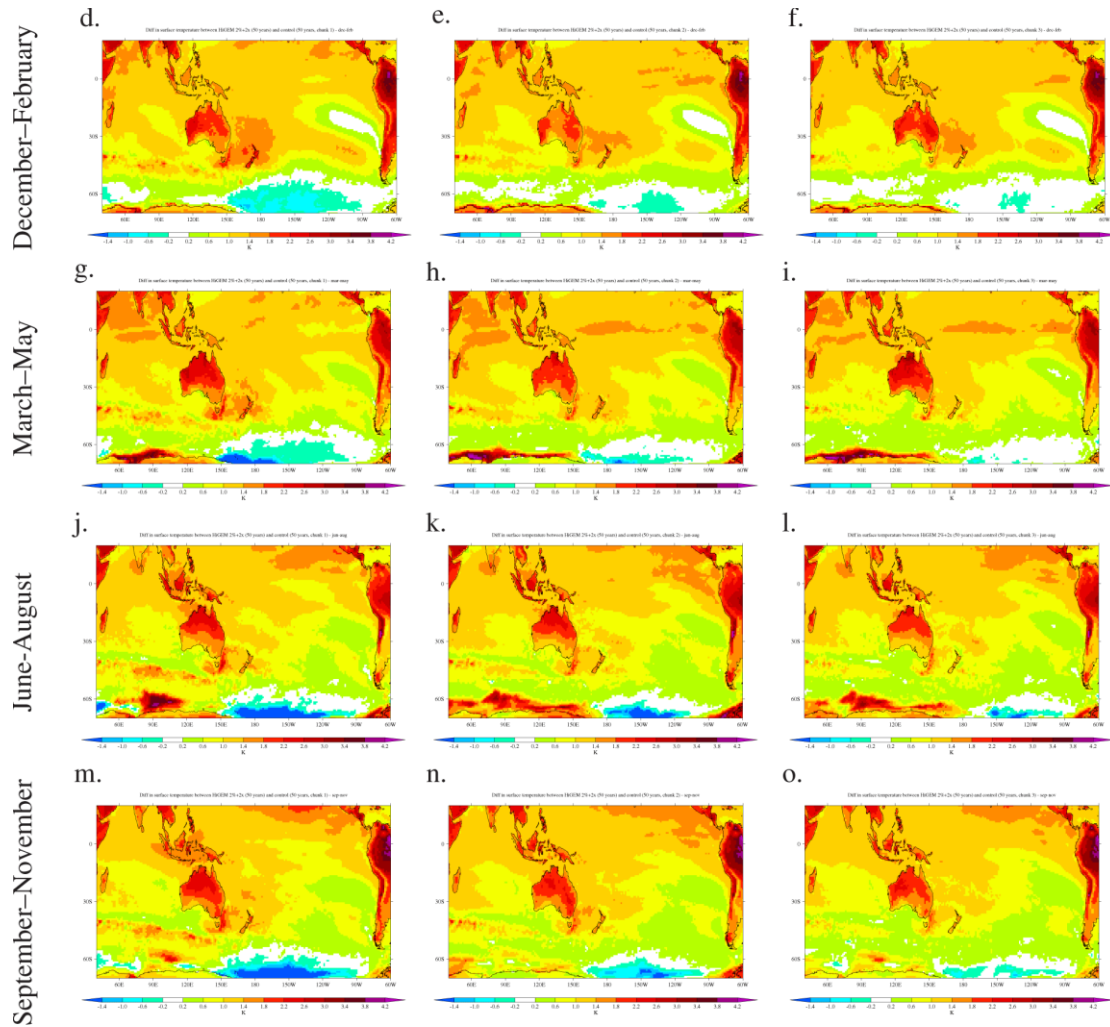


Figure 1: (Continued)

In Queensland, HiGEM produces seasonal-mean warmings of approximately 2°C in autumn (Fig. 1b) and winter (Fig. 1c), with smaller warmings of 1.75°C in spring (Fig. 1d) and in the summer wet season (Fig. 1a). The relatively lower (higher) warming in summer (autumn) is connected to increased (reduced) rainfall in that season, which will be discussed in section 3.3.

Coastal Queensland warms less than inland regions, due to the influence of the relatively cooler oceans. The Cape York Peninsula warms less than the rest of the state. In summer, sea-surface temperatures (SSTs) in the Tasman Sea show a greater warming than any of the other coastal waters (Fig. 1a).

It is unclear whether this increased warming is due to changes in ocean circulation or in surface heat or momentum exchange with the atmosphere. Several previous studies, however, have noted that the East Australian Current is likely to accelerate and penetrate further south in a warmer world (e.g. Cai et al. 2005; Ridgway 2007), which may explain the relatively warmer SSTs in 2 x CO₂. These warmer SSTs off the east coast likely provide an increased source of moisture and energy to the low-level trade easterlies, which then advect that moisture onto the east coast of Queensland. The effect of the locally enhanced SSTs on summer rainfall will be analysed further in section 3.3.

Similarly, a thin front of relatively warmer SSTs exists east of Tasmania in all seasons (Fig. 1a–d). HiGEM is able to simulate such fronts due to its 30 km, “eddy permitting” horizontal resolution in the ocean. (It is important to note, however, that the ability to resolve these features alone does not increase confidence in their existence in a warmer world.) These higher SSTs are associated with

changes to the low-level circulation (section 3.2) and rainfall (section 3.3) over the island. Since HiGEM is a coupled atmosphere–ocean GCM, it is not possible to determine whether the altered SSTs are driving changes in the circulation or the circulation changes are warming the SSTs.

Based on Pacific SSTs alone, HiGEM does not simulate a more “El Niño-like” basic state in response to greenhouse warming (Fig. 1a–d). There is considerable uncertainty in the response of the equatorial Pacific to increased CO₂, with some models simulating a pattern of SST change that resembles El Niño (i.e. a warmer equatorial Pacific relative to the sub-tropics) and others a pattern that resembles La Niña (i.e. a relatively cooler equatorial Pacific; Collins, 2005; Coelho and Goddard, 2009; Collins and others, 2010). Those models that simulate a more El Niño-like mean climate in a warmer world typically also show that the response of tropical rainfall resembles the El Niño teleconnection pattern. For example, much of Australia would be drier in such a model than in one that simulated an equitable Pacific warming or a La Niña-like SST pattern. HiGEM simulates relatively similar warming across the equatorial Pacific in all seasons; the mean state resembles neither El Niño nor La Niña (Fig. 1a–d).

To examine the effects of the smaller sample size of years in 2 x CO₂ (50) than in CTL (150), the seasonal mean climatological surface temperatures from 2 x CO₂ were compared those from three 50 year periods of CTL, as discussed in section 2.1. The seasonal surface-temperature changes between 2 x CO₂ and each 50 year CTL period are highly similar to each other and to the change with respect to the full 150 year CTL integration (Fig. 1e–p). For example, in summer the Tasman Sea is warmer than the surrounding waters regardless of the baseline 50 year CTL period used chosen (Fig. 1e–g). This indicates that the differences shown in Fig. 1a–d are robust; they are not due to the averaging of disparate 50 year periods from CTL.

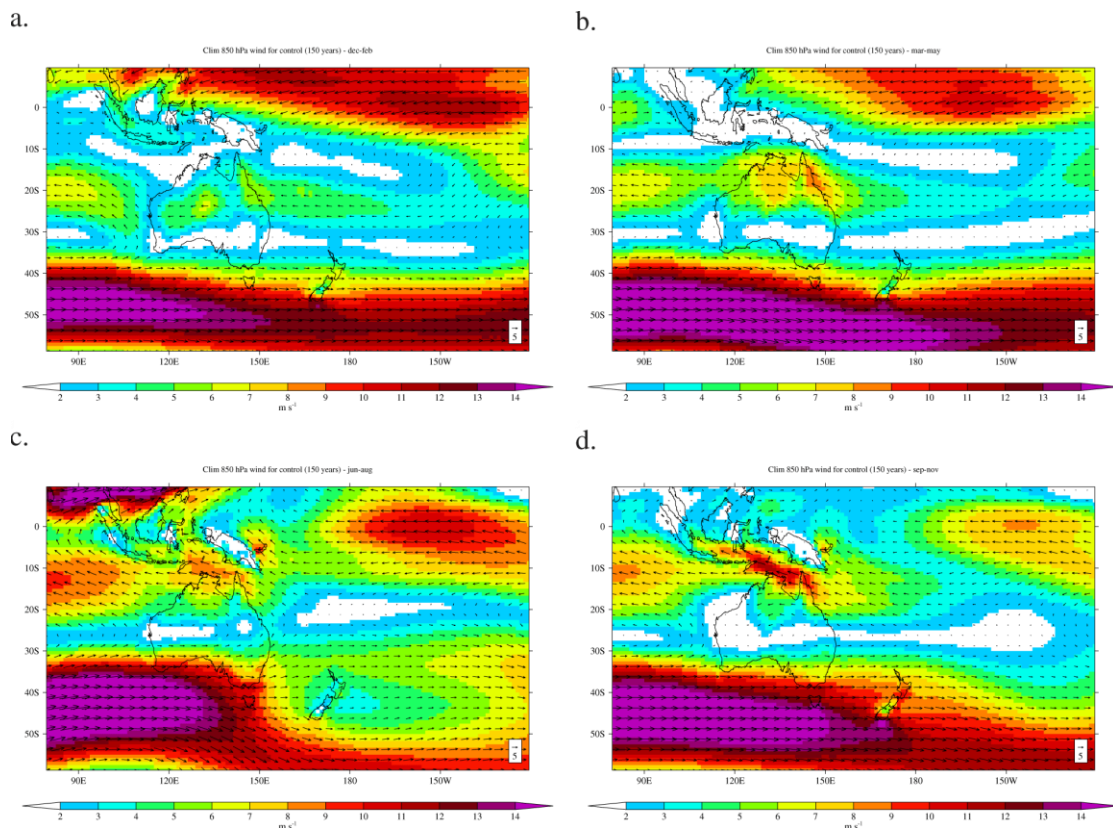


Figure 2: CTL Seasonal-mean climatological (vectors) 850 hPa wind direction and (colours) 850 hPa wind speed from CTL for (a) DJF, (b) MAM, (c) JJA and (d) SON

4.2 850 hPa circulation

In DJF, CTL simulates weak 850 hPa mean easterlies across much of the monsoon region of Australia (Fig. 2a), where weak westerlies exist in the European Centre for Medium Range Weather Forecasting 40-year reanalysis (ERA-40; Uppala et al. 2005) (not shown). This suggests that the CTL monsoon circulation is weaker than observed, which is consistent with the mean DJF dry bias and late monsoon onset in CTL found in Klingaman (2012a). The mean flow across much of Queensland in DJF is easterly, however, in both CTL and ERA-40, bringing moist oceanic air onshore.

In response to a doubling of atmospheric CO₂, HiGEM simulates an enhanced low-level summer monsoon circulation (Fig. 3a) relative to CTL. Anomalous westerly and northwesterly winds in DJF extend across the Maritime Continent and the north of Australia. The westerly anomalies in 2 x CO₂ act to reduce the mean easterlies in CTL, resulting in a slackening of the wind speed; the mean flow in 2 x CO₂ remains easterly (not shown). Still, the change in the 850 hPa circulation represents a stronger westerly summer monsoon circulation in 2 x CO₂ relative to CTL, which is associated with an increase in precipitation across northern Australia (section 3.3). The enhanced monsoon may result from the stronger land–sea temperature contrast in 2 x CO₂, due to the greater warming of the Australian continent relative to the surrounding oceans (Fig. 1a).

Weak westerly anomalies in MAM in 2 x CO₂ (Fig. 3b) have little effect on the mean easterlies in CTL (Fig. 2b). The onshore easterly flow to southeastern coastal Queensland increases slightly, strengthening the flow of moist oceanic air to that region. Overall, however, the autumn circulation over Queensland is little changed in 2 x CO₂. There is strong anomalous divergence over the Maritime Continent, however, possibly associated with a reduction in convective activity there. In JJA (Fig. 3c) and SON (Fig. 3d), the effect of 2 x CO₂ is to increase the easterly, onshore inflow of air in CTL (Figs. 2c and 2d) from the Pacific across Queensland. This effect is stronger in the north (south) of the state in JJA (SON).

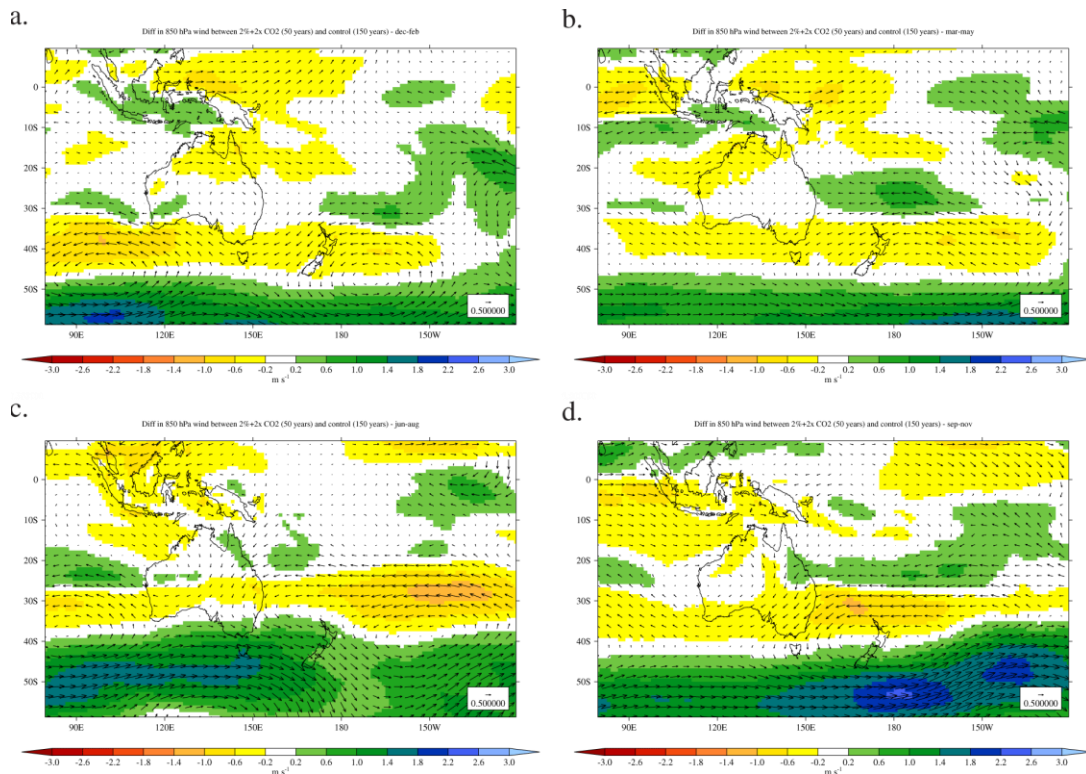


Figure 3: As in Fig. 1, but for the change in (vectors) 850 hPa wind direction and (colours) 850 hPa wind speed.

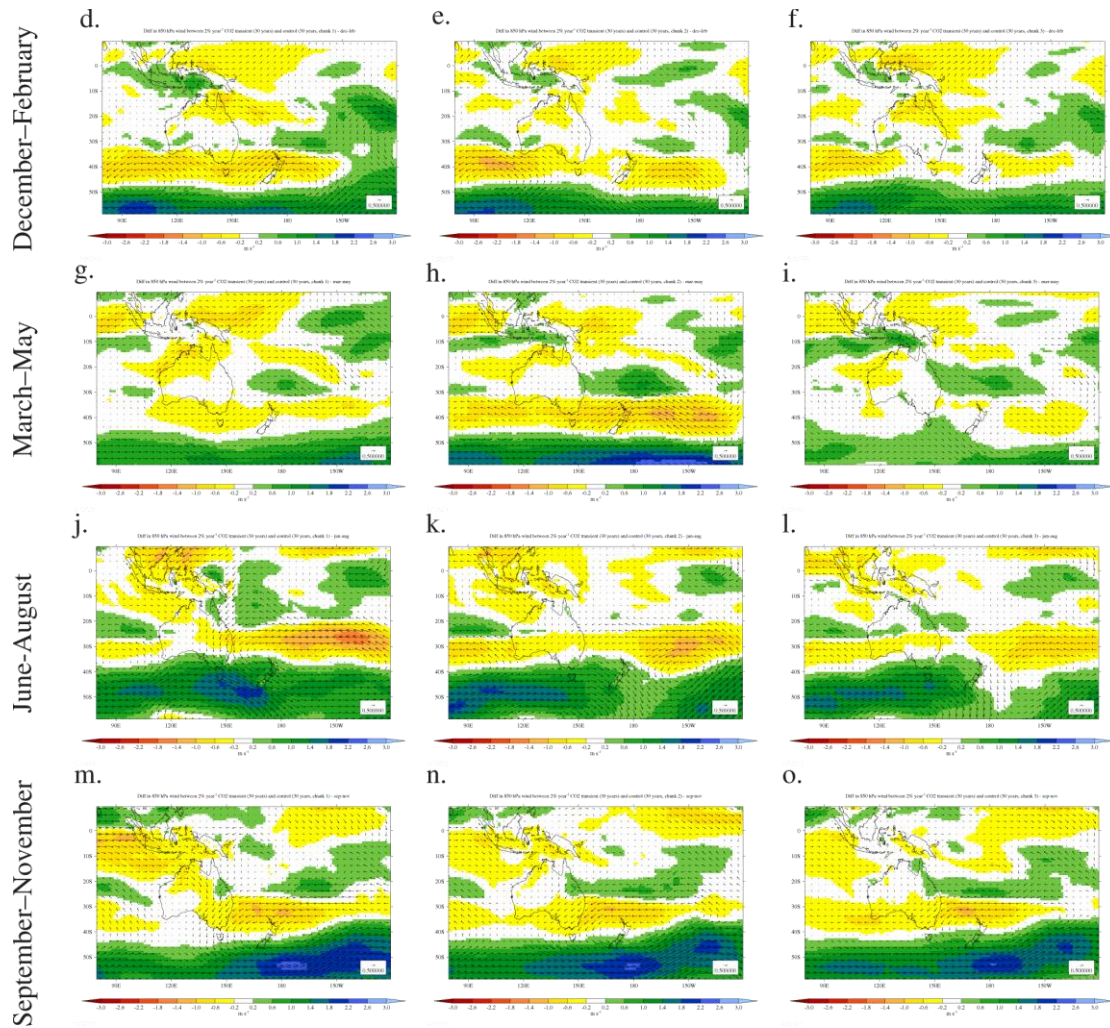


Figure 3: (continued)

The stronger easterlies across Queensland in JJA and SON are part of the zonal-mean easterly response to increased CO₂ in the subtropics, which is in turn associated with a poleward contraction of the Southern Ocean storm track. HiGEM simulates a southward shift of the Southern Ocean jet in all seasons in 2 x CO₂ (Figs. 3a–d), with westerly anomalies on the poleward side of the CTL jet and easterly anomalies on the equatorward side (Figs. 2a–d). These anomalies correspond to an acceleration of the jet near Antarctica and a deceleration near Australia; the response therefore resembles the positive phase of the Southern Annular Mode. Many other GCMs have simulated a poleward shift in the Southern Ocean storm track due to increased CO₂ and Antarctic stratospheric ozone depletion (Yin, 2005; Arblaster and Meehl, 2006; Cai and Cowan, 2007). As stratospheric ozone recovers during the 21st century, the position of the Southern Ocean storm track will be determined by the relative effects of ozone recovery—shifting the jet equatorward, towards Australia—and further CO₂ emissions—shifting the jet poleward (McLandsres et al. 2011; Polvani et al. 2011). It is important to note that ozone is held fixed at 1985 values in the HiGEM CTL and 2 x CO₂ simulations. Therefore, the response of the Southern Ocean jet in 2 x CO₂ is purely the response to increased CO₂, not to any changes in ozone.

As for surface temperature, the robustness of the 850 hPa circulation results was tested by comparing 2 x CO₂ to three 50 year means of CTL (Figs. 3e–p). Although the magnitudes of the 2 x CO₂ signals vary depending on the 50 year CTL period employed as the baseline, the general features noted above are present for all three baselines: a stronger westerly monsoon circulation in DJF (Figs. 3e–g), smaller westerly anomalies in MAM (Figs. 3h–j), increased onshore easterly flow in JJA (Figs. 3k–m) and SON (Figs. 3n–p) and a poleward contraction of the Southern Ocean westerly jet in all seasons.

4.3 Rainfall

4.3.1 Mean rainfall

Annual-mean Queensland rainfall changes little in 2 x CO₂ (Fig. 4a), with increases of 3–10 per cent in the northwestern and southeastern portions of the state and small decreases along the north eastern coast and in Cape York (Fig. 5a). The small annual-mean change, however, results from the compensation of two much larger seasonal changes: December–February rainfall increases by 12–60 mm (5–18 per cent) across the entire state (Figs. 4b and 5b), while autumn rainfall decreases by 12–60 mm (5–35 per cent) throughout Queensland (Fig. 4c and 5c). The amount of dry-season—winter and spring—rainfall shows little change (Figs. 4d and 4e), although in SON HiGEM projects a 5–45 per cent decrease in rainfall that is associated with a later onset of the November–April wet season (Fig. 5e). Changes in the length of the wet season are analysed in section 5. The following paragraphs discuss the DJF and MAM rainfall changes in greater detail.

Doubling atmospheric CO₂ in HiGEM accelerates the summer monsoon across northern Australia. Fig. 3a shows anomalous westerly and north westerly winds at 850 hPa throughout the monsoon region; Figs. 4b and 5b demonstrate that this enhanced circulation is associated with increased DJF rainfall. Precipitation increases by 5–18 per cent throughout northern Australia, including in Queensland, with localised changes of 18–33 per cent in central Australia near the present-day southern edge of the monsoon trough. These larger increases suggest that “marginal” monsoon regions in CTL—those that only occasionally lie within the monsoon trough—may be within the monsoon belt much more frequently in 2 x CO₂, as the monsoon belt extends south and intensifies.

The pattern of drying in MAM is highly similar to the pattern of increased rainfall in DJF. Rainfall decreases throughout northern Australia, including in Queensland. Coastal regions show the largest changes in rainfall amount, with some drying by more than 100 mm season⁻¹. As in DJF, the largest percentage changes occur along the southern edge of the monsoon trough in CTL, resulting in south western Queensland receiving only 60 per cent of the CTL average rainfall in 2 x CO₂. South eastern Queensland is also affected disproportionately to the rest of the state, with 15–25 per cent reductions in spring rainfall. Since the monsoon retreats from south to north, the spatial pattern of changes suggests that the monsoon withdraws more quickly in 2 x CO₂ than in CTL, leaving regions along the southern edge of the trough much drier in MAM. Differences in the onset and termination of the wet season between 2 x CO₂ and CTL will be discussed in section 5.

Although southern and western Australia are not a focus of this report, it is worth noting that rainfall declines in these regions in all seasons in 2 x CO₂. South Western Australia is most affected, drying by approximately 20 per cent in the annual mean (Fig. 5a); rainfall across Western Australia is reduced by 3–20 per cent, with the greatest changes along the coast. The southern coast of Australia, including much of Victoria, shows a 3–15 per cent drop in rainfall. The largest changes in rainfall amount occur during the winter wet season (Fig. 4d), particularly in southwestern Australia. These changes are consistent with the poleward shifts in the Southern Ocean storm track and the subtropical dry zone discussed in section 3.2 and shown in Fig. 3.

There are 10–20 per cent increases in annual rainfall to the south and east in Tasmania (Fig. 5a), which are driven mainly by wetter winters (Fig. 5d). This local increase is co-located with the “front” of relatively warm SSTs in 2 x CO₂ (section 3.1) which is also strongest in JJA (Fig. 1c). There also appears to be anomalous 850 hPa convergence over this region in JJA (Fig. 3c) in 2 x CO₂, which is a region of net divergence in CTL (Fig. 2c) due to a sharp south eastward shift in the extra-tropical storm track. The enhanced westerlies and anomalous convergence east of Tasmania in 2 x CO₂ may indicate a eastward extension of the storm track beyond the island and towards New Zealand. Aside from noting the co-location of anomalously warm SSTs, low-level convergence and increased rainfall, however, this report does not consider further the local maximum in rainfall east of Tasmania and in the Tasman Sea.

4.3.2 Significance of mean rainfall changes

As for surface temperatures and 850 hPa winds, the robustness of the changes in rainfall found for 2 x CO₂ against the complete CTL integration are assessed by comparing 2 x CO₂ to individual 50 year periods of CTL (Fig. 5f–t). The results of this comparison are shown for only the ratios of rainfall. For the annual-mean, Queensland in 2 x CO₂ is wetter than the first 50 years of CTL (Fig. 5f), but shows only small changes against the second and third 50 year periods (Figs. 5g and 5h). Ratio of summer (Fig. 5i–k) and autumn (Fig. 5l–n) rainfall are similar regardless of the 50 year CTL period chosen; all three periods agree with the patterns found when using the complete CTL integration (Figs. 5b and 5c). The effect of 2 x CO₂ on winter rainfall is highly variable, but climatological winter rainfall is extremely low and so small changes in the total amount will cause large percentage changes, as shown in Fig. 5o–q). Changes in SON precipitation in 2 x CO₂ are small when compared to the first 50 years of CTL (Fig. 5r), but Queensland dries considerably in 2 x CO₂ when ratios are taken against the second and third 50-year periods of CTL (Figs. 5s and 5t).

As a further test of the statistical significance of the sign of the rainfall changes between 2 x CO₂ and CTL, the difference in climatological rainfall is computed between 2 x CO₂ and every period of 50 consecutive years from CTL. For the 150 year CTL integration, there are 100 periods of 50 years; the analysis therefore produces 100 values of the rainfall difference between 2 x CO₂ and CTL as where D_n is the n th difference between 2 x CO₂ and CTL, R_{2xCO_2} is the rainfall from 2 x CO₂ and R_{CTL} is the rainfall from CTL; n ranges from 1 to 100. This is comparable to Monte Carlo or bootstrap resampling of CTL, except that instead of randomly choosing 50 years from CTL, the 50 year periods are constrained to be consecutive years. Fig. 6 shows, for each gridpoint, the fraction of values of D that are negative (i.e., the fraction of 50 year periods of CTL in which the rainfall is greater than the rainfall in 2 x CO₂). Where 2 x CO₂ is drier than CTL, this is effectively the confidence that the difference between 2 x CO₂ and CTL is less than zero. Where 2 x CO₂ is wetter than CTL, this is effectively unity minus the confidence that the difference between 2 x CO₂ and CTL is greater than zero. Therefore, the drying in southwestern 2 x CO₂ in the annual-mean is significant at the 1% level (99 per cent confidence; Fig. 6a).

$$D_n = \frac{\sum_{i=1}^{50} (R_{2xCO_2}^i)}{50} - \frac{\sum_{i=n}^{n+50} (R_{CTL}^i)}{50} \quad (1)$$

By this measure, there is no significant change in the annual-mean rainfall (Fig. 6a), consistent with the variability in the signals obtained from the three CTL baseline periods (Fig. 5f–h). This does not mean that the 2 x CO₂ result is unreliable, but that the rainfall in 2 x CO₂ is not significantly different from that CTL. The 2 x CO₂ rainfall in DJF (Fig. 6b) and MAM (Fig. 6) is significantly different from CTL at 5 per cent or higher in northern, western and southern Queensland; the signals along the eastern coastline are less reliable. The 2 x CO₂ rainfall for winter is indistinguishable from CTL (Fig. 6d), but there was little change in winter rainfall (Fig. 4d). The drying in SON in coastal Queensland in 2 x CO₂ is statistically significant at 1 per cent (Fig. 6e). The 2 x CO₂ rainfall changes against the complete CTL integration are therefore statistically robust for summer, autumn and spring: summer rainfall increases, while autumn and spring become drier. This suggests a compression of the wet season into DJF in 2 x CO₂, which will be discussed further in section 5.

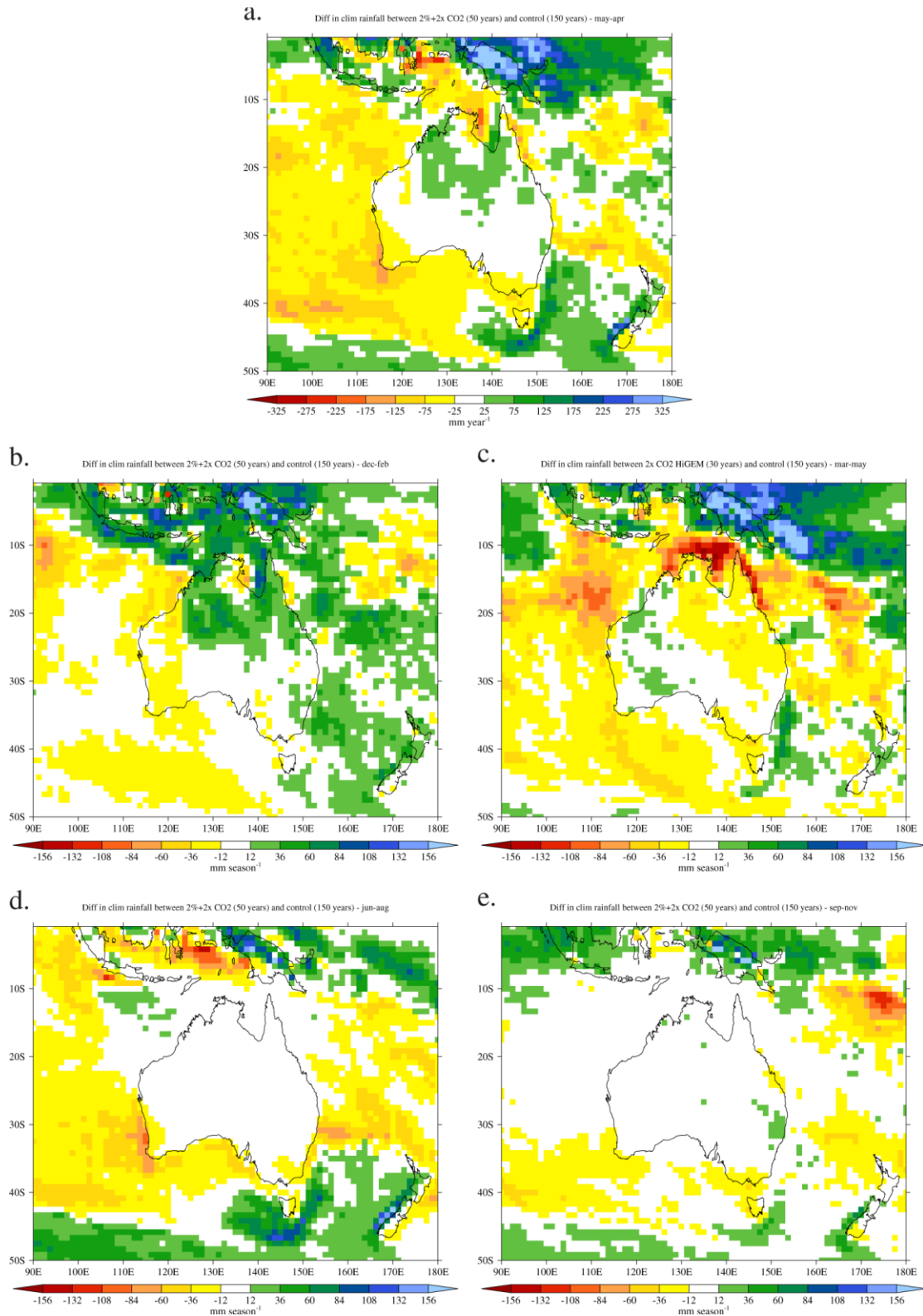


Figure 4: The difference (2xCO₂ minus CTL) in climatological rainfall for (a) May–April (mm year⁻¹), (b) December–February (mm season⁻¹), (c) March–May (mm season⁻¹), (d) June–August (mm season⁻¹) and (e) September–November (mm season⁻¹). The mean of all 150 years of CTL were used as the baseline against which 2 x CO₂ was compared. The contour interval for (a) is 50 mm year⁻¹, while for (b–e) it is 24 mm season⁻¹.

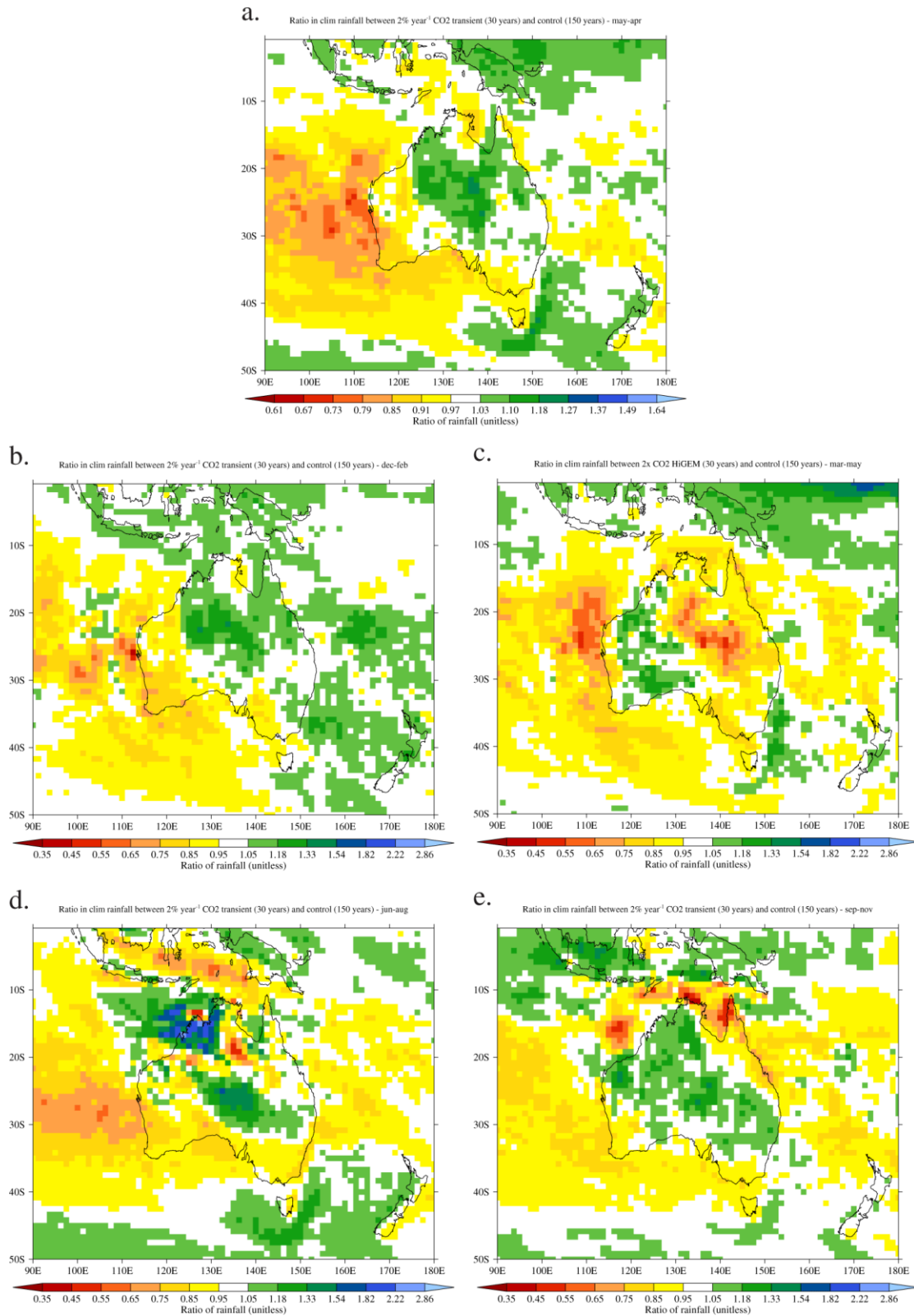


Figure 5: As in Fig. 3, but for ratios of rainfall (2 x CO₂ divided by CTL) for (a, f–h) May–April, (b, i–k) December–February, (c, l–n) March–May, (d, o–q) June–August and (e, r–t) September–November.

Projected changes in Queensland rainfall under double-CO₂ conditions in the HiGEM model

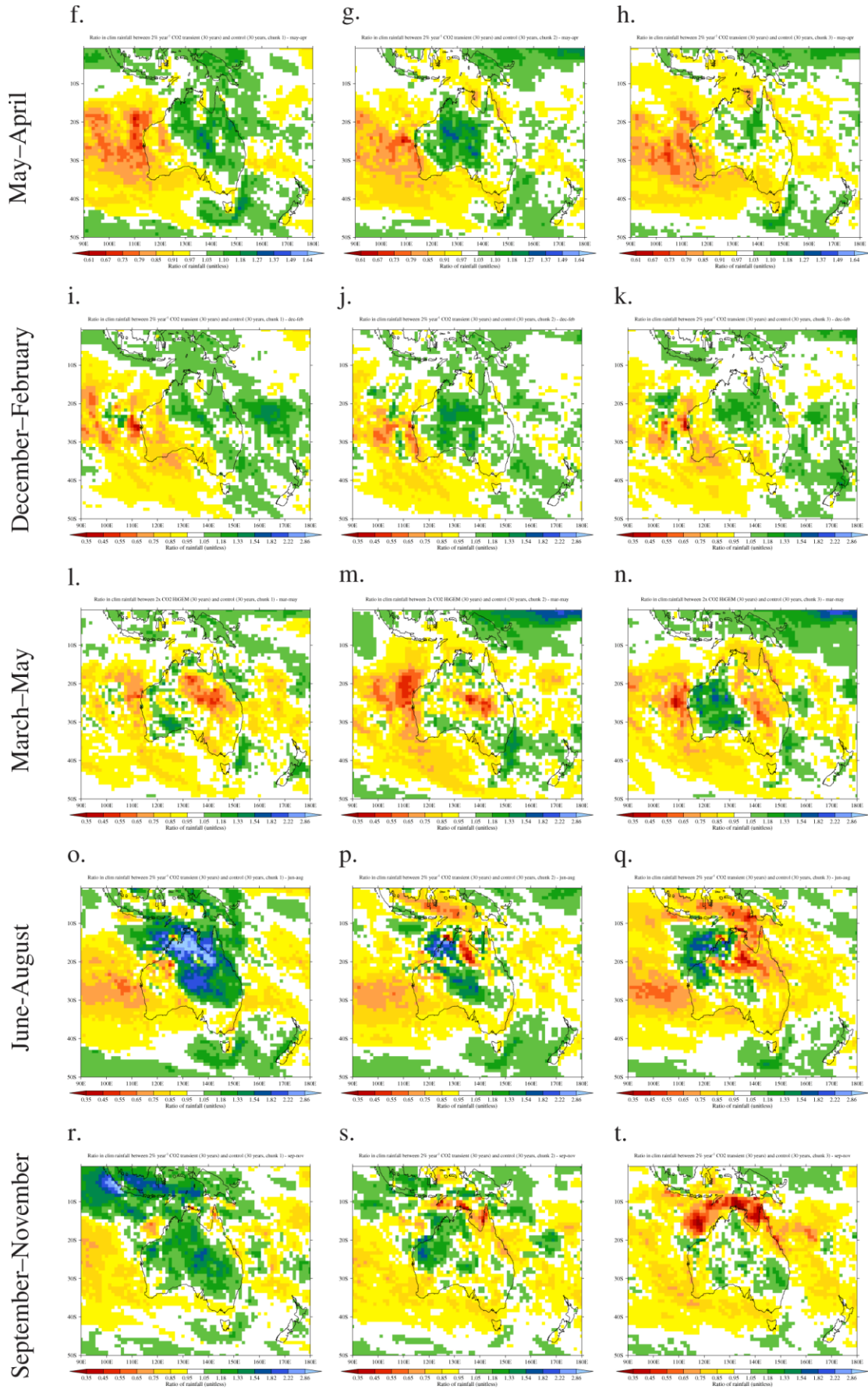


Figure 5: (continued)

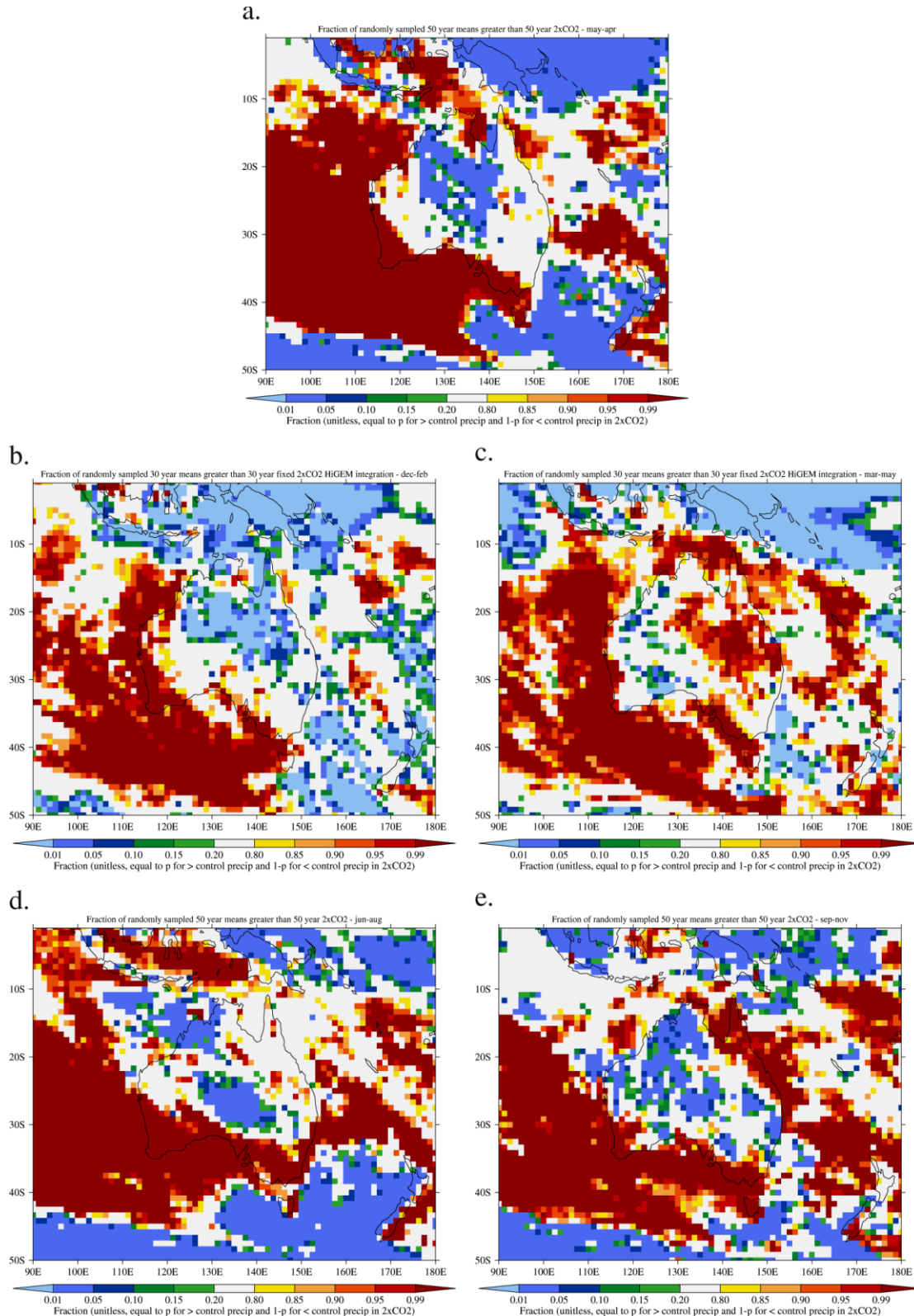


Figure 6: The fraction of 50-year periods in CTL with mean rainfall less than the mean rainfall in 2 x CO₂ for (a) the May–April annual-mean and seasonal means of (b) December–February, (c) March–May, (d) June–August and (e) September–November. The quantity shown is effectively the confidence level for a drying, or unity minus the confidence level for an increase in rainfall. White regions represent values between 0.20 and 0.80, which correspond to 2 x CO₂ mean rainfall that is statistically indistinguishable from CTL mean rainfall.

4.3.3 Frequency and intensity of daily rainfall

This section analyses the differences in the frequency and intensity of daily rainfall between 2 x CO₂ and CTL. Two thresholds for daily rainfall are used: 1 mm day⁻¹ and 5 mm day⁻¹. The former threshold represents changes in nearly all wet days, while the latter represents changes in moderate and heavy rainfall. Thresholds higher than 5 mm day⁻¹ are not applied here for brevity; the projected influence of climate change on daily rainfall extremes is presented in section 4. Changes in rainfall frequency and intensity are presented both as differences and ratios between 2 x CO₂ and CTL, to highlight regions of both large absolute changes and large changes relative to climatological values.

When atmospheric CO₂ is doubled, HiGEM projects a slight decrease in days with more than 1 mm day⁻¹ of rain in coastal Queensland: there are 2–6 fewer wet days annually along the eastern coast, with 6–10 fewer wet days in Cape York (Fig. 7a), representing a 4–10 per cent reduction in rainfall frequency (Fig. 7b). Nearly all Australian coastal regions experience a decline in the number of wet days in 2 x CO₂, particularly the southern coast. The mean daily rainfall intensity—the average amount of rain on each wet day—increases throughout Queensland by 0.4–1.5 mm day⁻¹ (Fig. 7c) or 4–16 per cent (Fig. 7d). The heavier rain on each wet day compensates for the reduced frequency of rainfall, producing little change in the total annual rainfall (Fig. 4a).

Despite an overall increase in DJF rainfall in 2 x CO₂ (Fig. 4b), there are 1–3 fewer wet days per summer in much of Queensland, particularly along the eastern coast and in Cape York (Fig. 7e), representing approximately a 5 per cent decrease (Fig. 7f). The mean intensity of summer rainfall is considerably greater in 2 x CO₂ than in CTL: the intensity increases by 5–30 per cent overall and by 15–30 per cent in the southeast. Wetter summers in 2 x CO₂ are therefore driven by much heavier rainfall on slightly fewer wet days, especially in southeastern Queensland.

By contrast, the drier autumns in 2 x CO₂ (Fig. 4c) are mainly due to a considerable decline in the number of rainy days: on average there are 2–4 fewer wet days season⁻¹ along the eastern coast and 3–5 fewer wet days in Cape York (Fig. 7i), equal to a 10–20 per cent reduction (Fig. 7j). Across inland Queensland the decreases are smaller—one or two fewer days per season—but the number of wet days is still 4–12 per cent less than in CTL. The intensity of autumn rainfall is slightly higher in 2 x CO₂ than CTL (Figs. 7k and 7l), but the increase is far less than for DJF and is evidently not enough to counteract the decline in rainfall frequency.

Changes in the frequency and intensity of wet days during the winter dry season are small (Figs. 7m–p), consistent with the small (Fig. 4d) and insignificant (Fig. 6d) changes in JJA rainfall in 2 x CO₂. The spring drying in 2 x CO₂ is caused by coincident slight decreases in the number of wet days (Figs. 7q and 7r) and their intensity (Fig. 7s and 7t). There are one or two fewer wet days season⁻¹ in 2 x CO₂ in SON.

Unlike in Queensland, the drying in southwestern and southeastern Australia is driven entirely by reductions in wet-day frequency (Fig. 7a): in southwestern (southeastern) Australia, the number of rainy days year⁻¹ declines by up to 20 per cent (12 per cent (Fig. 7b)). There is little change in mean daily precipitation intensity in these regions (Figs. 7c and 7d).

When the wet-day threshold is increased to 5 mm day⁻¹ across Queensland the magnitude of the differences in mean wet-day frequency decrease, while the changes in mean wet-day rainfall amount intensify considerably (Fig. 8). This suggests that the declines in wet-day frequency when using a 1 mm day⁻¹ threshold (Fig. 7) are primarily due to a reduction in the number of very light rain days—between 1 mm day⁻¹ and 5 mm day⁻¹. This effect is most apparent in summer: while the total number of DJF wet days declines in 2 x CO₂ (Fig. 7e), the number of wet days with more than 5 mm of rain remains steady (Fig. 8e).

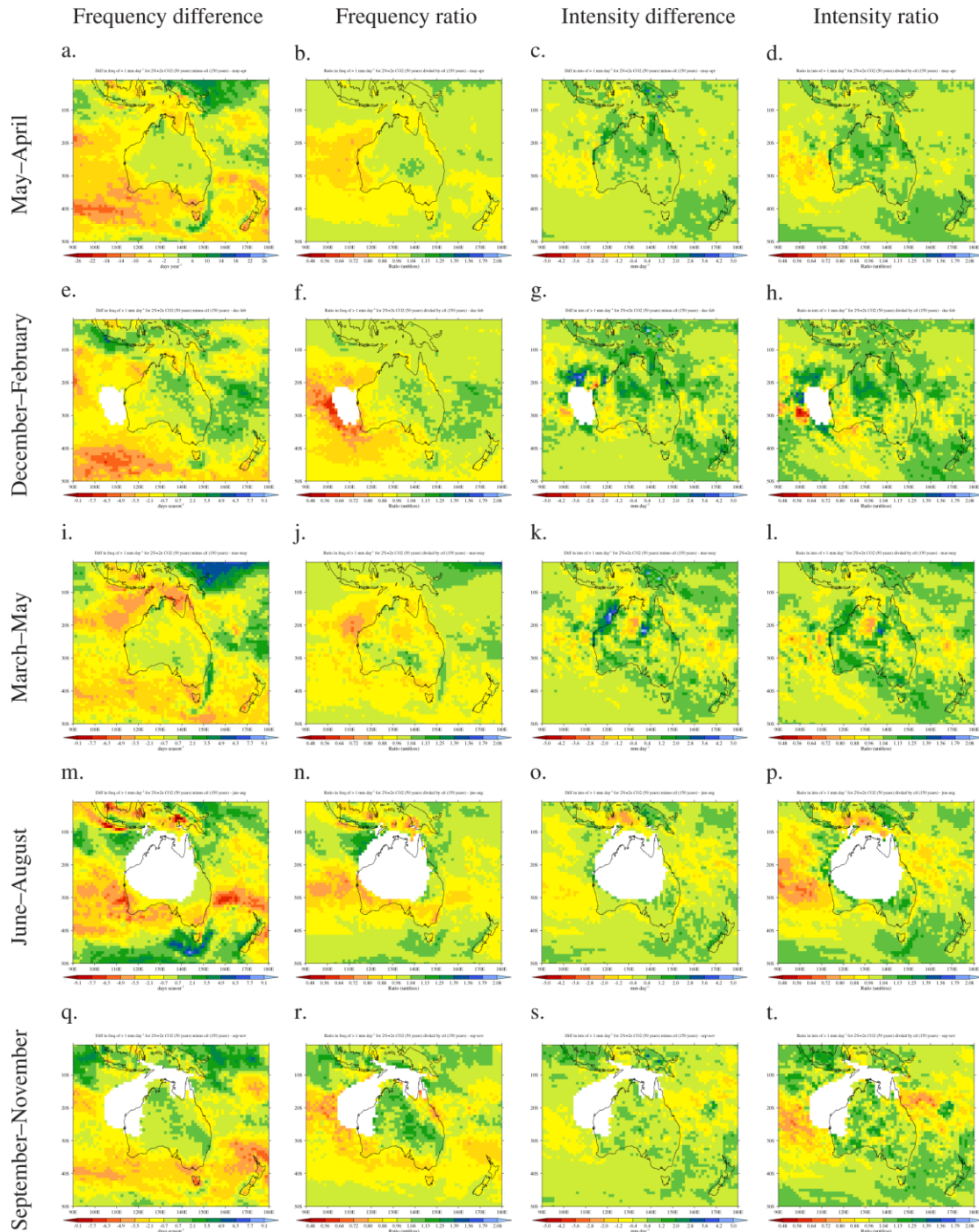


Figure 7: Using a 1 mm day⁻¹ threshold and for 2 x CO₂ minus or divided by CTL, (leftmost column) the difference in the mean number of wet days; (centre-left) the ratio of the mean number of wet days; (centre-right) the difference in the mean rainfall amount per wet day; (rightmost) the ratio of the mean rainfall amount per wet day. Differences and ratios are taken for (a–d) the May–April year, (e–h) December–February, (i–l) March–May, (m–p) June–August and (q–t) September–November. Regions where fewer than 5% of days in CTL and 2 x CO₂ are above the rainfall threshold are shown in white.

For the year (May–April) as a whole, HiGEM projects little change in the number of days with 5 mm of rain or more (Fig. 8a and 8b). The mean amount of rain on these days, however, increases by 4–25 per cent; this intensification of rainfall is strongest in southeastern Queensland, where the mean amount rises by 13–25 per cent. These increases are dominated by DJF (Figs. 8g and 8h) and MAM (Figs. 8k and 8l) which show similar rises in mean rainfall amount, despite DJF becoming wetter overall and MAM becoming drier.

The controlling influence on the mean rainfall changes in 2 x CO₂ between DJF and MAM, then, appears to be the number of wet days, particularly those more than 5 mm of rainfall. DJF becomes wetter overall because HiGEM projects little change in the frequency of wet days above 5 mm accumulation (Fig. 8e). MAM becomes drier overall because HiGEM projects a 10–20 per cent reduction in the frequency of these wet days. The mean accumulation on all wet days (Figs. 7h and 7l) and those with more than 5 mm accumulation (Figs. 7h and 8l) increases by similar amounts in both seasons, so rainfall frequency must be the controlling factor. This result agrees with the conclusions of Klingaman (2012c), which used the SILO gridded rainfall dataset to determine that total rainfall in Queensland was much more sensitive to the frequency of rainfall—particularly heavy rainfall—than to the mean intensity of rainfall.

4.4 Tropical cyclones

Although tropical cyclones have not been a focus of this analysis, the potentially large impact of changes in their frequency, intensity and tracks warrants at least a cursory analysis of their behaviour in 2 x CO₂. Klingaman (2012a) found that CTL represented well the spatial distribution of tropical cyclones in terms of genesis locations and tracks, but that the number of cyclones in the Southwest Pacific was much larger than in observations. It was not known whether this bias was due to HiGEM producing too many cyclones, to the tracking method erroneously detecting many weak disturbances as cyclones, or to some combination of the two effects.

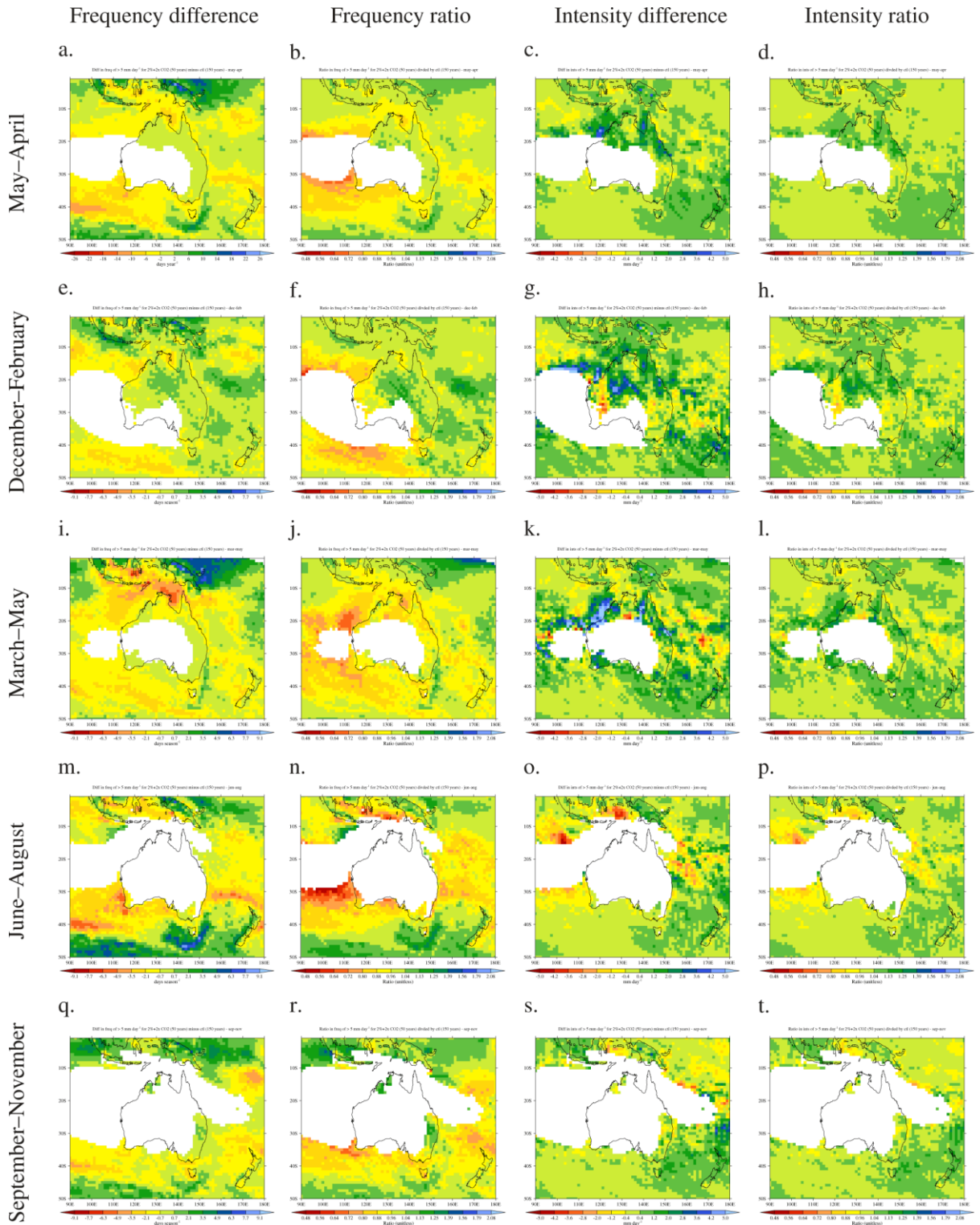


Figure 8: As in Fig. 7 but for a 5 mm day⁻¹ wet-day threshold

5 Projected changes in rainfall extremes

This section examines projected changes from HiGEM in the frequency—or return period—of intense rainfall in Queensland under 2 x CO₂ (section 4.1), as well as in the number of consecutive days of rainfall and the size of rainfall events (section 4.2). Differences in event duration and size are analysed for DJF and MAM only, as section 3.3 showed much smaller variations in JJA and SON rainfall between 2 x CO₂ and CTL.

5.1 Daily extremes

To determine how HiGEM projects the frequency of daily rainfall accumulations to change under doubled atmospheric CO₂, cumulative distribution functions (CDFs) of daily precipitation are constructed for Queensland (Fig. 10). All land gridpoints in 10–30°S and 138–154°E—approximately the State of Queensland—were included in the CDF's. No spatial averaging was performed; instead, the statistics were accumulated across the selected gridpoints. All days, including those with zero rainfall, were considered. The CDF value for 99, therefore, is the 1-in-100 day rainfall. It is important to note that accumulating the statistics of rainfall does not accumulate the probability; the CDF's do not represent the probability of a given rain rate occurring at any location in Queensland on any given day. Rather, the CDF's are effectively constructed for an indicative (but artificial) gridpoint that represents the average for the state.

The analysis was performed for 2 x CO₂, all 150 years of CTL and the three individual 50 year periods of CTL (section 2.1). The probability of having any rainfall can be determined from the lowest value on the probability curves in Fig. 10 [e.g. the probability of rainfall is 18 per cent (100 minus 82) in CTL when considering all seasons (the black curve in Fig. 10a)]. The ratios of the probability of a given daily rain accumulation between 2 x CO₂ and all 150 years of CTL are shown as solid blue curves in Fig. 10, which use the right-hand vertical axis; the ratios of 2 x CO₂ to each 50 year period of CTL are given by the dashed blue curves, again on the right-hand vertical axis.

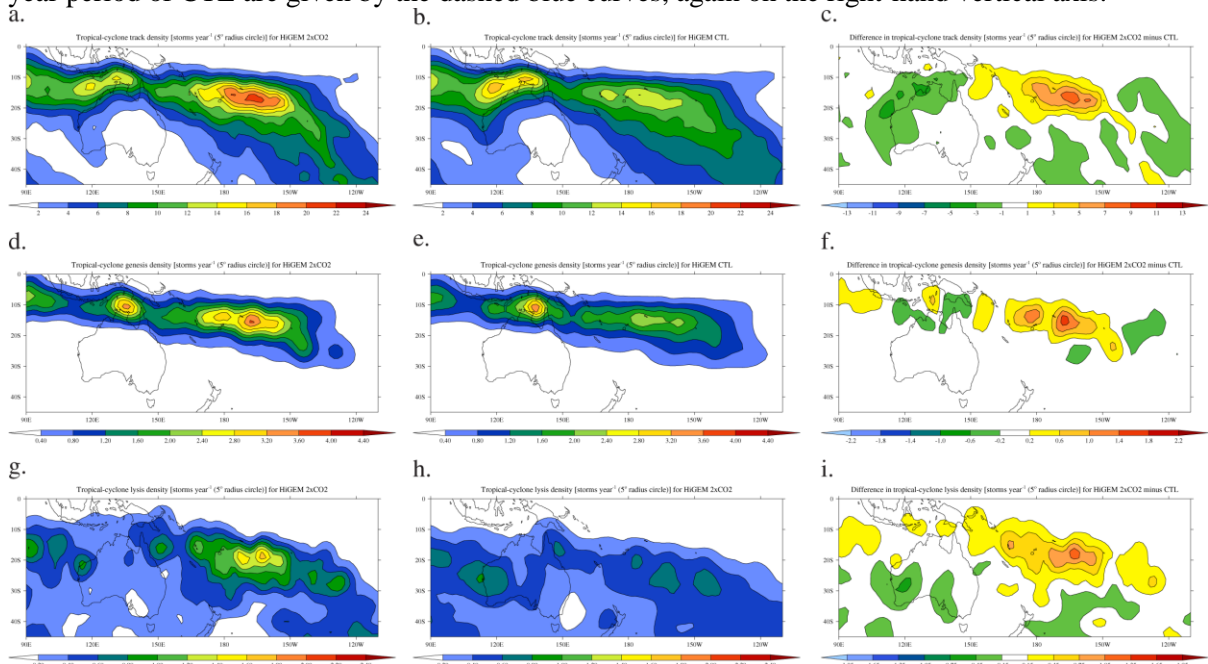


Figure 9: For (left column) 2xCO₂, (centre) CTL and (right) 2xCO₂ minus CTL, climatological densities [storms year⁻¹ (106 km²)⁻¹] of (a–c) cyclone tracks, (d–f) genesis locations and (g–i) lysis locations. Cyclones are tracked in all months years between October and May. Note that the contour intervals change between each row of

panels.

For all seasons together (May–April), the overall probability of rainfall in Queensland changes little in 2 x CO₂ relative to CTL (Fig. 10a). The probability of intense rainfall, however, increases substantially; the increase is stronger for heavier rain rates, such that the probability of more than a 100 mm accumulation rises by 30 per cent. Analysing the individual 50 year periods in CTL gives a range of 20–45 per cent for the increases in the frequency of at least a 100 mm accumulation. All three 50 year CTL baseline periods show that the probability of a 40 mm or greater accumulation rises under 2 x CO₂. Consistent with this, the return periods of constant accumulations above 40 mm decline in 2 x CO₂. The return period of an accumulation greater than 80 mm, for example, decreases from 914 days in CTL to 752 days in 2 x CO₂, a 17 per cent reduction.

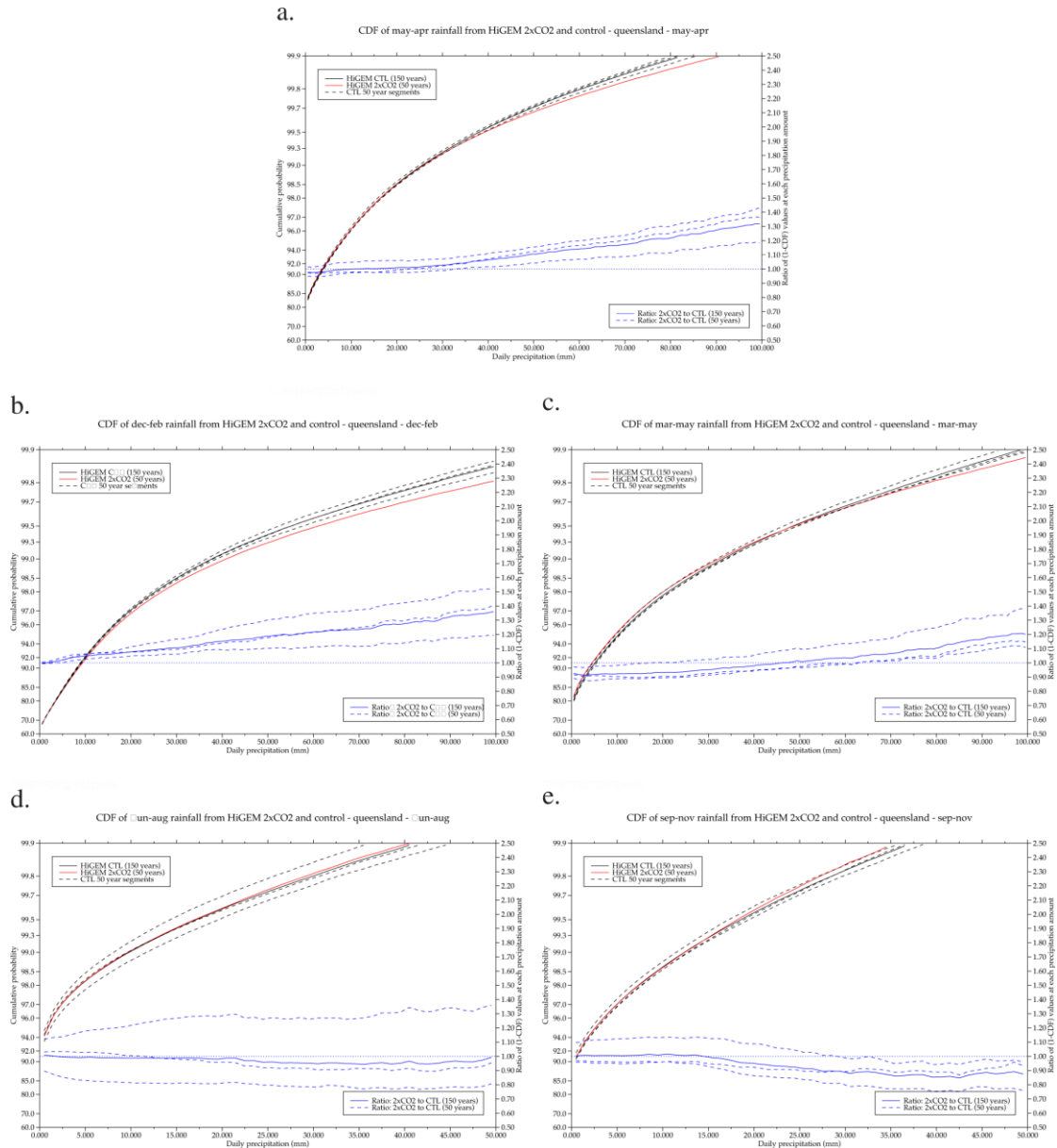


Figure 10: Cumulative distributions of daily rainfall for all land points in Queensland for (a) May–April, (b) December–February, (c) March–May, (d) June–August, (e) September–November using data from (solid black) all years of CTL, (solid red) all years of 2 x CO₂ and (dashed black) years 1–50, 51–100 and 101–150 of CTL. The blue lines show ratios of (solid) 2 x CO₂ to all years of CTL and (dashed) 2 x CO₂ to years 1–50, 51–100 and 101–150 of CTL.

Increases in the probability of extreme summer rainfall are primarily responsible for these annual changes (Fig. 10b). The probabilities of all but the lowest rain rates increase in 2 x CO₂ relative to all CTL baselines. A daily accumulation greater than 100 mm occurs 38 per cent more frequently in 2 x CO₂, with the 50 year CTL baselines giving a range of 20–52 per cent. The return period of an accumulation exceeding 80 mm declines from 418 days—approximately once every 4.5 summers—to 328 days—approximately once every 3.5 summers. Although the overall frequency of autumn rainfall declines (Fig. 10c), consistent with Fig. 7i, the probabilities of accumulations greater than 50–60 mm (depending on the CTL baseline) still increase in 2 x CO₂. An accumulation above 100 mm is 20 per cent more likely in 2 x CO₂ than CTL (10–40 per cent across the CTL baselines); the return period of at least an 80 mm accumulation declines from 570 days to 519 days. Thus, the mean drying in MAM across Queensland (Fig. 4c) obscures an increase in the probability of daily extreme rainfall that has been identified by this analysis.

Changes to JJA (Fig. 10c) and SON (Fig. 10d) extreme precipitation are weak and vary strongly with the CTL baseline chosen. The lone exception is a 10 per cent reduction in SON accumulations greater than 30 mm. These accumulations occur very rarely in HiGEM, however—an SON accumulation above 50 mm has a return period of nearly 25 years in CTL—so the results are likely not robust as there are few samples in the 50 years of 2 x CO₂ on which to base the statistical analysis.

5.2 Rainfall duration and event size

5.2.1 Rainfall Duration

Section 4.1 demonstrated that extreme daily rainfall becomes more likely in 2 x CO₂. Of greater importance for emergency-management applications (e.g. flood defence strategies), however, are changes to the probability of consecutive days of extreme daily rainfall. One day with a 100 mm accumulation may bring localised flooding, but three or four consecutive days with 100 mm accumulation each day could cause severe damage to agriculture and infrastructure on a regional scale.

To compute if HiGEM projects a change in the duration of extreme rainfall, the frequency of occurrence of “runs” (i.e., consecutive days) of precipitation greater than a threshold value are computed from CTL and 2 x CO₂. The precipitation threshold values are the percentiles of daily rainfall from CTL. These percentiles are computed at each HiGEM gridpoint in Queensland from the full 150 year CTL integration, using all days on which the rainfall exceeds 1 mm day⁻¹. The 90th percentile of rainfall, then, is equal to a 1-in-10 wet-day return period. (This is distinct from the 1-in-10 day return period.)

Using only wet days to define the percentiles enables the calculation to be equitable across Queensland, which is important given the large variance in the number of wet days across the state: there are three times more wet days in coastal Queensland and Cape York than in southwestern Queensland (Klingaman, 2012c). The data used to compute the rainfall percentiles are taken from the season (or May–April annual period) being analysed for event duration. For example, the distribution of runs for summer uses only summer rainfall to compute the percentile thresholds.

The frequency of runs of precipitation is computed for every 5th CTL rainfall percentile (e.g. 5 per cent, 10 per cent, 15 per cent) until the 90th percentile, after which the computation is performed for every integer percentile until the 99th percentile. The CTL percentiles are used for both the CTL and 2 x CO₂ integrations, to enable a clean comparison that is not influenced by the increase in precipitation intensity in 2 x CO₂ (section 3.3.3). As for the CDFs of daily rainfall in section 4.1, the statistics of rainfall duration are accumulated across all Queensland gridpoints. Fig. 11 displays the frequency of rainfall durations at each percentile—as events year⁻¹ gridpoint⁻¹ with all daily

accumulations at or above the percentile threshold—for CTL and the ratio of the frequencies of each duration for 2 x CO₂ divided by CTL.

For the May–April annual period, CTL shows the expected behaviour of a decreasing frequency of events with increasing percentile threshold and increasing event duration (Fig. 11a). In CTL, gridpoints in Queensland receive on average 2.6 one-day events year⁻¹ that exceed the 90th percentile of daily rainfall, but only 0.7 two day events year⁻¹ in which both days exceed the 90th percentile; three-day runs above the 90th percentile occur with a frequency of 0.26 year⁻¹. Events in which three or more days exceed the 99th percentile are extremely rare in CTL.

In 2 x CO₂, HiGEM projects an increased probability of long runs of rainfall for all thresholds exceeding the 80th percentile (Fig. 11b). The ratios for all events with a probability of less than 0.025 in CTL—or one per gridpoint per 40 years—are not shown, as these events are highly under-sampled in 2 x CO₂ (and likely even in CTL). The frequency of 4–6 day events in which each day exceeds the 90th percentile increases by 6–12 per cent per cent; similar increases are seen for 5–7 day events exceeding the 80th percentile of daily rainfall. At the extreme end of the spectrum, the probability of a four-day run of 95th percentile daily rainfall rises by 14 per cent. There are decreases in the probability of very long runs of light rainfall—below the 50th percentile—which suggest that in 2 x CO₂ there has been a dangerous shift away from long periods of light rain days and towards long periods of heavy rain.

Increases in the probability of consecutive days of heavy rainfall are greater in DJF than for May–April (Fig. 11d). All percentiles of daily rainfall greater than the 60th percentile show a greater number of long rainy spells in 2 x CO₂. (As discussed above, the percentiles here are computed based on summer rainfall in CTL, not May–April rainfall as in Fig. 11b). The frequency of four-day and five-day events exceeding the 90th percentile of daily summer rainfall increases by 15 per cent; four-day events above the 95th percentile are 23 per cent more likely in 2 x CO₂ than in CTL. This is consistent with the overall intensification of summer rainfall in DJF (Fig. 7b) and the increase in the probability of extreme daily accumulations (Fig. 10b). The reduction in wet days in MAM leads to a decrease in the frequency of long rainfall events in 2 x CO₂ at all but the most extreme percentiles (Fig. 11f). There is some indication that four-day runs of rainfall above the 90th percentile increase in 2 x CO₂ relative to CTL, but this is against a background of reductions in rainfall duration in spring.

It is important to note that many of the increases in extreme rainfall duration here are for events with a low probability of occurrence in either 2 x CO₂ or CTL. Although care has been taken to remove the most rare events—those that occur less than once every 40 years at a gridpoint, as discussed above—from the analysis, the percentage changes in the duration of extreme events will still be sensitive to small changes in their frequency. A longer 2 x CO₂ integration would provide greater confidence in these results, but such a simulation was not available. The robustness of the change across the percentiles—the fact that duration increases for heavy rainfall, but decreases for light rainfall—increases confidence in the general conclusion of substantial increases in the probability of consecutive days with extreme rainfall increases in Queensland in 2 x CO₂, primarily due to increases in the duration of heavy rainfall in summer.

5.2.2 Rainfall size event

Having determined that persistent extreme rainfall becomes more likely in 2 x CO₂ relative to CTL, particularly in DJF, it is logical to consider whether the area covered by extreme daily rain events changes in 2 x CO₂. This section analyses the spatial coherence of daily rainfall in 2 x CO₂ in CTL, using a method similar to that applied for the duration of rain events in section 4.2.1.

Percentiles of daily rainfall are computed from CTL at every land gridpoint in Queensland in the same manner as in section 4.2.1, using only days with greater than 1mm accumulation. The same percentile thresholds—in increments of five percent until the 90th percentile, then in increments of one percent until the 99th percentile—are applied to determine daily rain events. For each percentile

threshold, at each gridpoint, all days with rainfall accumulations above the threshold are extracted from CTL. For each selected day, the number of gridpoints within a two-gridpoint radius—24 gridpoints in total—that also have accumulations above the threshold are counted. To prevent counting each event multiple times, the precipitation at all gridpoints included in the event is reset to zero after each event is counted. The statistics of events are accumulated over all land gridpoints in Queensland. All events above a given percentile are then binned according to their size—using integer bins from 1 to 25—and the fraction of events that fall into each bin is computed. This is the quantity shown in Fig. 12; the integral of each column (i.e. for all sizes at a constant percentile threshold) is one, since the fractions are computed separately for each percentile threshold. For ease of interpretation, the size of the event is converted into an area (in 104 km²) by multiplying the number of gridpoints by the area of each HiGEM gridpoint (approximately 8100 km²).

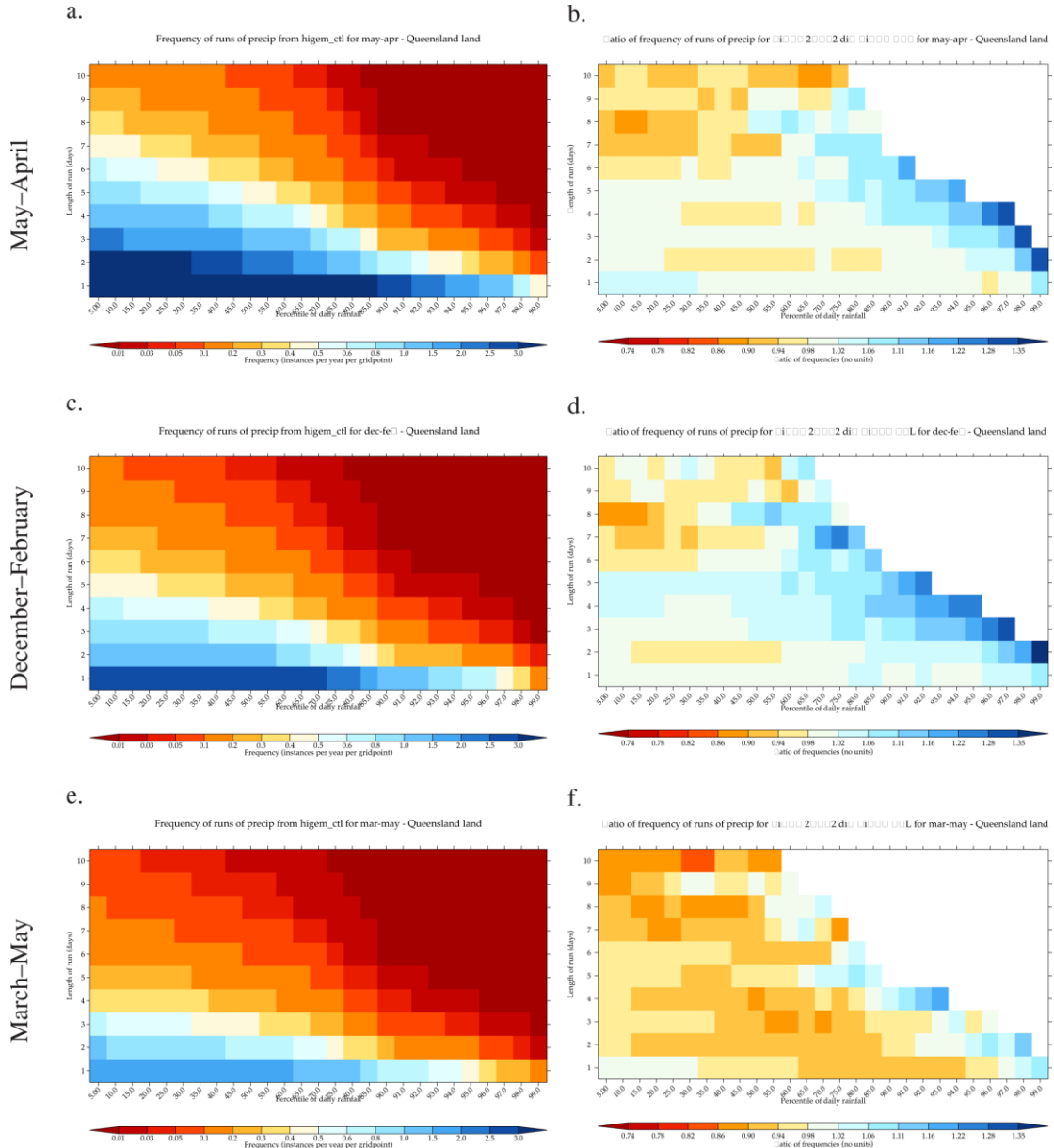


Figure 11: The frequency (events year⁻¹ gridpoint⁻¹) of consecutive days of precipitation exceeding a percentile threshold, using CTL rainfall to compute the percentiles, for (a) CTL for May–April rainfall, (b) 2 x CO₂ divided by CTL for May–April rainfall, (c) CTL for December–February rainfall, (d) 2 x CO₂ divided by CTL for December–February rainfall, (e) CTL for March–May rainfall and (f) 2 x CO₂ divided by CTL. Rainfall percentiles are computed from CTL for the season or year in question using all days with greater than 1 mm accumulation.

Using the May–April period, CTL shows the expected inverse relationship between the threshold intensity of daily rainfall and the size of the event: events with a light threshold (e.g. the 5th percentile of daily rainfall) typically cover larger areas (Fig. 12). The values shown on the horizontal axis in Fig. 12 are the lower threshold percentile of rainfall; the values shown for the 5th percentile are for all events exceeding the 5th percentile, not all events between the 5th and 10th percentiles. Similar inverse relationships are found for DJF (Fig. 12b) and MAM (Fig. 12c). Extreme daily rain events in DJF are more likely to cover a wider area than are similarly extreme events in MAM.

In the May–April annual period, DJF and MAM, HiGEM projects an increase in the spatial coherence of heavy daily accumulations in 2 x CO₂ (Figs. 12d–f). For threshold percentiles above the 70th percentile, there are relatively more occurrences of events covering a larger area and relatively fewer occurrences of events covering smaller areas. At the 95th percentile threshold, for example, there are 6–15 per cent fewer events that cover 2.45–8.10×10⁴ km² and 6–22 per cent more events that cover 9.72–12.9×10⁴ km². This indicates that when heavy precipitation occurs in 2 x CO₂, those heavy accumulations extend across a wider area of Queensland than they do in CTL.

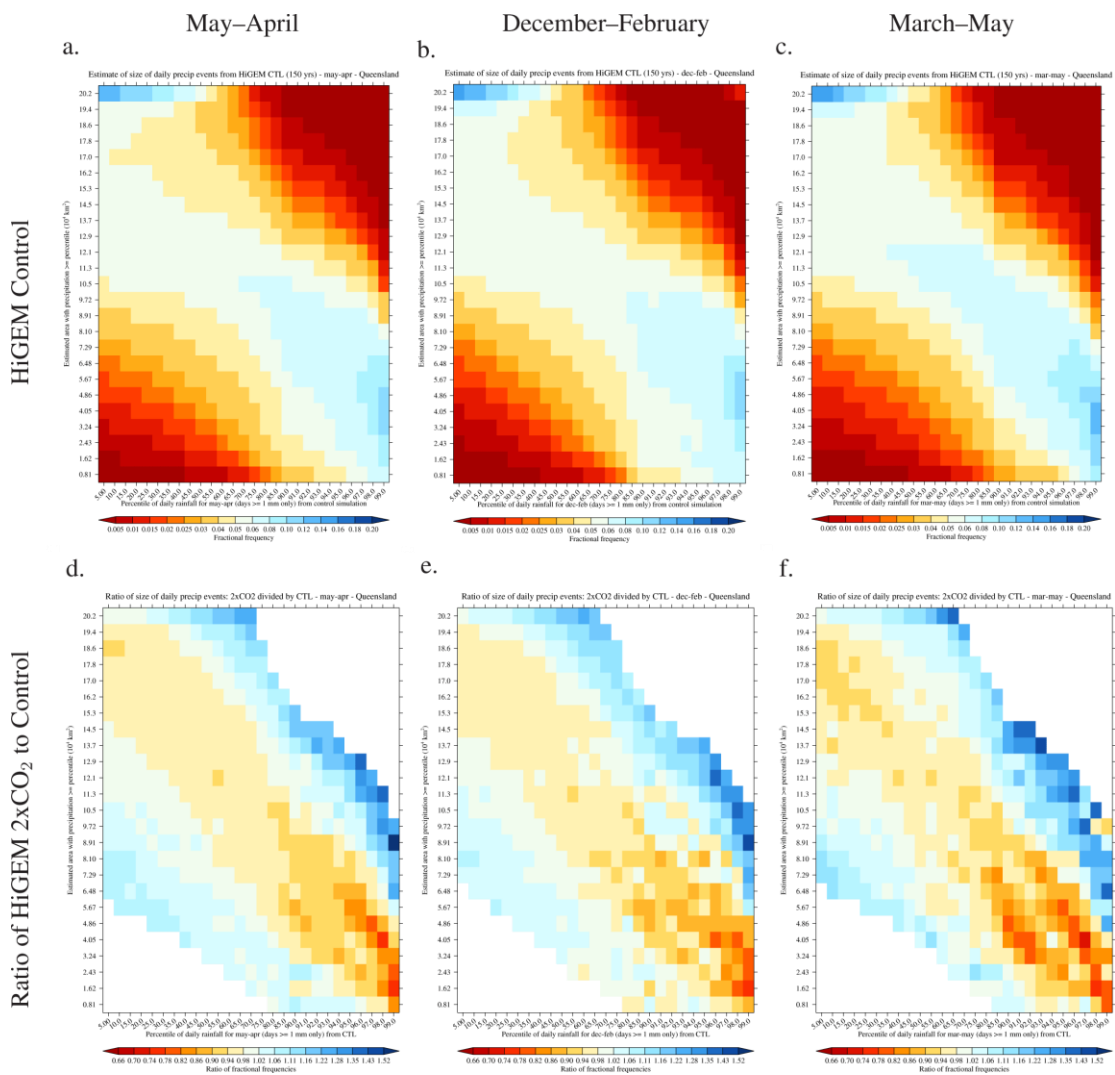


Figure 12: For all land gridpoints in Queensland, (a–c) the size distribution of CTL rain events exceeding each percentile of daily rainfall, expressed for each area bin (vertical axis, in 10⁴ km²) as a fraction of all events that exceed the given percentile (horizontal axis) for (a) May–April, (b) December–February and (c) March–May; (d–f) as in (a–c), but for the ratio of the 2 x CO₂ fractions to the CTL fractions. In (d–f), blue colours indicate rainfall event sizes that occur relatively more frequently in 2 x CO₂ than in CTL, while orange colours indicate event sizes that occur relatively less frequently; ratios are not shown for event sizes that occur less than 2% in CTL [equal to the 0.02 fractional frequency in (a–c)]. In all panels, the percentiles of daily rainfall are computed from CTL for the seasonal or annual period shown in the panel.

A summary of the changes to rainfall size and duration between 2 x CO₂ and CTL is provided in Fig. 13, which displays the mean duration and size of events exceeding each CTL percentile threshold for daily rainfall used in Figs. 11 and 12. The means are computed separately for DJF and MAM from all events occurring over land gridpoints in Queensland. Fig. 13a clearly demonstrates up to a 20 per cent increase in the duration of extreme rainfall events in DJF, while Fig. 13c shows up to a 15 per cent increase in the area encompassed by summer extreme rainfall. These increases are lower in MAM (Figs. 13b and 13d), particularly for duration.

When combined, the analysis presented in section 4 indicates that in 2 x CO₂, relative to CTL, heavy precipitation in Queensland occurs more frequently and with greater intensity (section 4.1), is more likely to persist at a given location for multiple days (section 4.2.1) and is more likely to cover a wider area on any given day (section 4.2.2). These conclusions have considerable implications for flood frequency and emergency preparedness; they will be discussed further in section 7.

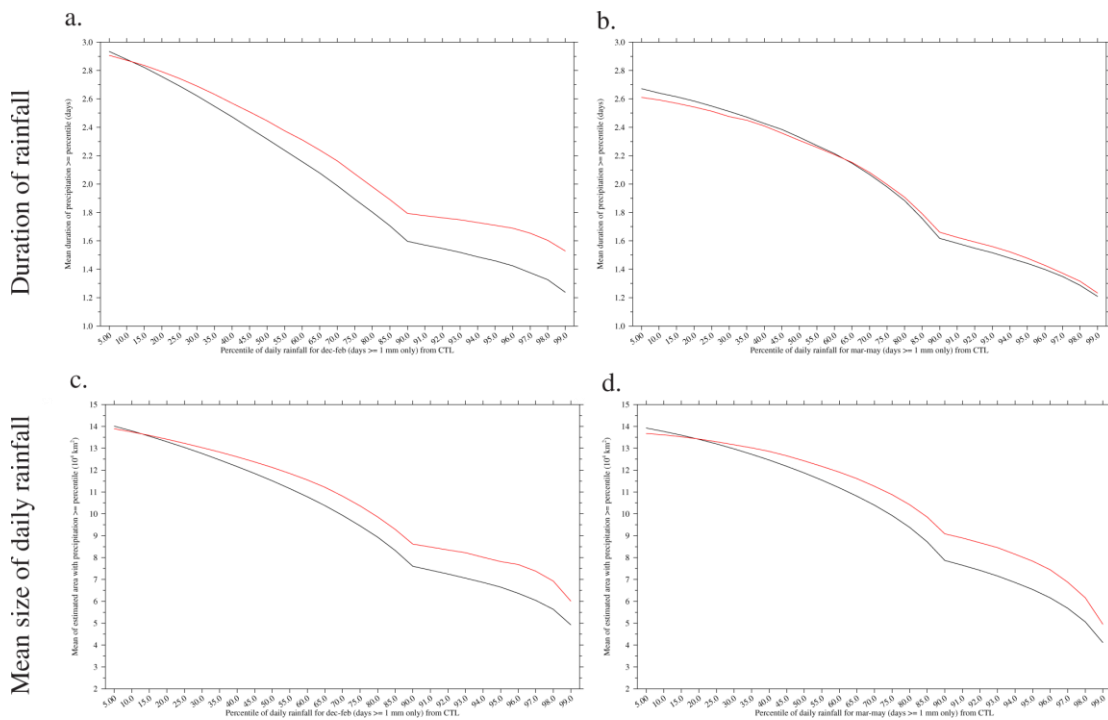


Figure 13: The mean over all Queensland land gridpoints of (a, b) duration of events (in days) exceeding each daily percentile threshold from CTL and (c, d) size of daily events (in 10⁴ km²) exceeding each percentile threshold from CTL for (black lines) CTL and (red lines) 2 x CO₂ using data from (a, c) DJF and (b, d) MAM. These are the means of the distributions from Fig. 11 for rainfall duration and Fig. 12 for event size.

Compression of the Queensland wet season

This section builds upon the results of section 3.3 for changes in Queensland seasonal-mean rainfall in 2 x CO₂. Those results showed that DJF becomes 5–18 per cent wetter, but MAM rainfall decreases by 5–40 per cent in the state, with the greatest drying in southwestern and southeastern Queensland. This suggested a compression of the present-day wet season, primarily due to an earlier termination in autumn. This section presents the differences between 2 x CO₂ and CTL in wet-season onset and termination dates (section 5.1), and in the contributions of each month in November–April to the total wet-season rainfall (section 5.2).

6.1 Onset and termination dates

The percentile method of Smith et al. (2008) is used to identify mean wet-season onset and termination dates at each gridpoint in CTL and 2 x CO₂. Smith et al. (2008) demonstrated using station rainfall data that the 15th and 85th percentiles of the September–April total accumulation, computed separately for each station and each year, were simple and robust descriptors of the beginning and end of the wet season across northern Australia. These thresholds are applied to CTL and 2 x CO₂ at every gridpoint for every September–April period; the mean onset and termination dates are then calculated for every gridpoint using all years of each integration.

In CTL, the wet-season onsets first in south-central Australia, then progresses north and then west and east; the latest onset dates are in Cape York and along the coast of Western Australia (Fig. 14a). This may seem counter-intuitive given that the summer monsoon trough moves from north to south, but it is important to remember that the seasonal cycle of rainfall is more equitable in central Australia, while the seasonal cycle is sharply peaked in DJF in the northern tropical regions. This leads to the 15th percentile threshold for onset being crossed earlier across central Australia (e.g. in southeastern Queensland) than in the tropical north (e.g. in Cape York). The spatial pattern of CTL onset dates in Fig. 14a agrees very well with that in Fig. 6 in Smith et al. (2008), but in CTL the dates are nearly uniformly 15 days later than those Smith et al. (2008) found from station observations. This is consistent with the conclusion of Klingaman (2012a) that the wet season in CTL is slightly delayed.

The pattern of CTL wet-season termination dates (Fig. 14c) also agrees with that of Smith et al. (2008), except that the CTL dates are approximately 10 days later than those observed. Thus, CTL produces a wet season of approximately the correct length, but one that is shifted later by 10–15 days relative to observations. HiGEM projects a compressed wet season in Queensland in 2 x CO₂. Along the eastern coast and in Cape York, wet-season onset dates are 2–12 days later on average in 2 x CO₂ than in CTL (Fig. 14b). This equates to a shift from a late-December onset in CTL to an early-January onset in 2 x CO₂. The later onset may be due to a reduction in SON rainfall along the coast (Fig. 5e), which would delay the crossing of the 15th percentile threshold since the total wet-season accumulation changes little (section 3.3).

Similarly, there are indications of a somewhat earlier wet-season onset in southwestern Queensland where SON rainfall increases slightly. Of greater significance, however, are the much earlier wet-season termination dates in 2 x CO₂ across the entire summer-monsoon domain (Fig. 14d). In southern Queensland, the termination dates are 10–16 days earlier than in CTL, representing a shift from early-to-mid March to mid-to-late February. Coastal termination dates are 6–12 days earlier. When combined with the later onset, this leads to wet seasons that are on average 8–20 days shorter across Queensland. Given that the CTL wet season is approximately 100 days long across much of the state (from Figs. 14a and 14c), this represents an 8–20 per cent reduction in wet-season length. The effect of the shorter wet season is not to reduce total rainfall—section 3.3 demonstrated that wet-

season accumulations are similar in 2 x CO₂ and CTL—but to compress the same rainfall into a shorter season. This agrees with the results of section 3.3.3 that the number of wet days in DJF and MAM decreases—particularly in MAM—but that the mean precipitation accumulation per wet day increases substantially, particularly in DJF.

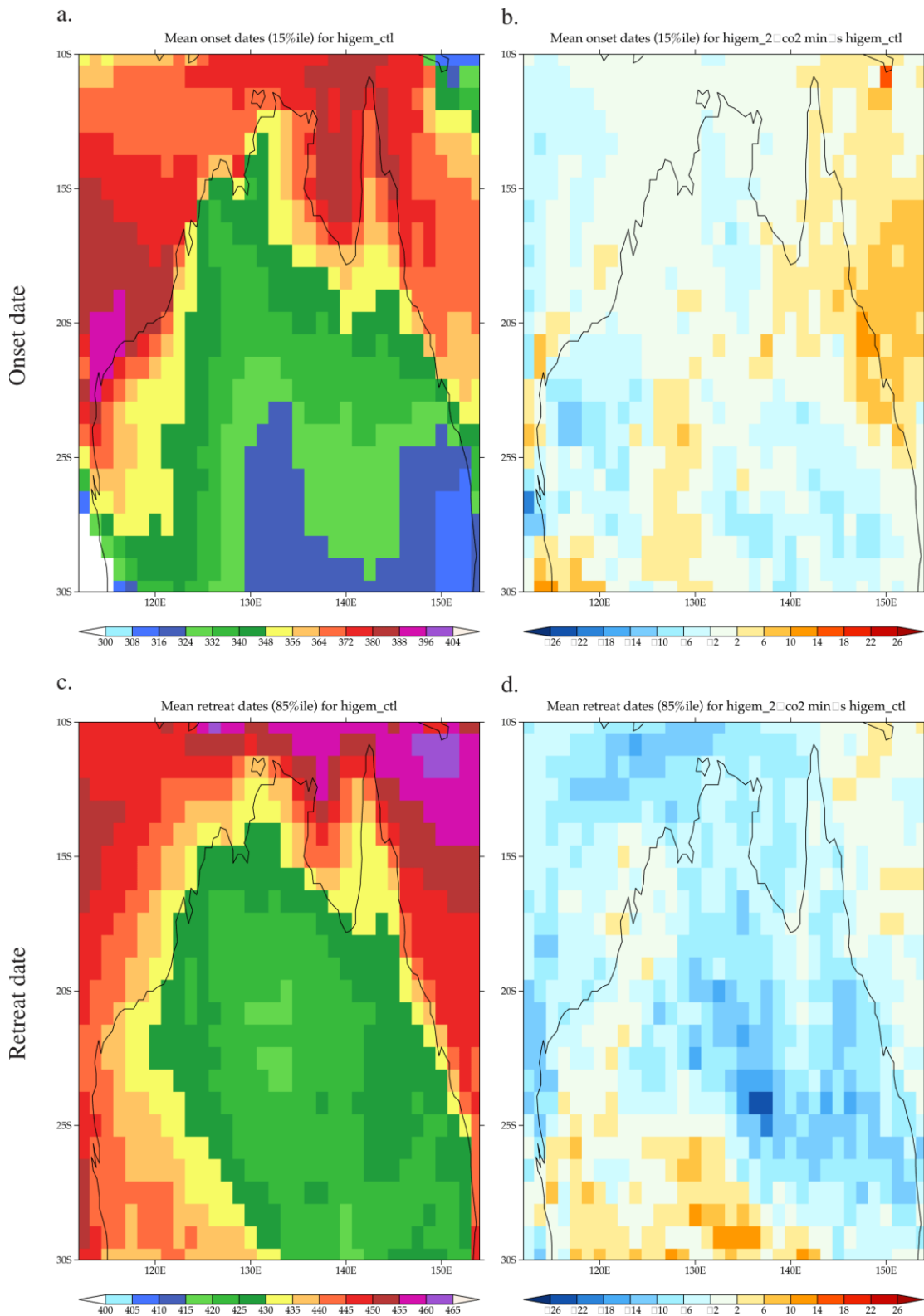


Figure 14: For the (a, b) wet-season onset date and (c, d) wet-season termination date, (a, c) the mean dates from CTL and (b, d) the differences in the mean dates between 2 x CO₂ and CTL.

6.2 Contributions of individual months to wet season totals

To further demonstrate the compression of the wet season in 2 x CO₂ relative to CTL, the linear regressions of monthly rainfall for each month in September–April on total September–April rainfall was computed for SILO (section 2.2), CTL and 2 x CO₂. SILO data are included as a validation of CTL. The regression coefficients effectively represent the fraction of September–April rainfall that falls in each month; they are the change in rainfall (mm) in each month for a 1 mm change in the September–April total. The September and October coefficients were found to be insubstantial throughout northern Australia in SILO and HiGEM; only those for November–April are shown in Fig. 15.

As previously discussed, the wet season in CTL runs slightly later than it does in observations; CTL produces too little rainfall in November and December (Figs. 15b and 15e, respectively) relative to SILO (Figs. 15a and 15d) and too much rainfall in March and April (Figs. 15n and 15q) compared to the gridded observations (Figs. 15m and 15p).

With respect to CTL, November and December contribute somewhat less to the September–April total rainfall in 2 x CO₂ (Figs. 15c and 15f), except in southern Queensland where December contributes somewhat more in 2 x CO₂. The latter result agrees with the slightly earlier mean wet-season onset date in this region (Fig. 14b). January and February are far more critical to the wet-season total in 2 x CO₂ (Figs. 15i and 15l) than CTL (Figs. 15h and 15k), with large increases in the regression coefficients in southern Queensland in January and in central and northern Queensland in February. By contrast, the regression coefficients decrease considerably in March and April relative to CTL, such that these months contribute far less to the wet-season rainfall in 2 x CO₂.

These results reinforce those of section 5.1: in Queensland the wet-season onset is slightly later (Fig. 14b) and the termination is much earlier (Fig. 14d) in 2 x CO₂, which is associated with total wet-season rainfall becoming far more sensitive to variations in January and February rainfall in 2 x CO₂ than in CTL. The wet season is therefore compressed into these months, with accumulations increasing in mid-summer and decreasing in late spring and throughout autumn.

7 Projected changes in inter-annual variability

7.1 Inter-annual variability in seasonal means

While section 3.3 presented the projected changes in climatological seasonal and annual rainfall in 2 x CO₂ against CTL, it is also prudent to consider the impacts of increased atmospheric CO₂ on year-to-year variations in Queensland rainfall. In this section, inter-annual variability is estimated using the coefficient of variation (CoV), which is equal to the inter-annual standard deviation of rainfall divided by the mean. Using the CoV instead of standard deviation limits the effects of changes in the climatological rainfall—which section 3.3.1 showed are large in DJF and MAM—and provides a more accurate representation of the magnitude of year-to-year variability about the long-term mean.

The CoV is computed for area-averaged Queensland rainfall in each season and for the May–April annual period. In addition to calculating the CoV over all years of CTL and 2 x CO₂, it is also computed for all 100 50-year periods in CTL—as in section 3.3.2—to provide a probability distribution function (PDF) against which the CoV from the 50-year 2 x CO₂ integration can be compared. Further, PDFs of the CoV are computed over all 40 10 year periods from 2 x CO₂ and each of the three 50 year blocks of CTL (i.e., years 1–50, 51–100 and 101–150) to estimate changes in inter-annual variability from decade to decade in each simulation. Fig. 16 shows the PDFs of the CoV for each season and for May–April, with vertical lines to denote the CoV over all years of CTL (black) and 2 x CO₂ (red).

Overall, HiGEM projects that inter-annual variation in Queensland rainfall, as a fraction of mean rainfall, will not be substantially affected by a doubling of atmospheric CO₂. The coefficients of variation in May–April (Fig. 16a), DJF (Fig. 16b) and MAM (Fig. 16c) area-averaged Queensland rainfall show very little change between CTL and 2 x CO₂. The CoV for 2 x CO₂ (red vertical line) lies well within the PDF of CoV values for the 100 50 year periods of CTL (black curve) for summer, autumn and annual rainfall. Further, the PDFs of CoV computed over 10 year periods of 2 x CO₂ show a similar spread as those from CTL, indicating there are no decades in 2 x CO₂ with inter-annual variability much lower or higher than in the decades in CTL. In the dry seasons, JJA (Fig. 16d) and SON (Fig. 16e), 2 x CO₂ shows slight decreases in inter-annual variability relative to CTL. The JJA CoV for 2 x CO₂ lies outside the (very tight) distribution of values from CTL, while the SON 2 x CO₂ CoV is near the lower end of the CTL distribution, indicating robust decreases in year to year variability in each season.

While there are some decades of high year-to-year variability in CTL—the purple dashed lines at the upper ends of the range in Figs. 16d and 16e—no such decades exist in 2 x CO₂. Based on this analysis, in a warmer world Queensland rainfall will vary inter-annually by a similar percentage of its long-term mean as in the present day. HiGEM projects large shifts in the long-term mean rainfall in DJF and MAM (section 3.3.1) but not in the magnitude of year-to-year variations relative to that mean.

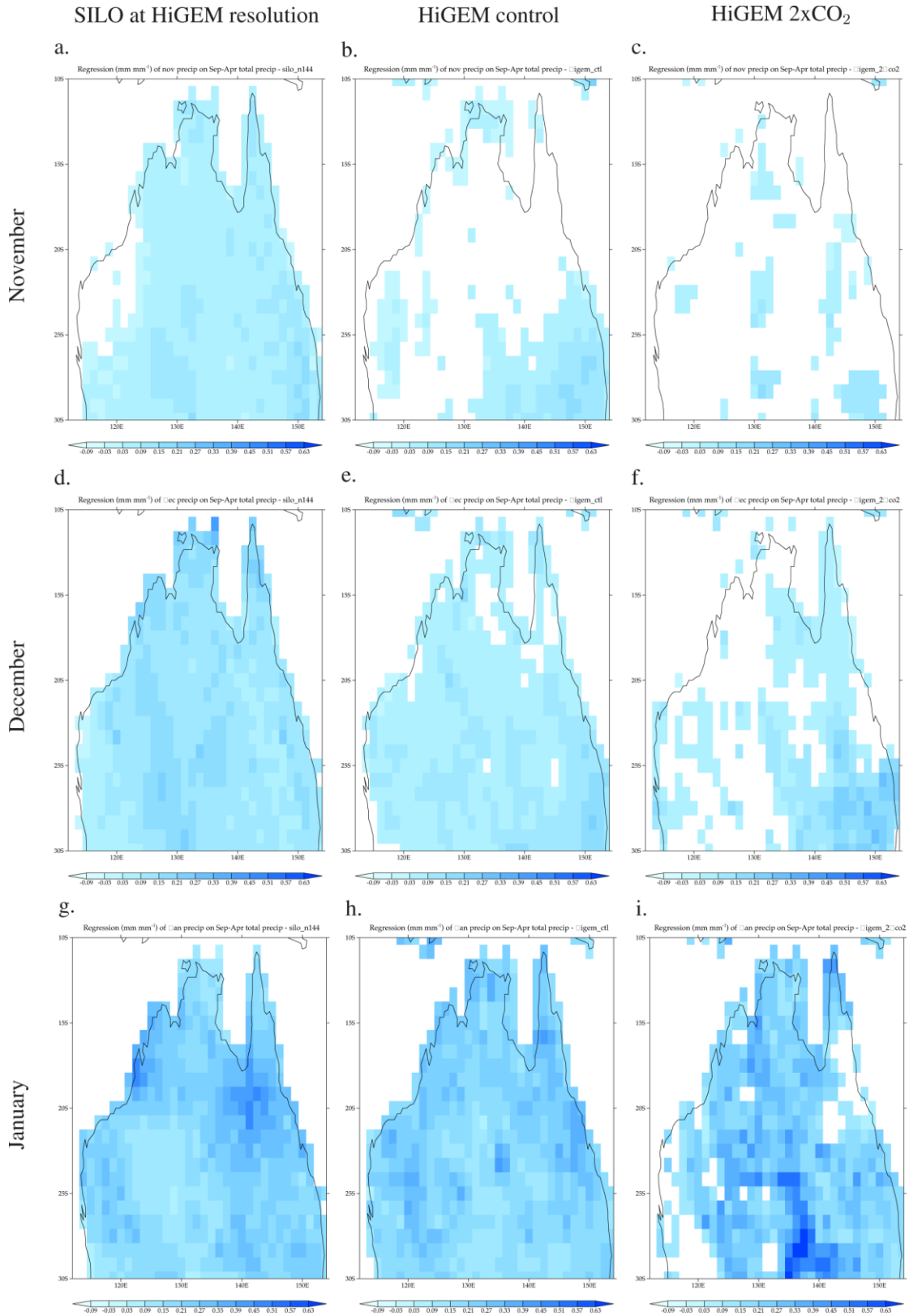
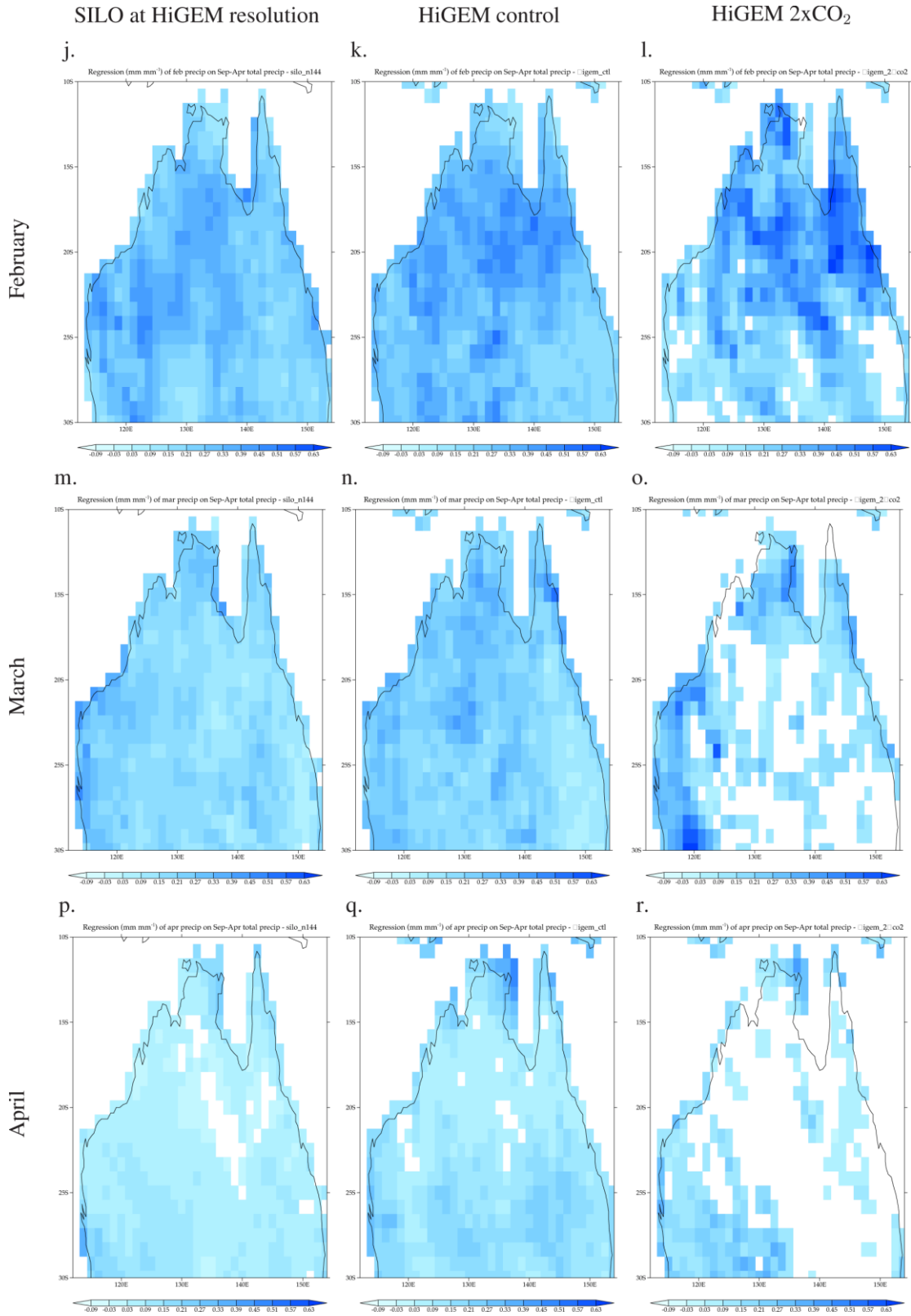


Figure 15: Linear regressions (mm mm⁻¹) of monthly rainfall on September–April total rainfall for (left column) SILO, (centre) CTL and (right) 2 x CO₂ for (a–c) November, (d–f) December, (g–i) January, (j–l) February, (m–o) March and (p–r) April. Regression coefficients are shown only where statistically significant at the 5% level.



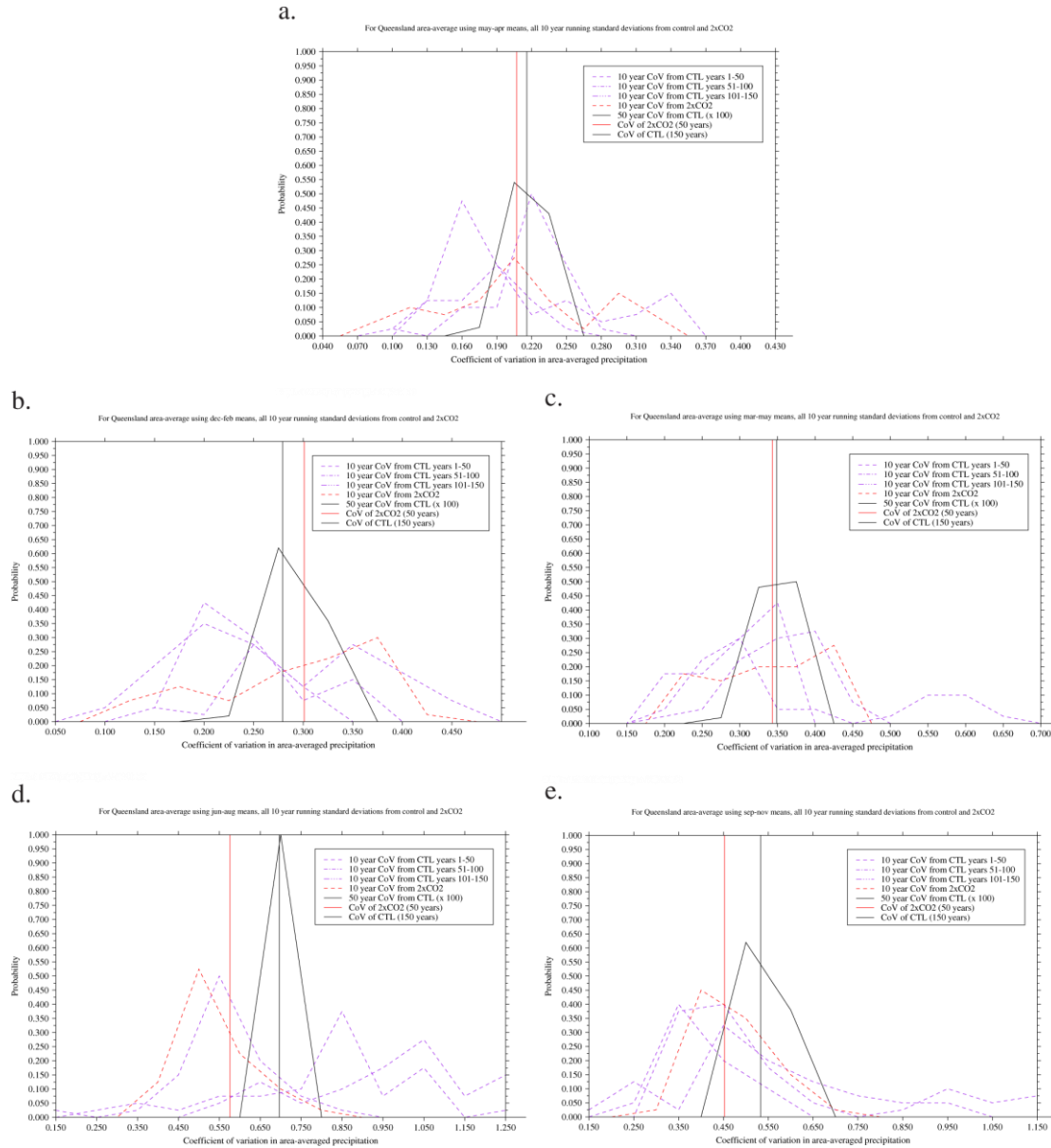


Figure 16: Probability distribution functions (PDFs) of the coefficient of variation (CoV, unitless) in Queensland area-averaged rainfall for (a) May–April, (b) December–February, (c) March–May, (d) June–August and (e) September–November. Lines show the PDFs for CoVs computed over (solid black) 50 year periods of 2xCO₂ (100 samples), (dashed purple) 10 year periods within each 50 year block of CTL (40 samples), (dashed red) 10 year periods within the 50 year 2 x CO₂. The vertical lines show the CoV using all years of (black) CTL and (red) 2 x CO₂.

7.2 Empirical Orthogonal Teleconnection patterns

This section examines how doubling atmospheric CO₂ concentrations modifies the EOT patterns of seasonal Queensland rainfall derived for HiGEM CTL in Klingaman (2012a). The first four EOTs of each season’s rainfall are computed for 2 x CO₂ by the method described in section 2.3 are compared to those from CTL in terms of spatial pattern and climate driver. For the latter, timeseries of SST, mean-sea-level pressure (MSLP), 850 hPa and 500 hPa winds and 500 hPa specific humidity are regressed onto each of the 2 x CO₂ and CTL EOTs.

In the case of 2 x CO₂, the all timeseries are linearly de-trended before calculating the regression coefficients, to remove any linear trends arising from the increased CO₂ forcing in 2 x CO₂. This is particularly necessary given that the climate of 2 x CO₂ is unlikely to be in balance with the

additional radiative forcing, which could lead to considerable trends as the system adjusts (section 2.1). For the CTL EOTs, these regressions are the same as those computed in Klingaman (2012a). Greater weight in this analysis will be given to those EOT patterns that Klingaman (2012a) determined were robustly simulated in CTL, compared to the EOT patterns computed from the SILO gridded rainfall dataset in Klingaman (2012b).

Changes in EOT patterns are examined for each of the four seasons separately: summer (section 6.2.1), autumn (section 6.2.2), winter (section 6.2.3) and spring (section 6.2.4). Table 1 summarises how doubling atmospheric CO₂ influences each the HiGEM EOTs from Klingaman (2012a).

7.2.1 December - February EOTs

In CTL (Fig. 17a) and 2 x CO₂ (Fig. 17e), the leading DJF EOT describes nearly state-wide variations in rainfall; there is little change in the spatial pattern of DJF EOT 1 due to doubling atmospheric CO₂. Klingaman (2012a) demonstrated that DJF EOT1 was significantly correlated with the El Niño Southern Oscillation (ENSO) in the SILO observations and CTL. This relationship is clearly shown by the regression of CTL SSTs on CTL DJF EOT1 (Fig. 18a). In 2 x CO₂, however, there is no significant correlation between equatorial Pacific SSTs and DJF EOT1 (Fig. 18d) and no significant correlations were found between 2 x CO₂ DJF EOT1 and the Niño 3, Niño 3.4 or Niño 4 SST indices (not shown). This suggests that the correlation between state-wide summer rainfall and ENSO weakens considerably in 2 x CO₂ from CTL.

The relatively short, 50-year period of 2 x CO₂ is likely insufficient to provide robust statistics of ENSO activity, however. Using a threshold of a Niño 4 SST anomaly of at least $\pm 0.5^{\circ}\text{C}$ for three months, there are only 10 (8) El Niño (La Niña) events in 2 x CO₂ using a 0.5°C . The small sample of events generates little confidence in any shifts in the relationship between ENSO and Queensland rainfall in 2 x CO₂. The ENSO–rainfall relationship in 2 x CO₂ is discussed further in section 7.

Aside from the lack of an ENSO teleconnection, the circulation patterns associated with 2 x CO₂ DJF EOT1 are remarkably similar to those for CTL DJF EOT1. At 850 hPa, both EOTs are related to an enhanced summer monsoon, with lower MSLP and an anomalously cyclonic circulation over Queensland (Figs. 18b and 18e). There is no anomalous convergence over the Maritime Continent or any indication of the positive SOI phase in wet summers in 2 x CO₂, both of which are consistent with the insignificant correlation with ENSO. Strong mid-tropospheric (500 hPa) moisture anomalies are centred over Queensland in both CTL (Fig. 18c) and 2xCO₂ (Fig. 18f) in positive DJF EOT1 seasons, associated with the enhanced transport of tropical moisture from ocean to land by the anomalous westerly winds.

Wet summers in Queensland in 2 x CO₂ are associated with very warm ocean temperatures along the east coast of Australia (Fig. 18d), a pattern which does not appear in CTL DJF EOT1 (Fig. 18a). These warm SST anomalies resemble those that Klingaman (2012b) found for MAM EOT1 in observations, which were associated with locally driven air–sea interactions during the late season summer monsoon. The occurrence of this pattern in 2 x CO₂ DJF EOT1, combined with the lack of an ENSO teleconnection, suggests that state-wide Queensland rainfall variations are associated with locally driven monsoon variations, rather than the remote effect of Pacific SSTs.

DJF EOT2 describes summer rainfall variations in southeast Queensland (Fig. 17b), which Klingaman (2012a) concluded were associated with coastal low-pressure systems and moist onshore easterlies. In 2 x CO₂, southeast Queensland summer rainfall becomes negatively correlated with that in the north and northwest of the state, suggesting a greater disconnect between those regions in a warmer world. The SST and circulation anomalies corresponding to wet DJF EOT2 seasons are broadly consistent between CTL (Figs. 18g–i) and 2 x CO₂ (Figs. 18j–l): warm SSTs extending in an arc from the east coast; lowered surface pressures along the coast, particularly near southeast Queensland; and an anomalous 500 hPa moisture source near the coastal lows.

HiGEM EOT	SILO EOT	Region in CTL	Mechanism in HiGEM CTL	Impact of 2xCO ₂
<i>DJF</i>				
EOT1	EOT1	State-wide	ENSO effects on monsoon	ENSO correlation weakens; monsoon relationship consistent
EOT2	EOT3	Southern	Coastal cyclones, onshore winds	Weaker onshore winds; coastal cyclones consistent
EOT3	None	Northwestern	Enhanced moisture transport	Region of influence restricted; same mechanism
EOT4	EOT2	Cape York	Tropical cyclone activity	No change to driver; decreased number of cyclones
<i>MAM</i>				
EOT1	EOT1	State-wide	Late-season monsoon	Region of influence restricted due to faster monsoon retreat
EOT2	EOT2	Central and south	Coastal cyclones	Influence only in SE; wet seasons correlated with El Niño
EOT3	None	Western	ENSO (decaying) effect on monsoon	No change; ENSO correlation robust
EOT4	None	Northern coastal	Tropical cyclone activity	No change to driver; decreased number of cyclones
<i>JJA</i>				
EOT1	EOT1	State-wide	ENSO (growing); onshore winds	ENSO correlation weakens; onshore winds robust
EOT2	EOT2	Southeastern	Southern Ocean blocking	No change to driver
EOT3	None	Northern	Southward moisture advection	No change to driver
EOT4	None	SE and western	Unknown; no significant regressions	Not applicable; no known driver
<i>SON</i>				
EOT1	EOT1	State-wide	ENSO (growing) and SAM	No change to drivers; ENSO and SAM correlations robust
EOT2	None	Coast and north	Moist air and low pressure offshore	No change to drivers
EOT3	None	Western	ENSO (decaying)	ENSO correlation weakens; moisture advection from north
EOT4	None	Southeast	Unknown; no significant regressions	Wet seasons correlated with El Niño

Table 1: For each HiGEM CTL EOT identified in (Klingaman, 2012a): the corresponding SILO EOT, if any, based on the analysis in (Klingaman, 2012a); the region of Queensland for which the EOT describes rainfall variations; the climate driver of the EOT, as determined in (Klingaman, 2012a); and a summary of the projected changes to that EOT based on the analysis in this report.

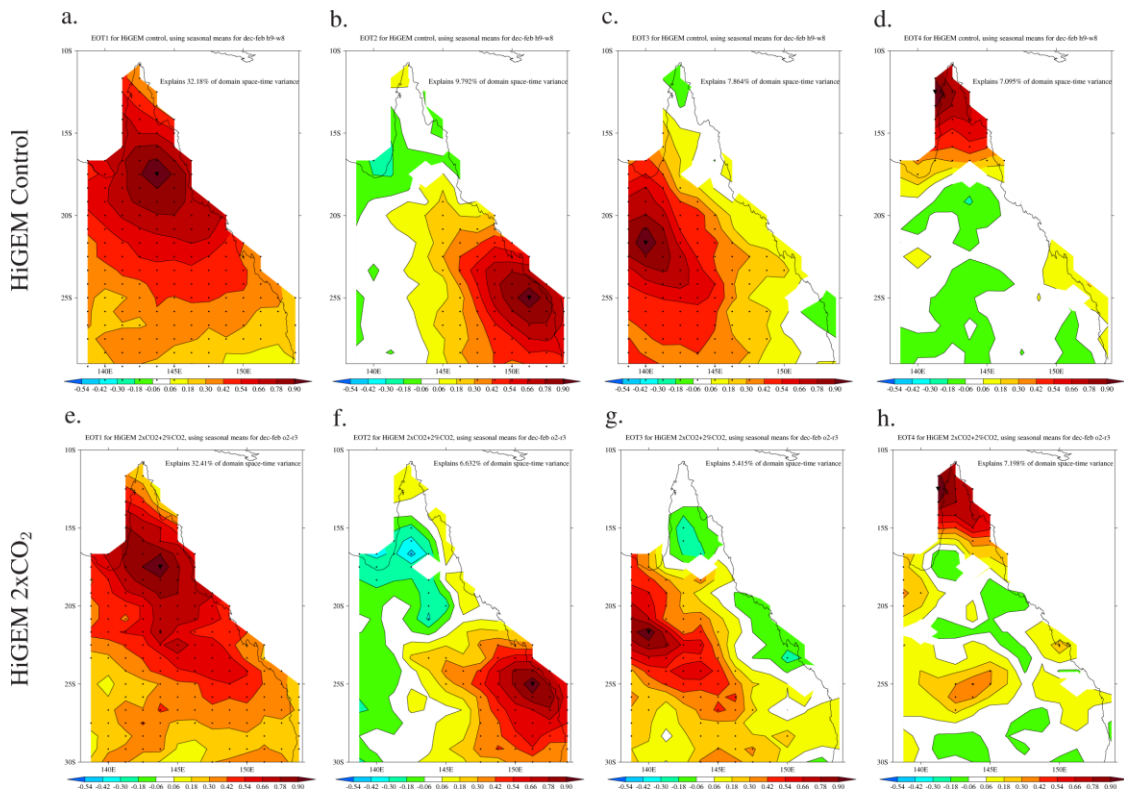


Figure 17: December–February Empirical Orthogonal Teleconnection patterns for (a–d) CTL and (e–h) 2 x CO₂, where the 2 x CO₂ patterns have been constrained to have the same central points as the CTL patterns. The values shown are the correlation coefficients of every point with the central point; stippling indicates correlations that are statistically significant at the 5% level.

In 2 x CO₂, however, there is no indication of blocking activity south of Australia (Fig. 18k) which was prominent in CTL (Fig. 18h) and drove the onshore easterlies. There is little indication of onshore winds in southeast Queensland in 2 x CO₂, although the anomalous low MSLP and enhanced

500 hPa moisture still indicate coastal lows as the driving mechanism for summer rainfall. The appearance of a dry mid-tropospheric anomaly over western Queensland in 2 x CO₂, likely due to dry-air advection from the interior of the continent, explains the anti-correlation between rainfall in the southeast and the northwest in 2 x CO₂.

Variations in western Queensland summer rainfall become less spatially coherent in 2 x CO₂, as indicated by a decreased region of significant correlations in 2 x CO₂ DJF EOT3 (Fig. 17g) relative to CTL DJF EOT3 (Fig. 17c). In 2 x CO₂, DJF EOT3 describes only rainfall in a band extending northwest–southeast; correlations between northwestern Queensland rainfall and rainfall in the southwest and central portions of the state decline considerably. Combined with the appearance of the anti-correlation between the southeast and northwest in 2 x CO₂ DJF EOT2 (Fig. 17f), these shifts suggest that rainfall variations in northwest Queensland become disconnected from those in the rest of the state in 2 x CO₂. The driving mechanism for DJF EOT3 remains the same in 2 x CO₂ (Figs. 18p–r) as in CTL (Figs. 18m–o): southward advection of moist air across the northwest of the state from the Gulf of Carpentaria. The anomalies in 500 hPa moisture cover only the northwest of Queensland in 2 x CO₂ (Fig. 18r), however, in contrast to the entire state in CTL (Fig. 18o), which may be due to the westward shift of the anomalous 500 hPa cyclonic circulation in 2 x CO₂ that in CTL was associated with the northerly wind anomalies. This likely explains the reduced correlations between summer rainfall in northwest Queensland and the rest of the state: the mechanism driving variations in northwest Queensland shifts west in 2 x CO₂ and no longer affects the entire state.

CTL DJF EOT4 (Fig. 17d) corresponds to DJF EOT2 in observations (Klingaman, 2012a); it describes rainfall variations in Cape York and is connected to the frequency of tropical cyclones. The spatial structure of this EOT remains consistent to CTL in 2 x CO₂ (Fig. 17h), as do its associated circulation patterns: anomalous westerlies across Cape York at 850 hPa (Fig. 18t for CTL and Fig. 18w for 2 x CO₂) and 500 hPa (Figs. 18u and 18x), with a stronger relationship between Cape York rainfall and 500 hPa specific humidity.

Regressions of seasonal tropical-cyclone track and genesis densities from 2 x CO₂ on 2 x CO₂ DJF EOT4 (Figs. 19c and 19d) reveal a similar pattern to the same regressions for CTL (Figs. 19a and 19b). In CTL and 2 x CO₂, summer rainfall variations in Cape York are connected to variability in tropical-cyclone counts in the Gulf of Carpentaria, across the Cape York Peninsula, and along the eastern coast of Queensland. Wet summers in Cape York are associated with increased tropical cyclogenesis in the Gulf of Carpentaria and, to a lesser extent, in the Coral Sea. There is therefore no change in 2 x CO₂ to this key driver of summer rainfall variability in northern Queensland.

Comparing the DJF EOT patterns from 2 x CO₂ reveals a possible weakening of the relationship between ENSO and state-wide rainfall variations, as well as the appearance of an anti-correlation between northwestern and southeastern Queensland rainfall. Apart from ENSO, however, the drivers of variations in summer Queensland rainfall remain robust in 2 x CO₂.

7.2.2 March - May EOTs

In observations and CTL, the leading spring EOT is connected to locally driven variations in the strength of the late-season summer monsoon (Klingaman, 2012b, a), which in CTL affect the entire state except for southeastern Queensland (Fig. 20a) where by March the wet season has already ended (Fig. 14c). 2 x CO₂ MAM EOT1 (Fig. 20e) explains rainfall variations over less of the state than its CTL counterpart, particularly in the south and east. The smaller area of significant correlations is likely to be due to the earlier retreat of the monsoon circulation in 2 x CO₂ (Fig. 14d), making rainfall variations in the north—where the central point for MAM EOT1 lies and where the monsoon is still active in 2 x CO₂ in March—less connected to those in the south. The climate driver of these rainfall variations remains the same, however, as the patterns of SSTs (Figs. 21a and 21d), MSLP and 850 hPa winds (Figs. 21b and 21e) and 500 hPa winds and specific humidity (Figs. 21c and 21f) are similar in 2xCO₂ and CTL. As in CTL, there is no significant correlation between state-wide autumn Queensland rainfall and ENSO in 2 x CO₂.

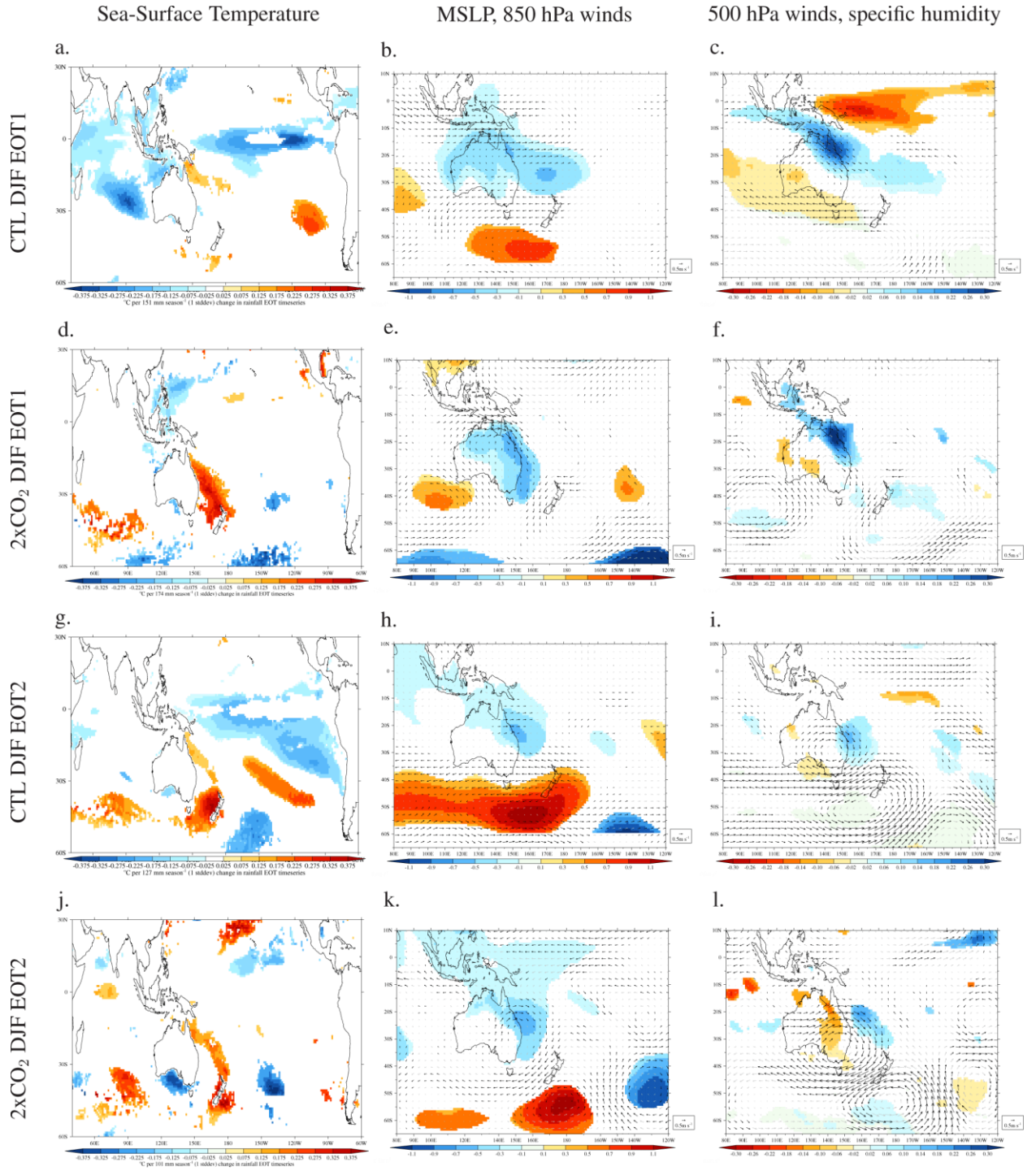


Figure 18: Coefficients of linear regression for gridpoint timeseries of DJF-mean (left column) SST (K); (centre, colours) mean-sea-level pressure (hPa) and (vectors) 850 hPa winds (m s^{-1}); (right, colours) 500 hPa specific humidity (g kg^{-1} and (vectors) 500 hPa winds (m s^{-1}) regressed on the timeseries of (a–c) CTL DJF EOT1; (d–f) $2 \times \text{CO}_2$ DJF EOT2; (g–i) CTL DJF EOT2; (j–l) $2 \times \text{CO}_2$ DJF EOT2; (m–o) CTL DJF EOT3; (p–r) CTL DJF EOT4; and (s–u) $2 \times \text{CO}_2$ DJF EOT4.

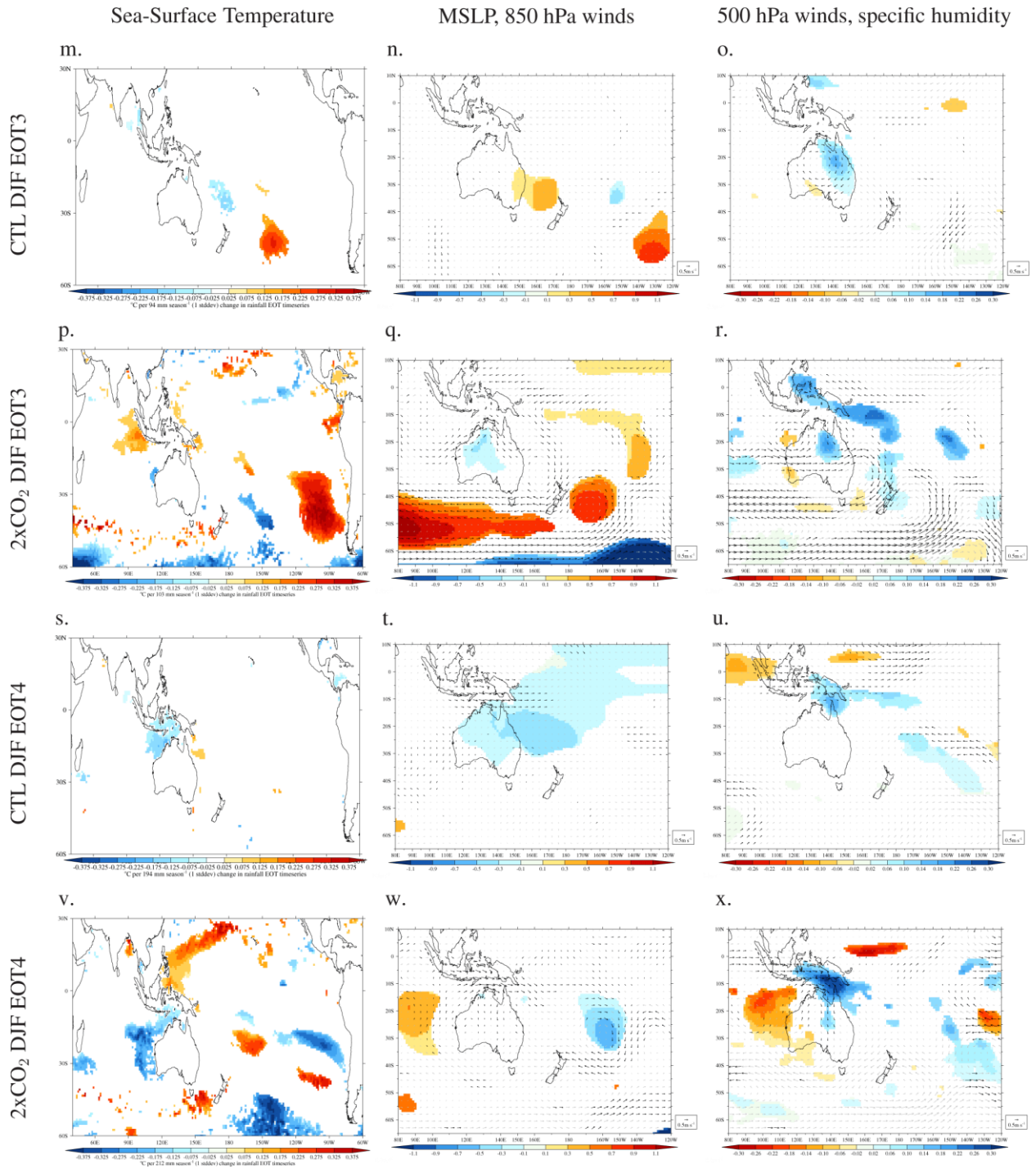


Figure 18: (continued)

The change in the spatial pattern of MAM EOT2 from CTL (Fig. 20b) to 2 x CO₂ (Fig. 20f) further demonstrates that southeastern Queensland autumn rainfall becomes less correlated with rainfall in the rest of the state in 2 x CO₂. In observations and CTL, this EOT was related to coastal cyclones and onshore winds (Fig. 21h) bringing anomalously moist air onshore (Fig. 21i). The regression of MSLP on MAMEOT2 weakens in 2 x CO₂, but there is still evidence on shore easterlies connected to an anomalous anti-cyclonic circulation in the Tasman Sea (Fig. 21k) and anomalously high specific humidity at 500 hPa (Fig. 21l).

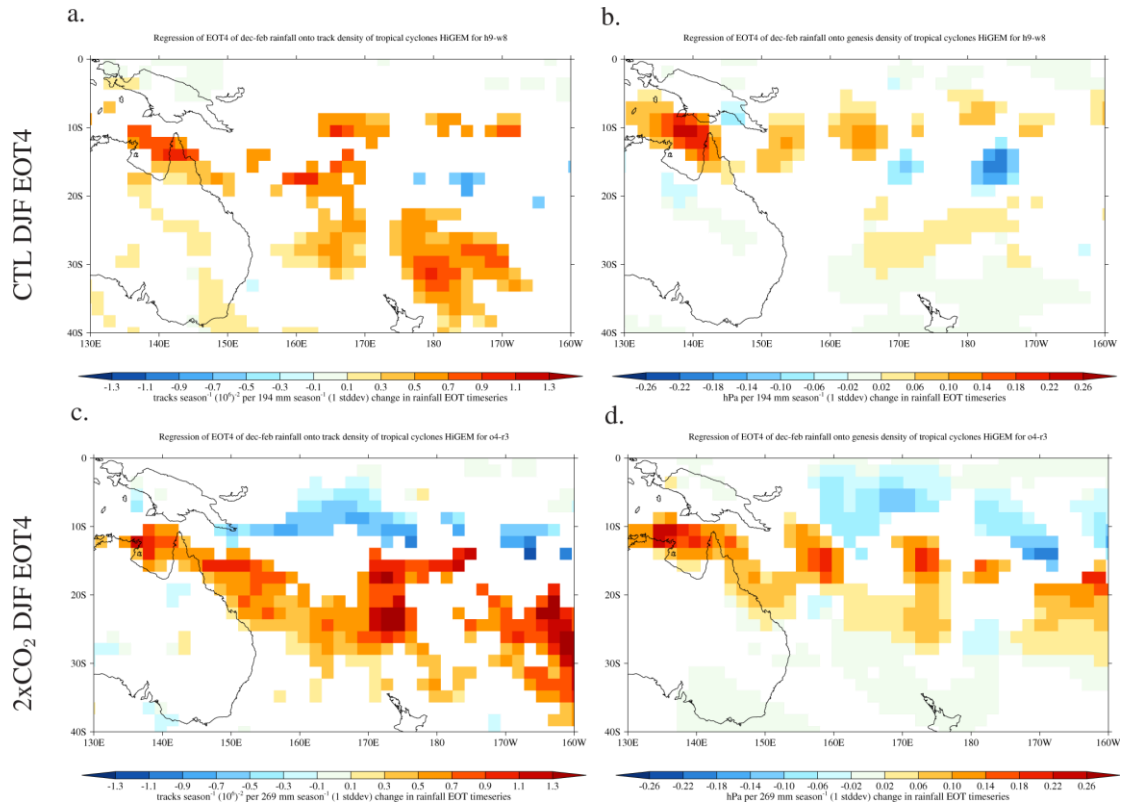


Figure 19: For (a,b) CTL DJF EOT4 and (c,d) 2xCO₂ EOT4, the regression of tropical-cyclone (a, c) track density and (b, d) genesis density on the EOT timeseries. Units are storms season⁻¹ (106 km²)⁻¹ around each gridpoint for a one standard-deviation change in the rainfall EOT timeseries.

Curiously, regressions of SST on 2 x CO₂ MAM EOT2 reveal a relationship between wet autumns in southeastern Queensland and El Niño conditions (Fig. 21j). This association is questionable for three reasons: (a) it reverses the traditional ENSO teleconnection; (b) the circulation patterns reveal little direct connection between the El Niño induced circulation anomalies—divergence and drying in the Maritime Continent and West Pacific, with convergence and moistening in the central Pacific—and the onshore wind anomalies over Queensland that drive MAM EOT 2; and (c) the relatively short 50 year period of 2 x CO₂ does not provide robust statistics of ENSO events (section 6.2.1). There is therefore little confidence in the positive correlation between El Niño SST anomalies and autumn rainfall in southeast Queensland.

In observations, MAM EOT3 represented the ENSO-driven variations in the late-season monsoon across northern Queensland (Klingaman, 2012b). HiGEM CTL correctly reproduced the ENSO correlation, but erroneously located the rainfall variations in western Queensland (Fig. 20c Klingaman, 2012b). This pattern is maintained in 2 x CO₂ (Fig. 20g), although there is also a hint of significant correlations in northern Cape York, in better agreement with SILO MAM EOT3. The relationship between wet autumns in western Queensland and an enhanced late-season monsoon strengthens in 2 x CO₂ (Figs. 21q and 21r) relative to CTL (Figs. 21n and 21o), with increased northwesterly flow into Queensland and greater mid-tropospheric moisture anomalies.

The correlation with ENSO also intensifies in 2 x CO₂, with the SST regression clearly showing La Niña conditions across the Pacific (Fig. 21p). HiGEM therefore projects a stronger relationship between ENSO, the late-season monsoon and western Queensland autumn rainfall. Confidence in this result, however, must be tempered by the incorrect location of the ENSO–rainfall teleconnection in CTL.

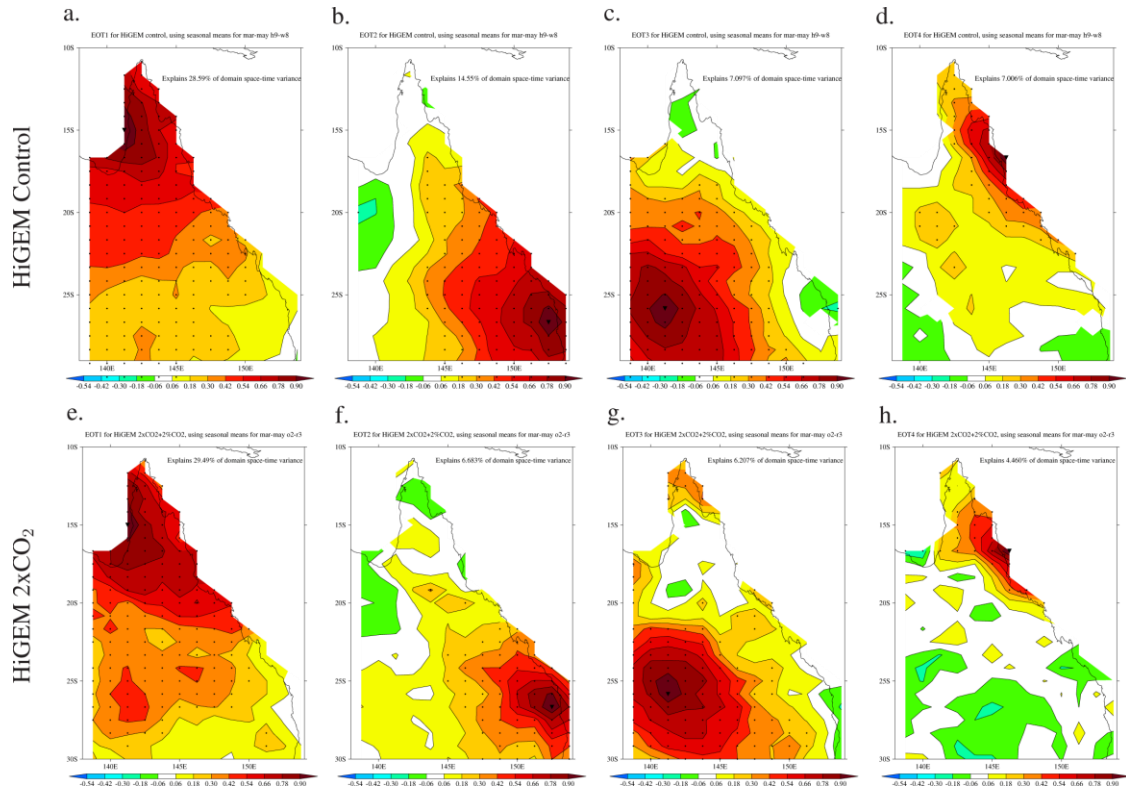


Figure 20: As in Fig. 17 but for March–May EOTs.

MAM EOT4 in CTL represents local variations in autumn rainfall along the northeastern coast (Fig. 20d), which is primarily connected to the strength of the onshore winds (Fig. 21u). There is little change in the spatial pattern (Fig. 20h) or mechanism (Fig. 21x) for this EOT in 2 x CO₂. There are considerable variations in the large-scale regression patterns for SST and mid-tropospheric winds and moisture on MAM EOT4 from CTL to 2 x CO₂, but these do not cleanly project onto any known modes of variability (e.g., ENSO, the monsoon circulation) and so are difficult to connect to any climate driver. Locally, in both CTL and 2 x CO₂ wet autumns along the northeast coast are connected to onshore winds.

7.2.3 June - August EOTs

State-wide variations in winter Queensland rainfall were found to be associated with ENSO in observations (Klingaman, 2012b) and CTL (Klingaman, 2012a). In 2 x CO₂, JJA EOT1 shows reduced correlations between the eastern and western halves of Queensland (Fig. 22e) compared to CTL (Fig. 22a), with the rainfall variations in the southwest becoming particularly isolated from the rest of the state. SST regressions demonstrate that, as for DJF EOT1 (Figs. 18a and 18d), the relationship between state-wide rainfall and ENSO weakens in winter in 2 x CO₂ (Fig. 23d) relative to CTL (Fig. 23a). Wet winters in Queensland remain related to warm SSTs in the Maritime Continent and to the north of Australia in 2 x CO₂, but there are no significant correlations with equatorial Pacific SSTs and no signals of the SOI in the MSLP regressions (Fig. 23e). Across Australia, however, the circulation patterns associated with JJA EOT1 in 2 x CO₂ (Figs. 23e and 23f) are consistent with those from CTL (Fig. 23b and 23c): anomalous northerly and northeasterly winds across Queensland bringing moist air south from the Maritime Continent across the region of warm SSTs.

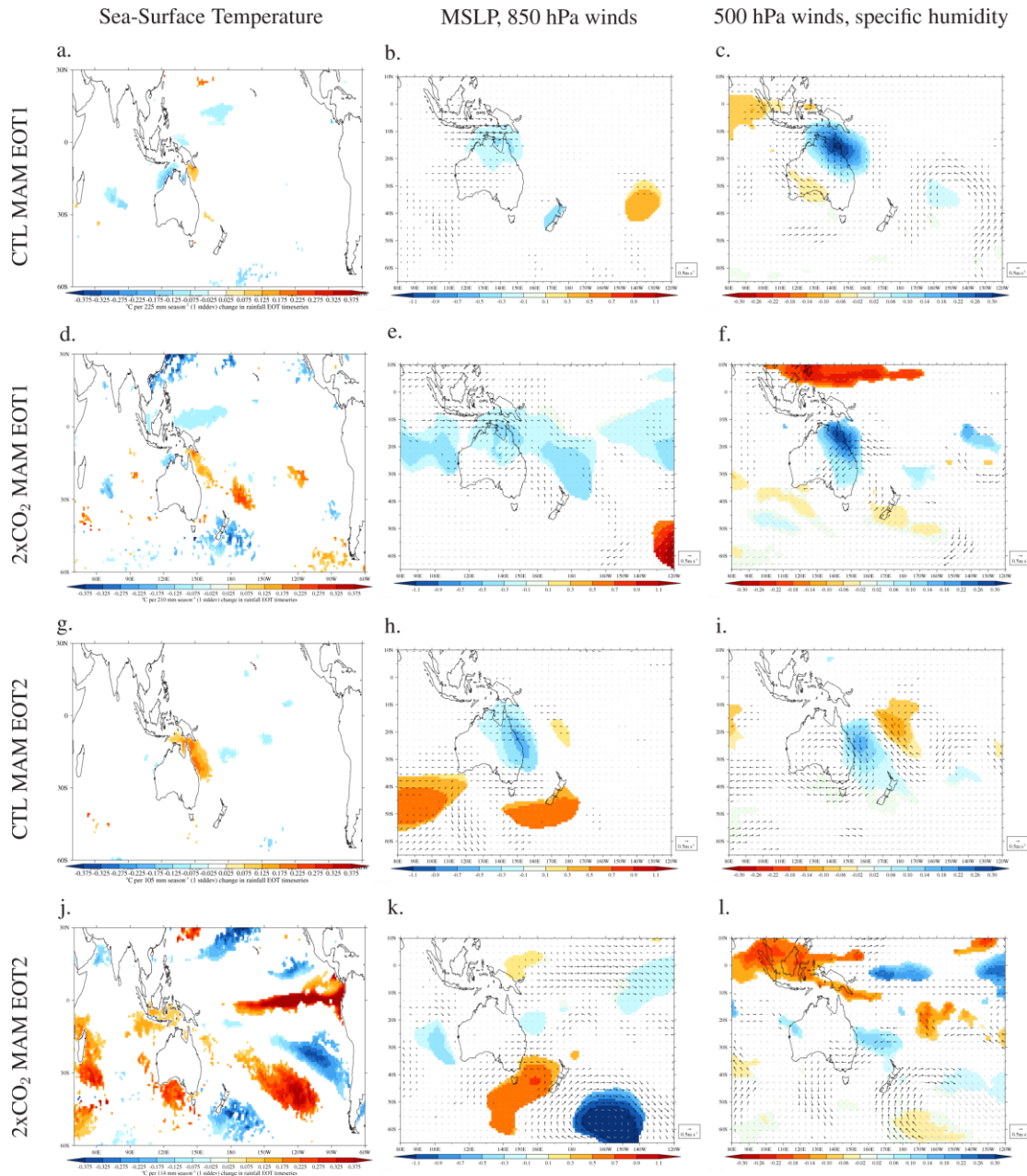


Figure 21: As in Fig.18 but for MAM seasonal-mean quantities regressed on the timeseries of MAM EOTs.

JJA EOT2 (Fig. 22b) describes rainfall variations in southern Queensland, primarily in the southeast, and in observations and CTL was shown to be driven by Southern Ocean blocking and onshore easterly winds (Fig. 23h Klingaman, 2012b, a). The spatial pattern of JJA EOT2 remains similar in 2 x CO₂ (Fig. 22f) with small increases in the correlation between southeastern Queensland and points further north along the east coast. The circulation patterns are broadly consistent between CTL (Figs. 23h and 23i) and 2 x CO₂ (Figs. 23k and 23l), although the anti-cyclone in the Southern Ocean reduces in extent; the onshore winds across southern Queensland remain statistically significant.

In CTL, HiGEM did not correctly simulate JJA EOT3—describing variations in dry-season precipitation in northern Queensland (Fig. 22c—from the SILO observations (Klingaman, 2012a), which was driven by coastal cyclones and the southward transport of moisture across northern Queensland (Klingaman, 2012b). There is little change between CTL JJA EOT3 and 2xCO₂ JJA EOT3, either in spatial pattern—comparing Figs. 22c and 22g— or in the regressions of SST, MSLP and 850 hPa and 500 hPa winds—comparing Figs. 23p–r and 23m–o. 2 x CO₂ shows a strong signal

of Southern Ocean blocking, but the circulation around the anti-cyclonic anomalies does not impact Queensland. Given that CTL failed to simulate this EOT correctly and that it essentially represents very small variations in dry-season precipitation, no further analysis of this pattern is warranted. No climate driver was found for CTL JJA EOT4 in Klingaman (2012a), which explains very little variance in Queensland winter rainfall. While the regression maps for this pattern are shown in Figs. 23s–u for CTL and Figs. 23v–x for 2 x CO₂, there is no significant driver for this pattern; it is not considered further.

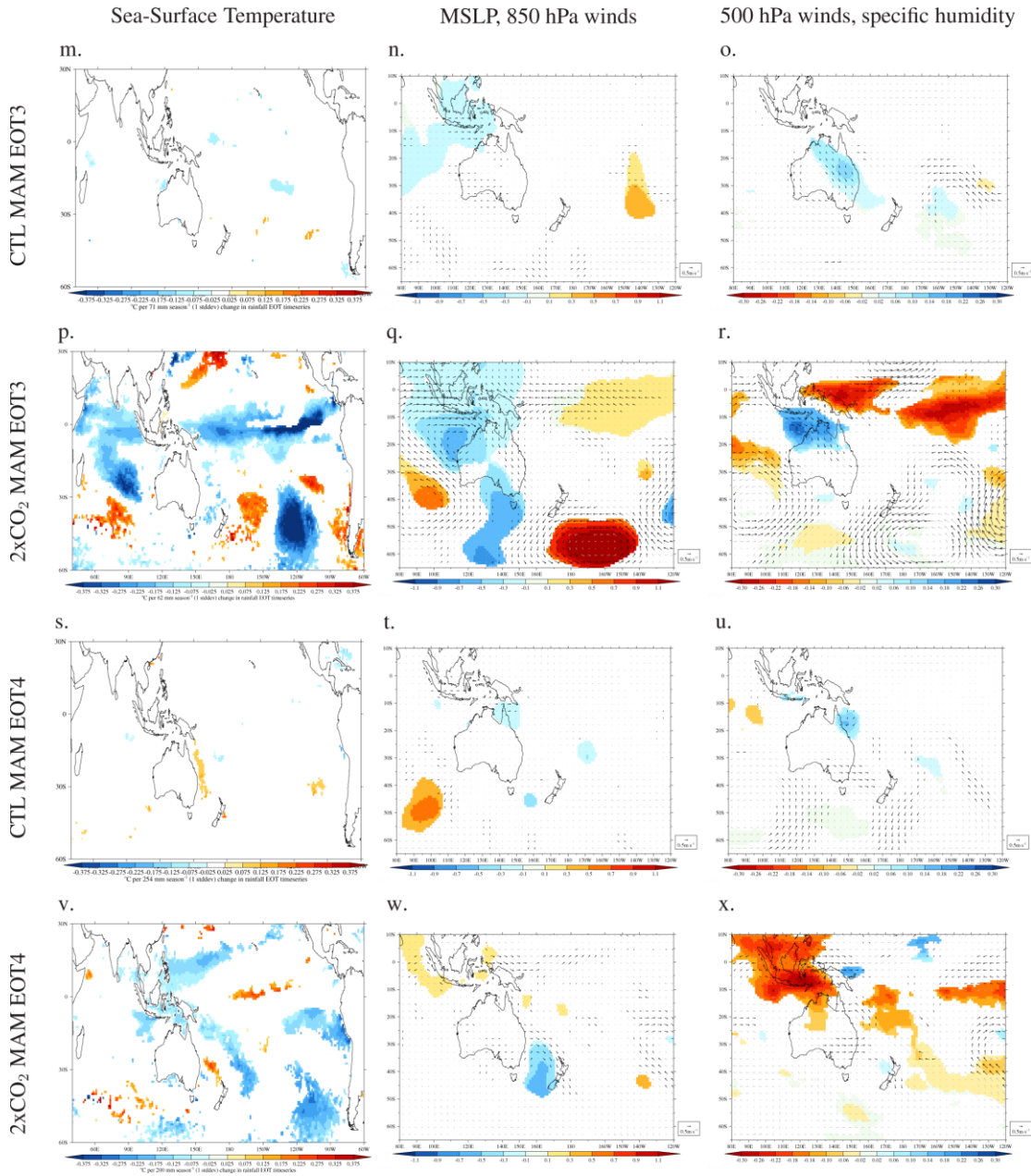


Figure 21: (continued)

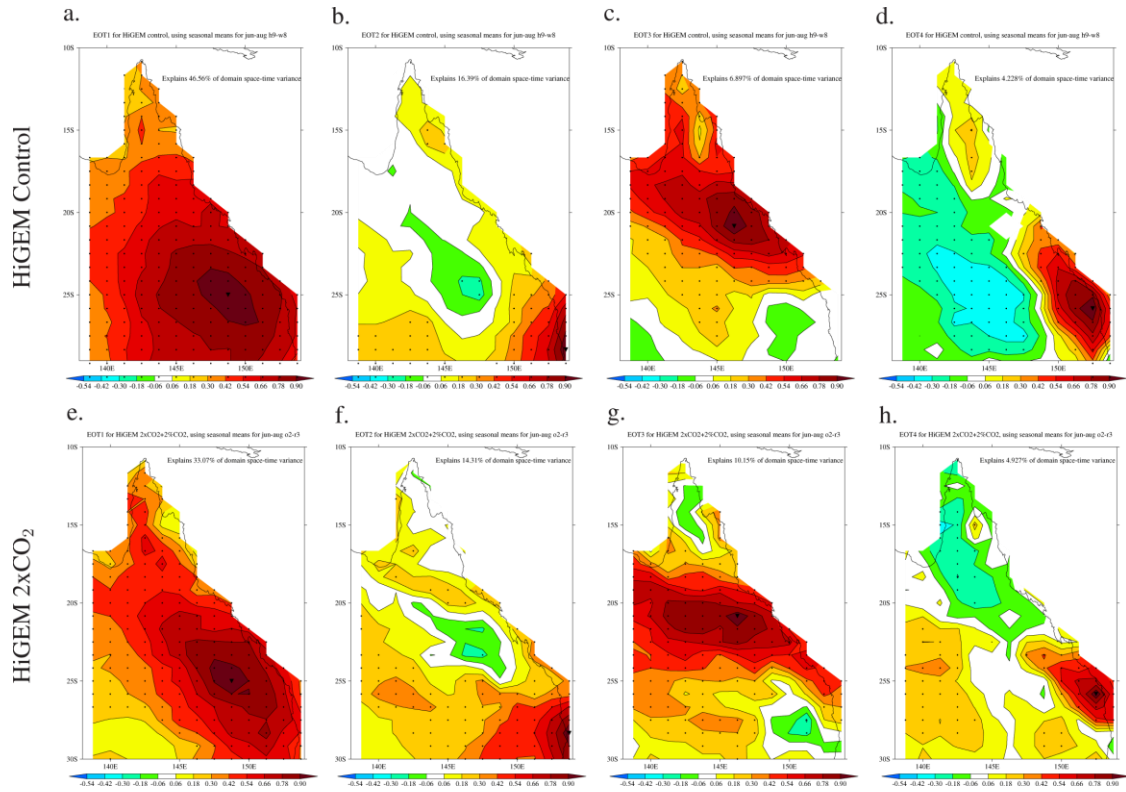


Figure 22: As in Fig. 17 but for June–August EOTs.

7.2.4 September - November EOTs

In spring, the leading, state-wide rainfall EOT is associated with ENSO and the SAM in observations (Klingaman, 2012b), HiGEM CTL (Fig. 25a Klingaman, 2012a) and 2 x CO₂ (Fig. 25d). Spring is the only season in 2 x CO₂ that features a robust, statistically significant teleconnection between ENSO and state-wide Queensland rainfall. Wet springs are dominated by La Niña conditions in the Pacific and warm SSTs around the Maritime Continent and to the north and east of Australia. There is essentially no change in the spatial pattern of SON EOT1 between CTL (Fig. 24a) and 2 x CO₂ (Fig. 24e). The circulation patterns are also consistent, with wet springs featuring an enhanced cyclonic flow and anomalously low MSLP over Australia and 500 hPa moisture anomalies across the Maritime Continent and into Queensland in both CTL (Figs. 25b and 25c) and 2 x CO₂ (Figs. 25e and 25f). The positive correlation seen in CTL between SON EOT1 and the SAM (Fig. 26a Klingaman, 2012a) remains robust in 2 x CO₂ (Fig. 26b), albeit with a slightly weaker regression coefficients.

Since HiGEM CTL did not reproduce either SON EOT2 or SON EOT3 from the SILO observations (Klingaman, 2012a), the 2 x CO₂ EOT patterns beyond the EOT1 are discussed only briefly. SON EOT2, which describes spring rainfall variability in coastal Queensland, does not change between CTL (Fig. 24b) and 2 x CO₂ (Fig. 24f). Wet springs along the coast in 2xCO₂ remain driven by the southward transport of moist air from the equator, with anomalous northwesterly winds at both 850 hPa (Fig. 25k) and 500 hPa (Fig. 25l), consistent with CTL (Figs. 25h and 25i). SON EOT3 was associated with weakening ENSO events in CTL (Fig. 24m)—as in SILO SON EOT2— but as with MAM EOT3, HiGEM erroneously centred the ENSO-driven rainfall variations in the southwest of Queensland (Fig. 24c) instead of the north (Klingaman, 2012a). In 2 x CO₂, SON EOT3 is restricted even further to the southwest (Fig. 24g) but is no longer connected to ENSO (Fig. 24q). Instead, rainfall in southwest Queensland is driven by anomalously moist northerly flow at 500 hPa (Fig. 24r) that is connected to a cyclonic circulation over Western Australia that draws air from the Indian Ocean across northern Australia.

In 2 x CO₂, SON EOT4 displays a relationship between El Niño (Fig. 25v) and wet springs in southeast Queensland (Fig. 24h), similar to that for MAM EOT2 (Fig. 21j) that also describes rainfall

variations in the southeast. Given the small sample size of ENSO events in 2 x CO₂ (section 6.2.1) and the lack of a connection between SON EOT4 and ENSO in CTL (Fig. 25s), these results should be viewed sceptically.

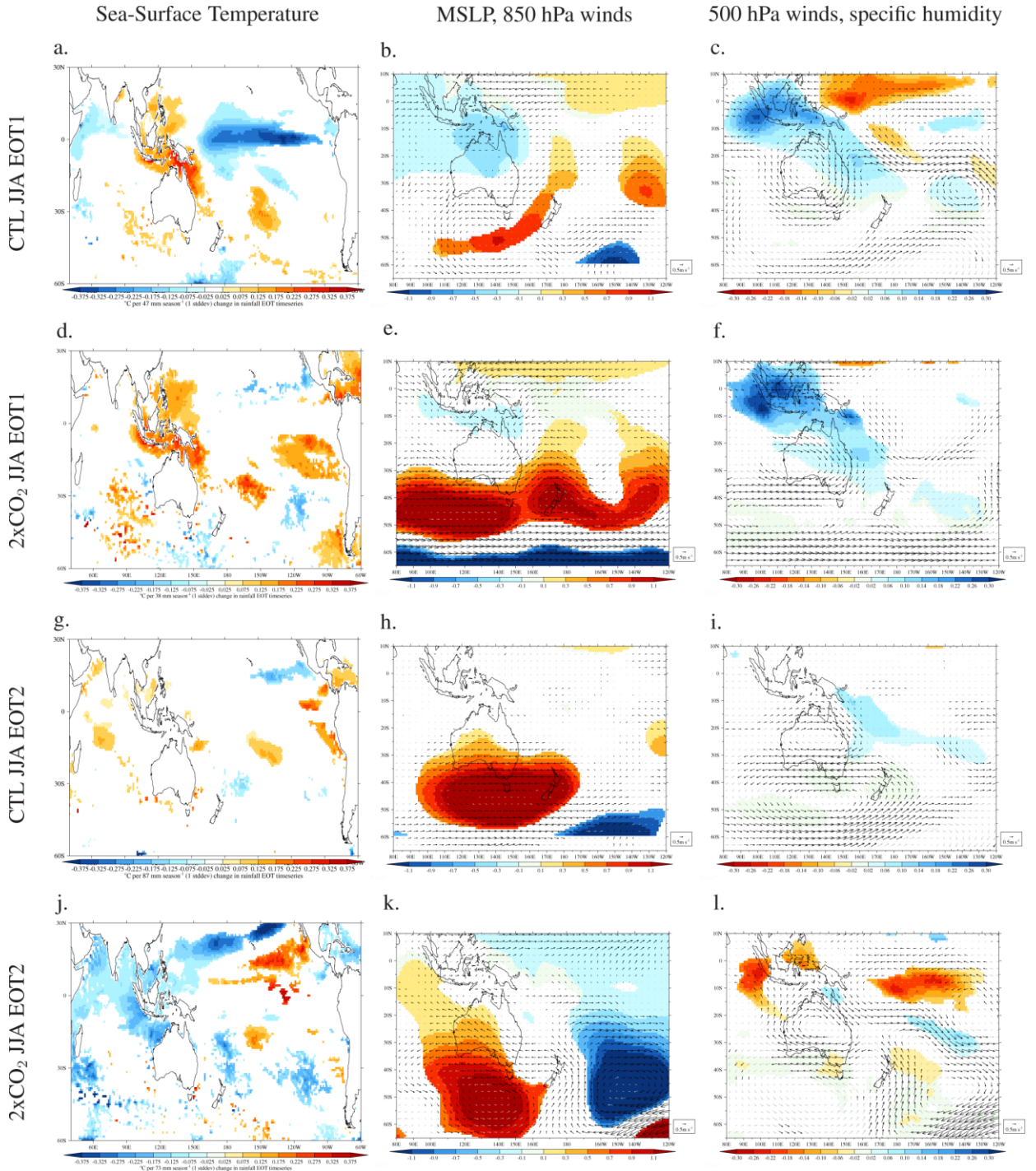
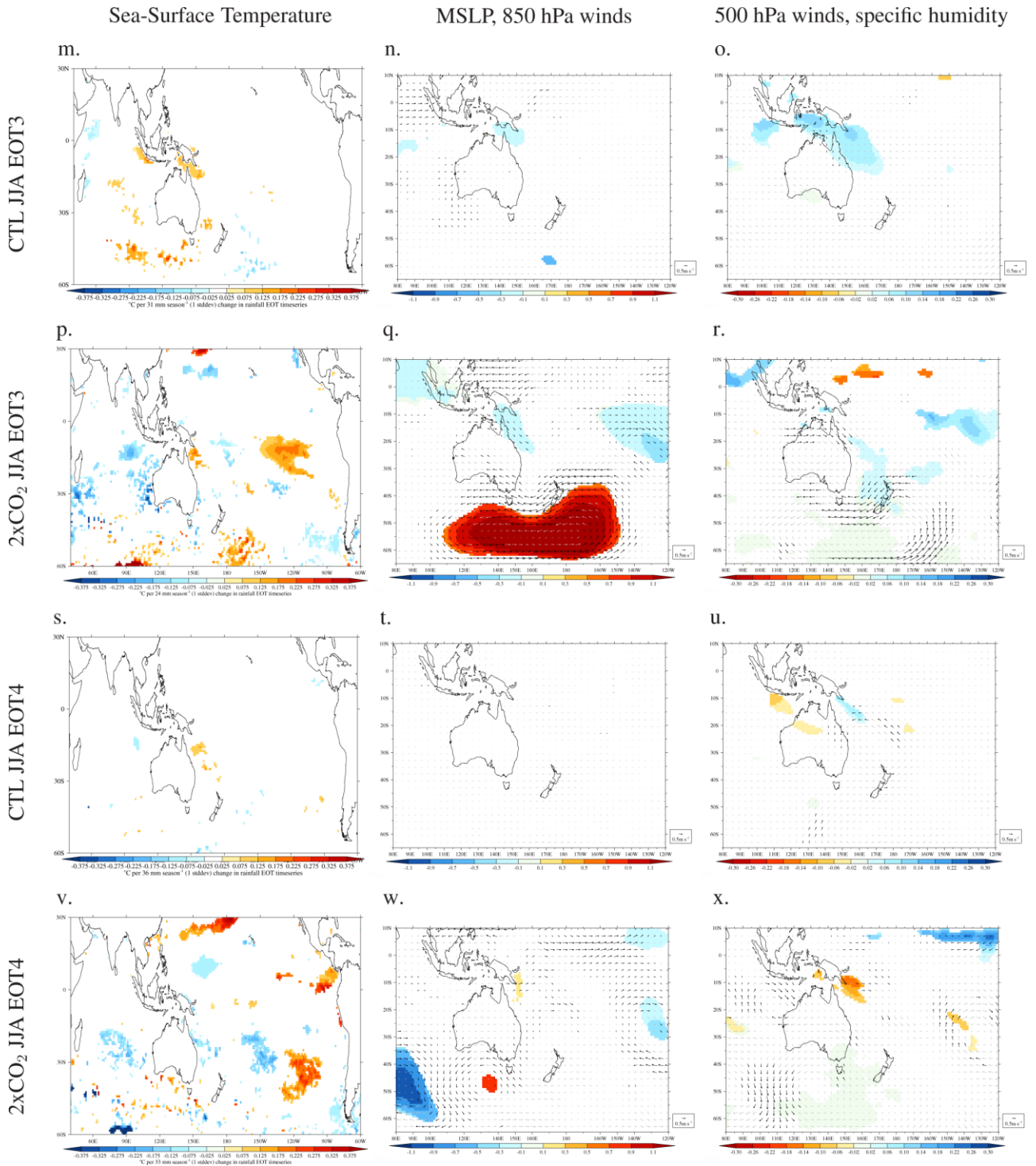


Figure 23: As in Fig.18 but for JJA seasonal-mean quantities regressed on the timeseries of JJA EOTs.



(Figure 23: continued)

Projected changes in Queensland rainfall under double-CO₂ conditions in the HiGEM model

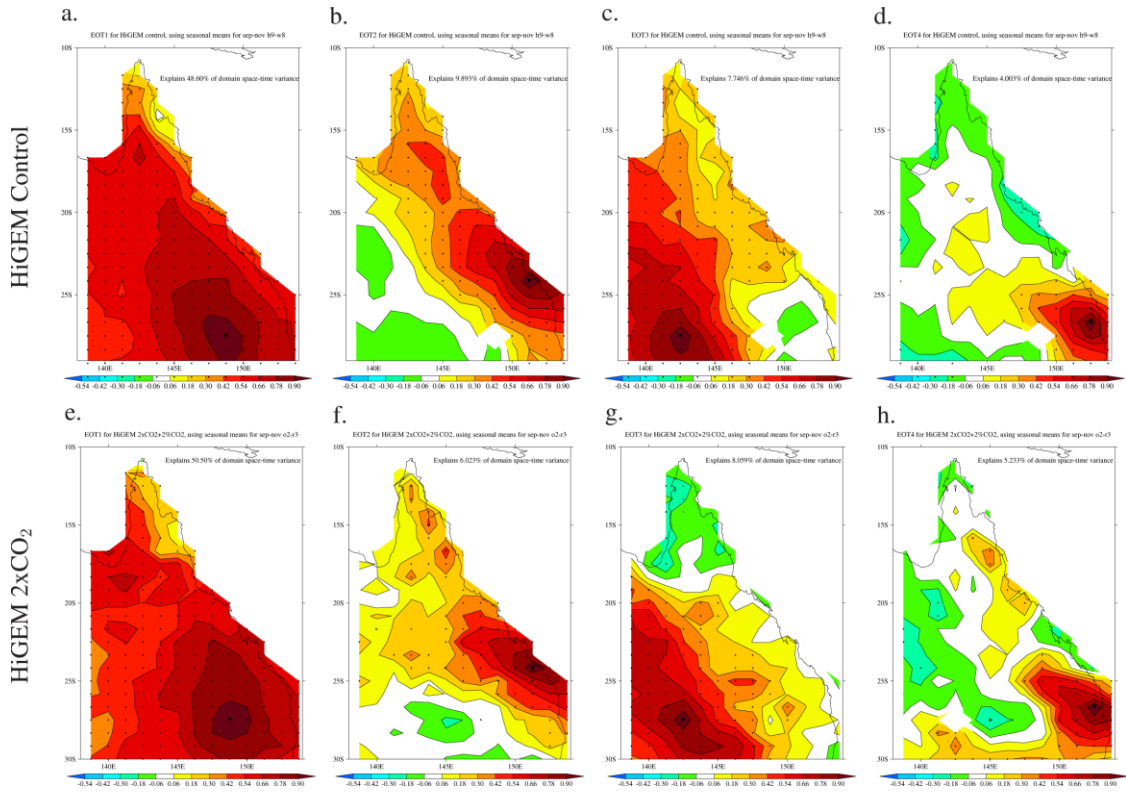


Figure 24: As in Fig. 17 but for September–November EOTs.

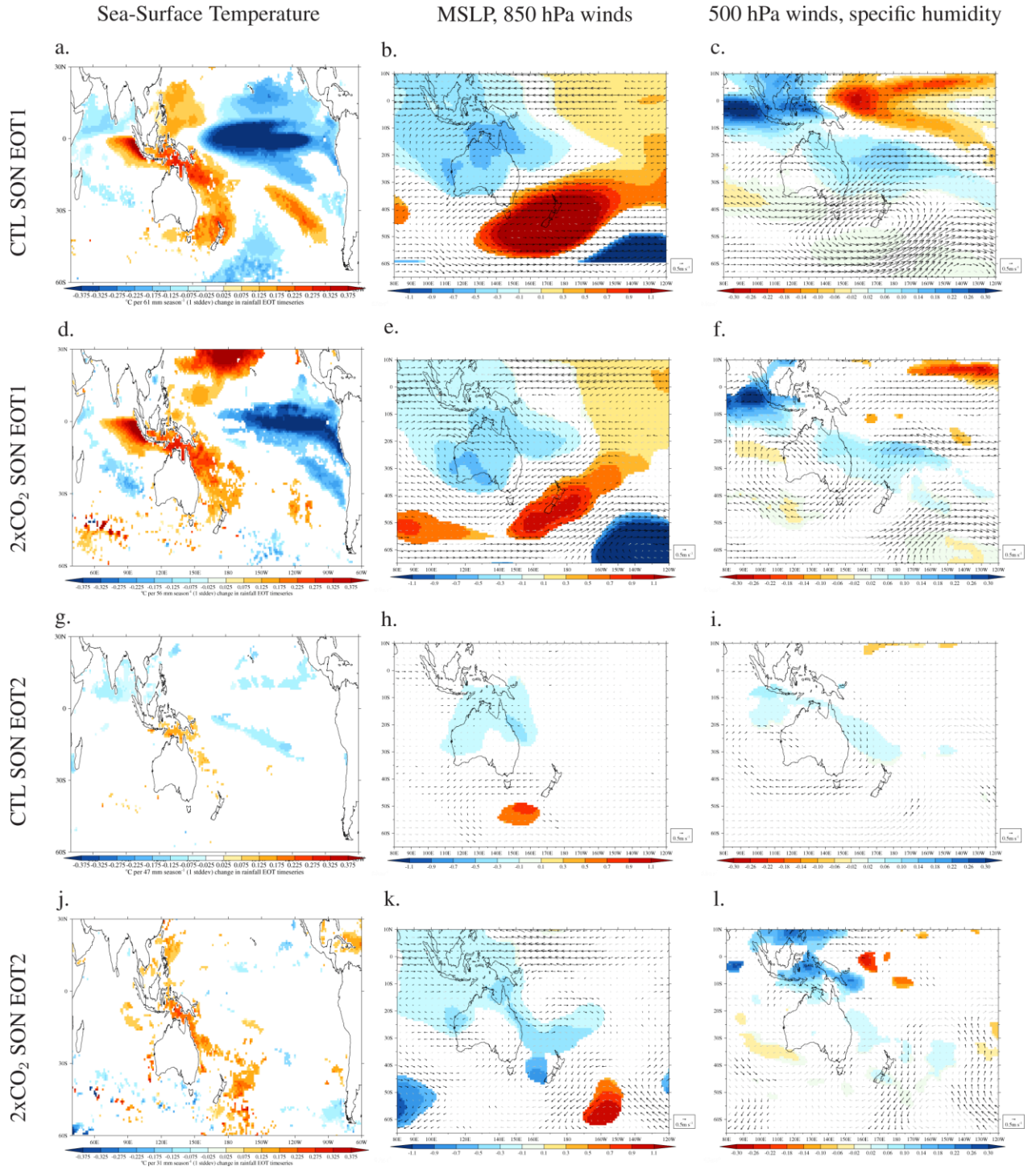
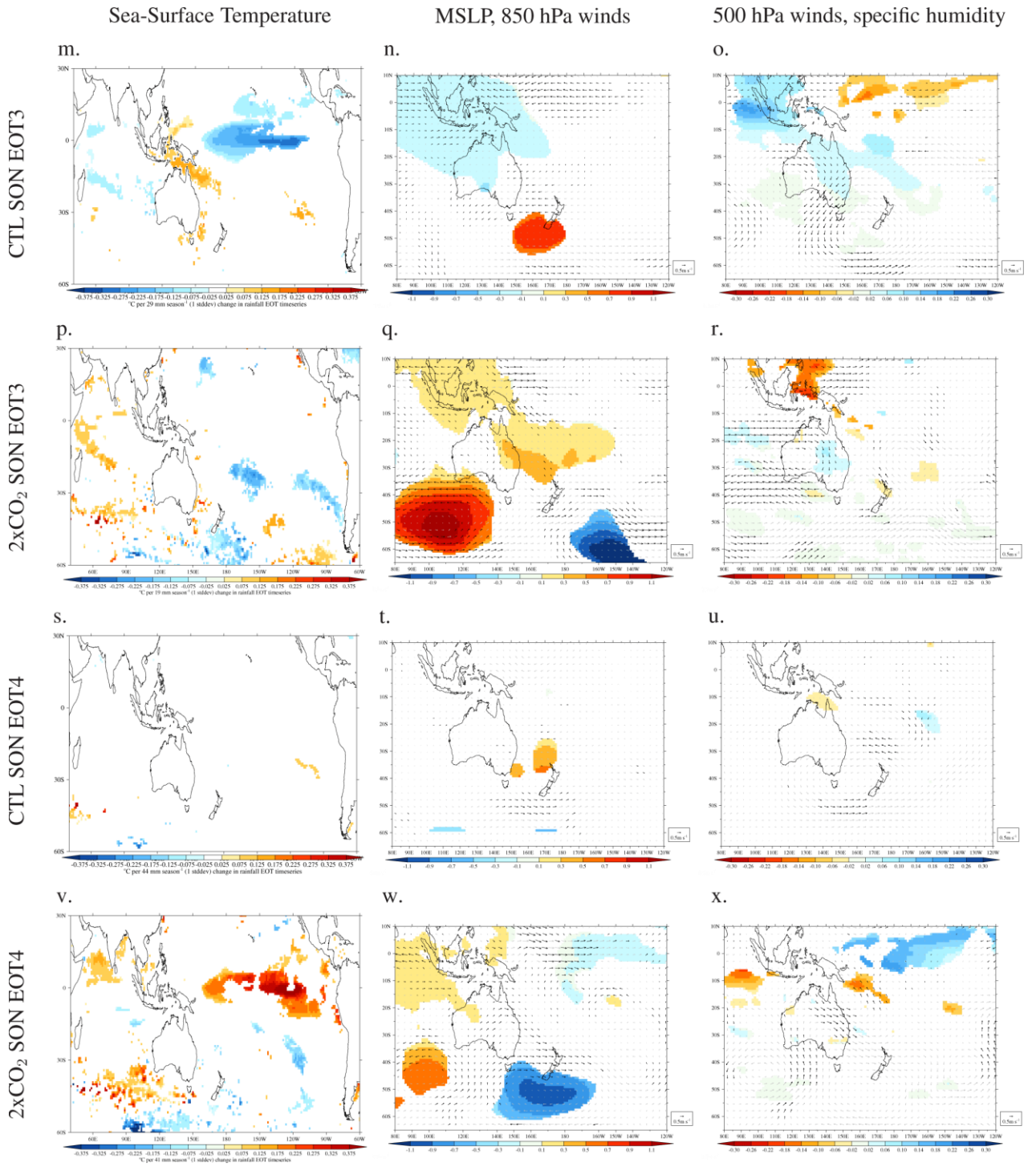


Figure 25: As in Fig. 18 but for SON seasonal-mean quantities regressed on the timeseries of SON EOTs.



Projected changes in Queensland rainfall under double-CO₂ conditions in the HiGEM model

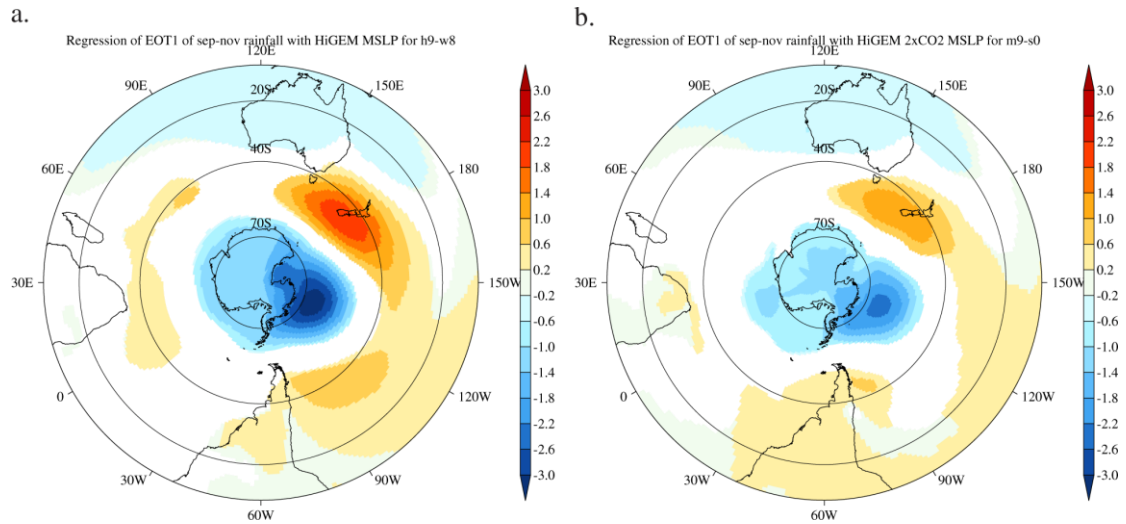


Figure 26: (a) As in Fig. 25a but for MSLP only; (b) as in Fig. 25d but for MSLP only.

8 Discussion

The projected compression of the present-day wet season under doubled atmospheric CO₂, combined with the tendency toward more frequent and intense extreme events, would have considerable consequences for agriculture, hydrology and infrastructure. With the same total precipitation projected to fall in a shorter wet season, soils would become saturated more quickly in summer, potentially leading to dangerous levels of runoff into river basins and more frequent inland flooding. Summers become wetter in 2 x CO₂ because the average intensity of daily rainfall increases, while the number of wet days remains roughly similar to the present-day. Heavier rainfall events are associated with greater runoff, particularly when soils are already saturated from previous events, and hence the increased average intensity points to an increased risk of flooding. The projected increases in the frequency, intensity, duration and size of extreme daily rainfall events would also lead to more and heavier floods throughout the state, particularly in summer when these increases are largest.

A shorter, sharper wet season would also lead to a greater need for water storage in Queensland. HiGEM 2 x CO₂ projects that much of Queensland will rely more strongly on intense mid-summer rains for its annual rainfall. Under such a scenario, capturing and storing mid-summer rainfall would become increasingly important, as precipitation in the surrounding seasons (i.e., autumn and late spring) is projected to decline. Further, if the mid-summer rains fail then the entire year will likely be dry, due to the overall decrease in average precipitation in the other seasons. Sequestering water from plentiful years would therefore become even more critical to maintaining adequate water supplies in the state.

In the context of the above results, it is worth highlighting that HiGEM 2 x CO₂ projected no change in inter-annual rainfall variability in a warmer world. This suggests that the primary effect of increased carbon dioxide in this model is to produce a shift in the mean climate, rather than to increase or reduce climate variability. Although HiGEM projects that summers will become wetter overall and autumns drier overall, the differences between wet and dry years remain roughly the same as the present day. Importantly, these results still imply increases in the probability of extremely wet summers and extremely dry autumns—as viewed from the perspective of the present-day climate—but HiGEM projects that the cause of these changes is a shift in the mean, rather than increased climate variability. Climate variability does not “compound” climate change in this model. The changes in the mean rainfall in 2 x CO₂ are due to most years becoming wetter or drier than the CTL average, not to a few extreme, outlying years in 2 x CO₂ influencing the mean rainfall.

Projected changes in decadal variability were not analysed in this report. This was in part because there are only 50 years of model data from 2 x CO₂, which would have produced few samples with which to attempt to detect any changes in decadal variability. Further, Klingaman (2012a) found that HiGEM CTL had much lower-than-observed levels of decadal variability in Queensland rainfall. This was thought to be due to a lack of decadal variability in Pacific Ocean temperatures—either from an Inter-decadal Pacific Oscillation or from decadal variability in ENSO activity—which have previously been shown to be a key driver of decadal rainfall variations in eastern Australia (e.g. Power et al. 1999, 2006).

Associated with the small changes in inter-annual rainfall variability, HiGEM 2 x CO₂ projected only minor variations in the climate drivers of Queensland rainfall. EOT analysis on 2 x CO₂ found that most of the climate drivers identified in CTL (Klingaman, 2012a) remained robust in a warmer world, including the strength and moisture content of onshore winds—important for southeastern and coastal Queensland rainfall—and tropical cyclones—critical for Cape York summer rainfall.

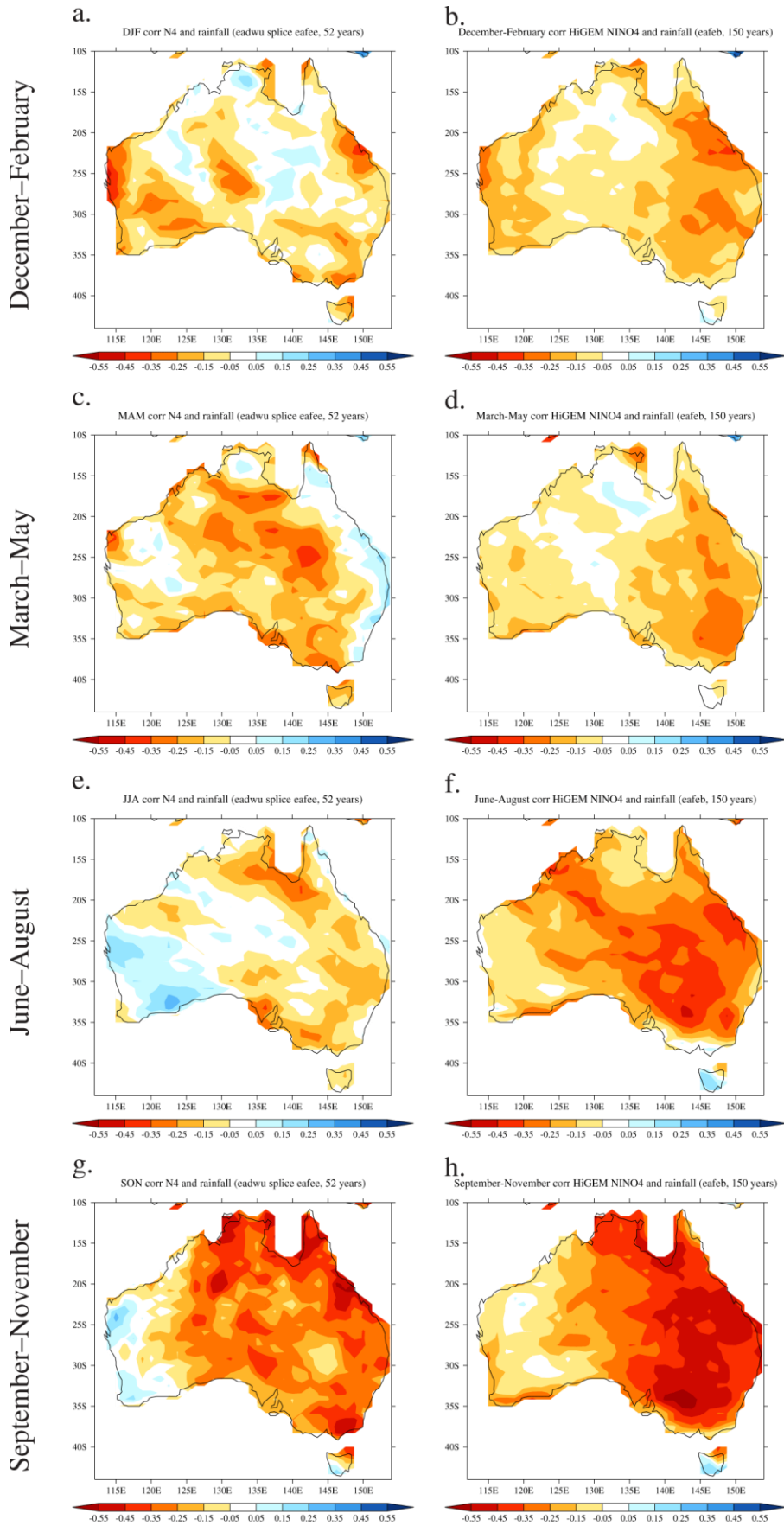


Figure 27: Linear correlations between seasonal-mean Niño 4 SSTs and gridpoint rainfall for (left column) 2 x CO₂ and (right column) CTL in (a, b) December–February, (c, d) March–May, (e, f) June–August and (g, h) September–November. The 2 x CO₂ rainfall and SSTs were de-trended prior to computing the correlation.

The only climate driver to weaken substantially was ENSO, which was no longer associated with the leading EOTs in summer and winter. This decline in the teleconnection between ENSO and state-wide summer and winter rainfall is also reflected in the overall correlation between Niño 4 SSTs and seasonal-mean rainfall in 2 x CO₂ (Fig. 27). HiGEM 2 x CO₂ projects weaker correlations between eastern Australian rainfall and ENSO in all seasons, particularly in summer (Fig. 27a) and winter (Fig. 27e) relative to CTL (Figs. 27b and 27f).

The cause of this systematic weakening of the teleconnection is unclear. It is possible that the weaker correlations arise from sampling variability, as there are only 50 years of data available from 2 x CO₂. A longer 2 x CO₂ integration or multiple ensemble members would allow this hypothesis to be tested and the sources of any statistically robust reduction in the ENSO correlation to be identified.

There are two key caveats associated with these results that limit their direct applicability to adaptation decisions.

First, these results are based on analysis of only a single model. Klingaman (2012a) found that the HiGEM control simulation accurately reproduced many of the key climate drivers of Queensland rainfall. While this increases our confidence in the projected rainfall changes from HiGEM 2 x CO₂, that simulation should not be interpreted as an accurate prediction of the impact of increased CO₂ on Queensland rainfall. Rather, 2 x CO₂ is one possible future scenario generated from a climate model that has been shown to perform well for Queensland climate under a present-day forcing scenario. Ideally, adaptation decisions would be based on projections from a set of climate models that all faithfully simulate the observed climate drivers of Queensland rainfall.

The potential exists to extend the EOT-based model validation technique of Klingaman (2012a) to a suite of models, to distinguish between the better- and lesser-performing models for Queensland. Such analysis would be much better able to reduce uncertainty in future projections of Queensland rainfall and inform adaptation decisions.

A second caveat is that HiGEM 2 x CO₂ projects only the CO₂-forced change in Queensland future climate. All other forcings, including methane, ozone and aerosols, were left fixed at present-day values. While CO₂ is likely to be the largest driver of future global climate change, non-CO₂ forcings will certainly play a role as well, particularly on the regional scale. HiGEM 2 x CO₂ therefore does not represent a complete picture of the late-21st century climate, as it does not include these additional forcings.

This does not invalidate the findings of this report, which was intended to examine the response of Queensland rainfall to increasing atmospheric CO₂. It does mean, however, the direct comparisons cannot be made between the HiGEM 2 x CO₂ results and those from climate models running IPCC SRES or Representative Concentration Pathway (RCP) scenarios. For these two reasons, it is critical that these results are interpreted only as the projections from one model of CO₂-driven changes in Queensland rainfall.

9 Summary and conclusions

This report has examined projected changes in Queensland climate under approximately double the present day atmospheric carbon-dioxide (CO₂) concentrations (690 parts per million) from the HiGEM climate model. HiGEM is a high-resolution (90 km in the atmosphere, 30 km in the ocean) coupled atmosphere–ocean general circulation model based on the U.K. Met Office Hadley Centre’s HadGEM1 model. Previous research (Klingaman, 2012a) has found that under present-day climate forcings, HiGEM reliably simulates most of the key climate drivers of inter-annual rainfall variability in Queensland. This increases our confidence in the model’s ability to project changes due to increased CO₂ in both Queensland rainfall itself and the climate drivers of inter-annual rainfall variability.

Fifty years of the HiGEM doubled-CO₂ (2 x CO₂) projections were compared to the 150-year present-day control simulation (CTL) analysed in Klingaman (2012a). The 690 ppm of CO₂ in 2 x CO₂ is roughly equivalent to the CO₂ concentration at 2090 under the moderate-emissions IPCC SRES A1B scenario. It is important to note, however, that in 2 x CO₂ only the CO₂ concentration has been increased; other forcings (e.g. methane, aerosols and ozone) were left at their present-day values.

In 2 x CO₂, HiGEM projects that Queensland land-surface temperatures warm by approximately 2°C, with the greatest warming during the dry season in winter when the skies are predominantly clear (Fig. 1). Consistent with many other climate models, the land warms more than the ocean; the interior of Queensland therefore warms more than the coastal regions. HiGEM simulates neither an “El Niño-like” nor a “La Niña-like” pattern of warming in the equatorial Pacific.

The summer monsoon circulation strengthens in 2 x CO₂, with increased westerly winds at 850 hPa across northern Australia (Fig. 3a). This results in anomalous low-level convergence over Queensland, as the stronger westerlies encounter the climatological easterly trades (Fig. 2). By contrast, in autumn the late-season monsoon weakens considerably, with easterly anomalies and anomalous low-level divergence over much of northern Australia, including Queensland (Fig. 3b). This represents an acceleration of the present-day seasonal cycle, in which the monsoon circulation becomes more intense in summer but retreats more quickly in autumn.

There is little change in annual-total rainfall across Queensland in 2 x CO₂ (Figs. 4 and 5). The annual total signal results from the cancellation of two large, oppositely signed seasonal changes: summer rainfall increases by 10–20 per cent relative to CTL, while autumn rainfall declines by 10–40 per cent. These results agree with those for the monsoon circulation.

The seasonal signals are greatest in southern Queensland, where the southern boundary of the monsoon trough often lies, and which would therefore be most affected by the stronger, more extensive westerlies in summer and the quicker withdraw of the monsoon in autumn.

HiGEM 2 x CO₂ therefore projects a compression of the present-day November–April wet season: the wet-season onsets 6–10 days later and terminates 10–20 days earlier in 2 x CO₂ than in CTL (Fig. 14). Total wet-season rainfall, however, is similar in 2 x CO₂ and CTL. Consequently, the mid-summer (January and February) rains constitute a much higher fraction of the wet-season total in 2 x CO₂, with far lower contributions from November, December, March and April (Fig. 15).

As for total rainfall, the magnitude of these changes is greatest in southern Queensland. In 2 x CO₂, summers become wetter in Queensland due a 5–30 per cent increase in average rainfall intensity, while the average number of wet days per season slightly decreases relative to CTL (Figs. 7 and 8). In many regions of Queensland, the intensity increases are greater than that predicted by the Clausius–Clapeyron relationship for either the global-mean or Queensland-mean temperature increase. This is likely because 2 x CO₂ simulates an intensified summer monsoon circulation, providing more oceanic moisture to the monsoon rains over land and increasing relative humidity. By contrast, in autumn the

mean rainfall intensity remains similar to CTL, but the number of wet days per season declines considerably—by 10–20 per cent across the state—consistent with the earlier retreat of the monsoon circulation.

In southern Australia, 2 x CO₂ shows a 10–25 per cent reduction in total rainfall, with decreases in all seasons but especially in winter in southwest Western Australia (Fig. 4). The Southern Ocean storm track shifts poleward in 2 x CO₂, away from Australia and toward Antarctica, in line with many other climate models forced with only CO₂ increases (Arblaster and Meehl, 2006; McLandress et al., 2011). The decline in southern Australia rainfall is mainly due to a reduction in the number of wet days (Fig. 7), consistent with fewer rain-bearing extra-tropical cyclones.

HiGEM projects a considerable increase in the frequency and intensity of extreme rainfall in Queensland, particularly in summer, under increased CO₂ (Fig. 10). Considering all seasons together, the probability of a 100 mm daily accumulation rises by 30 per cent; in summer, however, the probability increases by approximately 40 per cent due to the enhanced monsoon. Even in autumn, when total rainfall declines, 100 mm daily accumulations occur 20 per cent more frequently in 2 x CO₂ than in CTL. Perhaps most importantly for flood risk and emergency management, the duration and size of extreme events also increases in 2 x CO₂ (Figs. 11 and 12). For summer, the probability of consecutive days above the 99th percentile of rainfall (based on CTL percentiles) increases by 20 per cent in 2 x CO₂ over CTL; the average area covered by a rain event exceeding the 99th percentile rises by 15 per cent. The increases in average duration and size of events are smaller in autumn, but those quantities do still increase despite the reduction in total rainfall.

The number of tropical cyclones per season near the northern coast of Australia declines slightly in 2 x CO₂ (Fig. 9). HiGEM projects an eastward shift in tropical-cyclone activity, away from the coast of Australia and into the open waters of the southwest Pacific.

An Empirical Orthogonal Teleconnection analysis of 2 x CO₂ found that most climate drivers identified in CTL (Klingaman, 2012a) and from observations and reanalysis data (Klingaman, 2012b) remained robust in a warmer world (Table 1). The teleconnection between state-wide rainfall and ENSO activity weakened in 2 x CO₂, particularly for summer (Fig. 17) and winter (Fig. 22) rainfall, but it is difficult to draw robust conclusions about future changes in ENSO or its teleconnections from only 50 years of 2 x CO₂ data. The overall correlation between ENSO and eastern Australia rainfall also declined in all seasons in 2 x CO₂ (Fig. 27), but these results may also be the result of sampling variability.

The EOT analysis also showed that southeastern and southwestern Queensland became more disconnected from the rest of the state. The EOT patterns describing variations in those regions were focused more strongly in those regions in 2 x CO₂ than in CTL, showing few significant correlations to other regions of the state, as in CTL. This was seen particularly strongly in autumn (Fig. 20), which suggests that it is the result of the monsoon withdrawing more quickly from southern Queensland, weakening the relationship between those regions and the rest of the state, which is still influenced by the monsoon for at least part of the season. It may be, therefore, that one effect of increased atmospheric CO₂ is to isolate climate variations in southeastern and southwestern Queensland from those in the rest of the state.

It is important to note that these results are the projections from only one model, albeit a high-resolution model shown to have a realistic representation of the climate drivers of Queensland rainfall, in response to a doubling of atmospheric CO₂. The experiment does not conform to a standard IPCC SRES or RCP scenario, since the CO₂ concentrations are fixed at 690 ppm and other forcings (e.g. aerosols, methane and ozone) have not changed. Thus, when making adaptation decisions, these results must be used alongside projections from other models that have included all forcings.

10 References

- Arblaster, J. and G. A. Meehl, 2006: Contributions of external forcings to Southern Annular Mode trends. *J. Climate*, 19, 2896–2905.
- Cai, W. and T. Cowan, 2007: Trends in Southern Hemisphere circulation in IPCC AR4 models over 1950–99: Ozone depletion versus greenhouse forcing. *J. Climate*, 20, 681–693.
- Cai, W., G. Shi, T. Cowan, D. Bi, and J. Ribbe, 2005: The response of the Southern Annular Mode, the East Australian Current and the southern mid-latitude ocean circulation to global warming. *Geophys. Res. Lett.*, 32, L23 706.
- Coelho, C. A. S. and L. Goddard, 2009: El Niño-induced tropical droughts in climate change projections. *J. Climate*, 22, 6456–6476.
- Collins, M., 2005: El Niño or La Niña-like climate change? *Clim. Dynam.*, 24, 89–104.
- Collins, M. et al., 2010: The impact of global warming on the tropical Pacific Ocean and El Niño. *Nature Geoscience*, 3, 391–397.
- Compo, G. et al., 2011: The twentieth century reanalysis project. *Q. J. R. Meteorol. Soc.*, 137, 1–28.
- Flato, G. M. and G. J. Boer, 2001: Warming asymmetry in climate change simulations. *Geophys. Res. Lett.*, 28, 195–198.
- Gualdi, S., E. Scoccimarro, and A. Navarra, 2008: Changes in tropical cyclone activity due to global warming: Results from a high-resolution coupled general circulation model. *J. Climate*, 21, 5204–5228.
- Hodges, K. I., 1996: Spherical nonparametric estimators applied to the UGAMP model integration for AMIP. *Mon. Wea. Rev.*, 124, 2914–2932.
- Jeffrey, S. J., 2001: Using spatial interpolation to construct a comprehensive archive of Australian climate data. *Environ. Modell. Softw.*, 16, 309–330.
- Klingaman, N. P., 2012a: The ability of HiGEM to simulate Queensland’s rainfall and its drivers. QCCCE Research Report 4, Department of Environment and Resource Management, Queensland Government, Brisbane, Australia.
- Klingaman, N. P., 2012b: Empirical orthogonal teleconnection analysis of inter-annual variability in Queensland rainfall. QCCCE Research Report 3, Department of Environment and Resource Management, Queensland Government, Brisbane, Australia.
- Klingaman, N. P., 2012c: Is the inter-annual variability in Queensland rainfall due to variability in rainfall frequency, intensity or both? QCCCE Research Report 2, Department of Environment and Resource Management, Queensland Government, Brisbane, Australia.
- Lavender, S. L. and K. J. E. Walsh, 2011: Dynamically downscaled simulations of Australian region tropical cyclones in current and future climates. *Geophys. Res. Lett.*, 38 (10), 1–6.
- Lough, J. M., 1997: Regional indices of climate variation: temperature and rainfall in Queensland, Australia. *Int. J. Climatol.*, 17, 55–66.
- McLandress, C., T. G. Shepherd, J. F. Scinocca, D. A. Plummer, M. Sigmond, A. I. Jonsson, and M. C. Reader, 2011: Separating the dynamical effects of climate change and ozone depletion. Part II: Southern Hemisphere troposphere. *J. Climate*, 24, 1850–1868.
- Moise, A. F. and D. A. Hudson, 2008: Probabilistic predictions of climate change for Australia and Africa using the reliability ensemble average of IPCC CMIP3 model simulations. *J. Geophys. Res.*, 113, D15 113.
- Polvani, L., M. Previdi, and C. Deser, 2011: Large cancellation, due to ozone recovery, of future Southern Hemisphere atmospheric circulation trends. *Geophys. Res. Lett.*, 38, L04 707.
- Power, S., T. Casey, C. Folland, A. Colman, and V. Mehta, 1999: Inter-decadal modulation of the impact of ENSO on Australia. *Clim. Dynam.*, 15, 319–324.
- Power, S., M. Haylock, R. Colman, and X. Wang, 2006: The predictability of interdecadal changes in ENSO activity and ENSO teleconnections. *J. Climate*, 19, 4755–4771.
- Ridgway, K. R., 2007: Long-term trend and decadal variability of the southward penetration of the East Australian Current. *Geophys. Res. Lett.*, 34, L13 613.
- Ringer, M. A., G. M. Martin, C. Z. Greeves, T. J. Hinton, P. M. James, V. D. Pope, A. A. Scaife, and R. A. Stratton, 2006: The physical properties of the atmosphere in the new Hadley Centre global

- environmental model (HadGEM1). Part II: Aspects of variability and regional climate. *J. Climate*, 19, 1302–1326.
- Roberts, M. J., et al., 2009: Impact of resolution on the tropical Pacific circulation in a matrix of coupled models. *J. Climate*, 22, 2541–2556.
- Shaffrey, L., et al., 2009: U.K. HiGEM: The new U.K. high-resolution global environment model—Model description and basic evaluation. *J. Climate*, 22, 1861–1896.
- Smith, I., 2004: An assessment of recent trends in Australian rainfall. *Aust. Met. Mag.*, 53, 163–173.
- Smith, I. N., L. Wilson, and R. Suppiah, 2008: Characteristics of the North Australian rainy season. *J. Climate*, 21, 4298–4311.
- Suppiah, R., K. J. Hennessy, P. H. Whetton, K. McInnes, I. Macadam, J. Bathols, J. Ricketts, and C. M. Page, 2007: Australian climate change projections derived from simulations performed for the IPCC 4th Assessment Report. *Aust. Met. Mag.*, 131–152.
- Uppala, S. M. et al., 2005: The ERA-40 re-analysis. *Q. J. R. Meteorol. Soc.*, 131, 2961–3012.
- Yin, J. H., 2005: A consistent poleward shift of the storm tracks in simulations of 21st century climate. *Geophys. Res. Lett.*, 32, L18 701.
- Zhao, M., I.M. Held, S.-J. Lin, and G. A. Vecchi, 2009: Simulations of global hurricane climatology, interannual variability and response to global warming using a 50-km resolution GCM. *J. Climate*, 22, 6653–6678.